Evaluation of Organic Barrier Coatings for Wastewater Digesters Using Electrochemical Impedance Spectroscopy

A thesis submitted to
the Faculty of Graduate Studies and Research
in Partial Fulfillment of the requirements for the degree

Master of Applied Science

by

Thomas Miller

Department of Civil and Environmental Engineering
Carleton University

Ottawa-Carleton Institute of Civil and Environmental Engineering
Defence Date: January 2009

Your file Votre référence
ISBN: 978-0-494-63210-9
Our file Notre référence
ISBN: 978-0-494-63210-9

Abstract

This study involved the investigation of the potential use of electrochemical impendence spectroscopy (EIS) to quantify the performance of barrier coatings proposed for use in wastewater digesters under varying environmental conditions, and also to optimize the chemical conditions and the experimental method to obtain an accelerated test procedure. To achieve these objectives a detailed experimental program has been carried out. This included the evaluation of two commercially available barrier coatings using EIS: a Rubberized Epoxy Barrier Coating (REBC) and a PolyUrethane Barrier Coating (PUBC). In the preliminary investigation, the feasibility and efficacy of EIS were investigated on the REBC and the PUBC samples that were sandwiched between two metal plates at room temperature and in dry conditions (*in air*). Using this method, coatings containing artificial defects and exposed to different environments were studied to determine if EIS could detect and measure faults in coatings. The preliminary metal plate tests were limited because they did not permit the continuous monitoring of EIS spectra in the simulated wastewater digester solution, so an apparatus, called a Tait cell, was used to carry out repetitive in-situ EIS tests on the barrier coatings. The Tait cell also was used to carry out EIS tests on the coatings at different temperatures. These experiments have shown that the REBC used in this study is not a good barrier coating, even at room temperature and when exposed to non-aggressive solutions like NaCl. On the other hand, the PUBC used in this study showed excellent protective properties, even when exposed to highly acidic solutions at temperatures up to 60°C. The EIS technique was shown to detect small changes in both coatings, and the Tait cell proved to be an effective means of performing in-situ EIS scans.

Acknowledgements

I would like to thank my thesis supervisor Professor O. Burkan Isgor for his advice, guidance, support and patience during the difficult process of carrying out my M.A.Sc. research. I could not have completed this work without him.

I would like Dr. Glenn McRae and Dr. Dave McCracken for their guidance and advice provided during the experimental work and the writing of this thesis.

I would like to thank Mr.Pedro Escudero of Carboline Canada.

I would like to thank my mother, father, sister, and my girlfriend for their constant encouragement and support.

I would also like to thank Mr Pouria Ghods, and Mr. Kostas Karadakis for being great colleagues and friends.

Finally, I would like to express my deep appreciation for Ontario Centres for Excellence (OCE), Carboline Canada, CANMET MTL and NRCAN for their financial and in kind support, without which this research would not be possible.

Table of Contents

List of Figures

List of Tables

1. Introduction

1.1. Background

In developed countries, over 75 percent of the population is served by centralized water collection and treatment systems; the remaining population uses on-site cleaning methods such as septic systems. In the year 2000, approximately 208 million people in the U.S. were served by centralized collection systems [EPA 2004]. In North America, it is estimated that over 20,000 municipal wastewater treatment facilities (of which 16,000 are in the US) are in operation. As an example, the Ashbridges Bay Wastewater Treatment Plant in Toronto is the largest wastewater treatment plant in Canada, processing approximately 818,000 cubic metres of wastewater per day [KMK 2004]; however, a large portion of the existing plants in Canada serve smaller communities. Regardless of the size of the plant, the wastewater treatment generally follows five steps [Peavy 1985, EPA 1975]:

1) Preliminary treatment, in which the wastewater is passed through screens to eliminate large objects;
2) Primary treatment, in which the wastewater is kept in settlement tanks so that solid particles can be physically separated;
3) Secondary treatment, in which biological treatment processes (i.e. micro-organisms) are used to remove very small particles from wastewater;
4) Final treatment, in which the wastewater is disinfected with chemical agents such as chlorine;

5) Processing of solids, or digestion, in which the solids (i.e. sludge that includes biomass and pathogens) from primary and secondary treatment processes are sent to digesters where they are further cleaned using bacteria and are reduced to bio-solids and gaseous products.

One of the most common and efficient methods of processing solids is through anaerobic digestion, in which anaerobic bacteria are used in a temperature-controlled closed digester to reduce the sludge to bio-solids and gaseous products such as methane, carbon dioxide and relatively small amounts of hydrogen sulphide (H_2S). Methane produced during the processing of solids can be used for energy production. Bio-solids comprise a wet soil-like material which is high in organic content and nutrients (e.g. nitrogen and phosphorous), and which can be reused as fertilizer, incinerated or sent to a landfill. A typical anaerobic digester, from the wastewater treatment plant of the City of Sante Fe, USA, is illustrated in Figure 1-1a. Digesters may range in size and shape, but they generally consist of a cylindrical container that is capped with a fixed or floating cover (see Figure 1-1b).

Digesters used in the processing of solids are generally made of reinforced or prestressed concrete. As presented later, the treatment process of sludge in a digester creates an acidic environment known to be deleterious to concrete [Estoup et al. 1997]. Should concrete come into contact with the waste water sludge gypsum would form in the concrete, this can leads to the deterioration of the mechanical properties of concrete, cracking, and eventual failure of the structure [Crites and Tchobanoglous 1998]. The deterioration and eventual failure of these structures may have significant health, environmental and economic impacts, and therefore preventative measures must be taken

to reduce the effect of this aggressive environment on the concrete. The main method used to achieve this goal is to apply high-performance barrier coatings on the interior faces, (*i.e.*, the walls, the bottom and the cover of the digesters) to prevent the chemically aggressive sludge from contacting the concrete. Traditionally, many different types of coatings have been used for this purpose, including, but not limited to, coal-tar epoxies, polyamide epoxies, vinyl esters, polyester mortars, novolac epoxies, solvent-based epoxies and polyurethanes. Coating failures observed in treatment plants generally involve cracking and dis-bondedment of the coatings, which is caused by low coating elasticity that limits the integrity of the coating when the concrete substrate moves and cracks. As a consequence, recent practice is to use coatings which exhibit significantly higher elasticity [O'Dea 2007], such as 100%-solids per volume polyurethanes (*i.e.,* there is no solvent to evaporate during the curing process) [Khanna 2008].

1.2. Anaerobic Digestion

Anaerobic digestion follows a three-step process: hydrolysis, acidogenesis, and methanogenesis [Gray 2004]. In the hydrolysis stage complex organic molecules in the sludge are made soluble and hydrolyzed to smaller molecules. For example, carbohydrates and proteins are converted into simpler compounds such as glucose and amino acids. In the acidogenesis stage, acid-forming bacteria convert the products of the hydrolysis stage into short-chain organic acids, hydrogen and carbon dioxide. Finally in the methanogenesis stage, the volatile acids are converted into methane and carbon dioxide. These three steps occur simultaneously during anaerobic digestion.

The acid-forming bacteria are relatively tolerant to fluctuations in pH and temperature, and have the ability to metabolize dissolved oxygen. They also have a fairly

rapid growth rate. In contrast, the methanogenesis bacteria are not tolerant to pH and temperature changes. They are anaerobes with slow growth rates. These two sets of bacteria operate in equilibrium, in which the rate of acid and hydrogen gas formation by acid-forming bacteria is matched by the rate of creation of methane and carbon dioxide by methanogenesis bacteria. [Gray 2004]

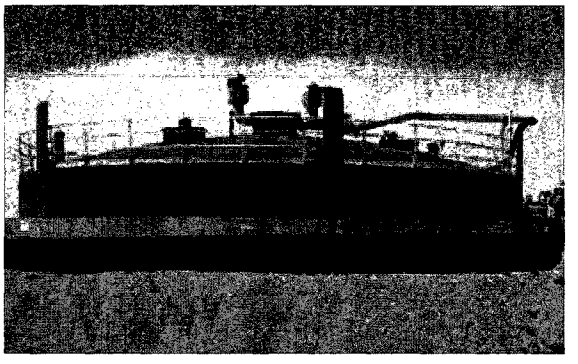

(a) Anaerobic digester of the water treatment plant of the City of Sante Fe. [Taken from the webpage of the City of Sante Fe, USA]

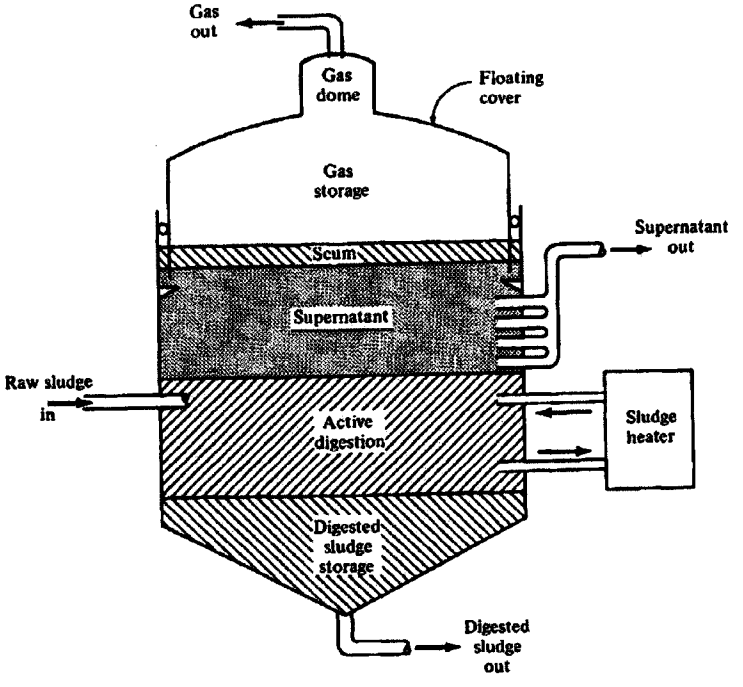

(b) Scematic of a typical anaerobic digester. [Peavy 1985]

Figure 1-1 Anaerobic digesters.

There is also another possible mechanism of acidification that is not related to the anaerobic processes. Sulphates can be found in most water supplies and wastewater systems. Under anaerobic conditions, sulphate is reduced to sulphide by bacteria, which results in the formation of H_2S. Equations 1-1 and 1-2 show this process [Tchobanoglous 1979]:

$$SO_4^{2-} + \text{organic matter} \xrightarrow{bacteria} S^{2-} + H_2O + CO_2 \qquad 1\text{-}1$$

$$S^{2-} + 2\,H^{+} \rightarrow H_2S \qquad 1\text{-}2$$

Ideally, anaerobic digesters work in the absence of oxygen; however, oxygen can leak into the digester from the expansion joints, movable parts, or faults in the cover, so that localized oxygen-rich areas may exist under the cover and above the sludge line. These areas are prone to further acidification, and hence to deterioration. When the environment changes from anaerobic to aerobic (*i.e.* oxygenated) conditions, the hydrogen sulphide is converted to sulphuric acid, and can thereby drop the pH of the environment to lower than the optimum pH of the digester.

The physical and chemical nature of sludge will vary among different wastewater treatment plants. The variations are mainly due to the relative amounts of industrial waste, residential waste and storm water flow, as well as the treatment method. Primary sludge (sludge from the primary treatment) has a density of 1 - 1.03 g/cm^3, while the density of activated sludge (sludge from the secondary treatment) is approximately 1 g/cm^3 [Turovskiy et al. 2006]. Table 1-1 and 1-2 show the particle size distribution of primary and activated sludge, respectively.

Table 1-3 shows the components of wastewater sludge in North America. Table 1-4 gives the major mineral components in sludge.

Table 1-1 Particle size distribution of primary sludge. [Turovskiy et al. 2006]

Size (mm)	Primary Sludge (%)
> 7	5 – 20
1 – 7	9 – 33
< 1	50 – 88
< 0.2	45

Table 1-2 Particle size distribution of activated sludge. [Turovskiy et al. 2006]

Size (mm)	Activated Sludge (%)
> 3	0.4
1 - 3	1.6
1 – 0.2	8
< 0.2	90

Table 1-3 Typical wastewater sludge characteristics in North America. [Turovskiy et al. 2006]

	Primary Sludge		Activated Sludge	
Item	**Range**	**Typical**	**Range**	**Typical**
Total dry solids (TS) (%)	2 - 7	5	0.4 - 1.5	1
Volatile solids (% of TS)	60 - 80	65	60 - 80	75
Specific gravity		1.02		1.01
Grease and fats				
Ether soluble (% of TS)	6 - 30			
Ether extract (% of TS)	7 - 35		5-12	
Protein (% of TS)	20 - 30	25	32 - 41	
Nitrogen (N, % of TS)	1.5 - 4.0	2.5	2.4 - 5.0	
Phosphorus (P_2O_5, % of TS)	0.8 – 2.8	1.6	2.8 – 11.0	
Potash (K_2O, % of TS)	0 - 1	0.4	0.5 – 0.7	
Cellulose (% of TS)	9 - 13	10		7
Iron (not as sulphide, % of TS)	2 - 4	2.5		
Silica (SiO_2, % of TS)	15 – 20			8
pH	5 - 8	6	6.5 – 8.0	7
Alkalinity (mg/L as $CaCO_3$)	500 - 1500	600	580 – 1100	
Organic acids (mg/L as HAc*)	200 - 2000	500	1100 - 1700	
Energy content				
kJ/kg	23300	18600	23300	
Btu/lb	10000	8000	10000	

*HAc: Acetic acid equivalent

Table 1-4 Major mineral constituents of sludge as percentage of total mineral constituents. [Turovskiy et al. 2006]

Content	Raw primary sludge	Raw activated sludge	Digested mixture of primary and activated sludge
SiO_2	21.5 – 55.9	17.6 – 33.8	27.3 – 35.7
Al_2O_3	0.3 – 18.9	7.3 – 26.9	8.7 – 9.3
Fe_3O_4	4.9 – 13.9	7.2 – 18.7	11.4 – 13.6
CaO	11.8 – 35.9	8.9 – 16.7	12.5 – 15.6
MgO	2.1 – 4.3	1.4 – 11.4	1.5 – 3.6
K_2O	0.7 – 3.4	0.8 – 3.9	1.8 – 2.8
Na_2O	0.8 – 4.2	1.9 – 8.3	2.6 – 4.7
SO_3	2.0 – 7.5	1.5 – 6.8	3.0 – 7.2
ZnO	0.1 – 0.2	0.2 - 0.3	0.1 – 0.3
CuO	0.1 – 0.8	0.1 – 0.2	0.2 – 0.3
NiO	0.2 – 2.9	0.2 – 3.4	0.2 – 1.0
Cr_2O_3	0.8 – 3.1	0.0 – 2.4	1.3 – 1.9

1.3. Problem Definition

The performance of coatings in wastewater treatment plants is currently monitored using real-time in-situ testing. For this purpose, sample concrete coupons are prepared, and then the coating to be tested is applied on these coupons as shown in Figure 1-2. These coupons are placed in an operating digester for approximately two years, or longer. The inspection of the coupons after this exposure time (see Figure 1-3) provides belated information about the performance of the applied coating. Although in-service testing is important, it is considered that even the shortest time of two years is too long to have to wait to find out if a coating is working.

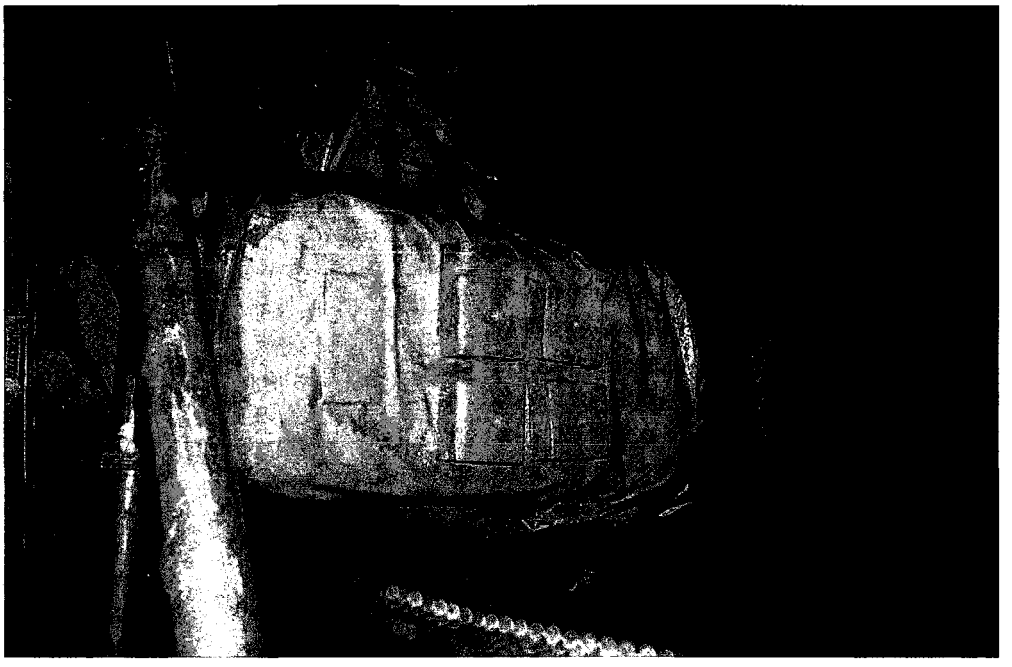

Figure 1-2 Current in-service coatings test: sprayed coupons before in-situ testing; specimens are 10 cm x 10 cm x 5 cm.

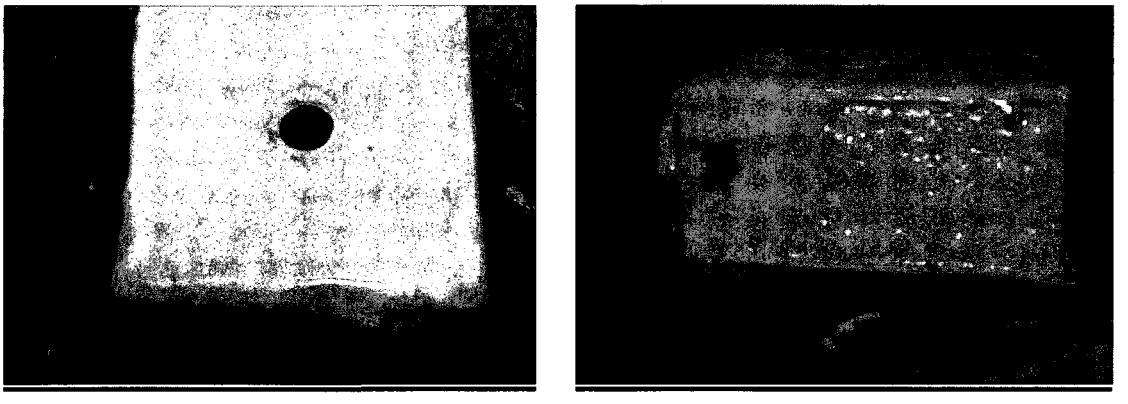

Figure 1-3 Current in-service coatings test: coupons are inspected after two years of exposure; specimens are 10 cm x 10 cm x 5 cm.

Currently, communities are required to process their wastewater to minimize the contamination of natural water resources. There is a demand [EPA 2004, EPA 2007] for better processes' to reduce the environmental impact of wastewater treatment plants.

Higher levels of treatment usually require higher anaerobic digestion capacity in the processing of solids. One way for treatment plants to increase their capacity is to decrease the time needed for the contaminated sludge to stay inside anaerobic digesters.

The operating temperature has an important effect on the growth, performance, and type of anaerobic bacteria, and consequently has a large impact on the overall digester performance [Grady et al. 1999]. Most digesters operate in the so-called mesophyllic temperature range of 30-38°C, usually at 35°C. However, digesters can also be designed to operate in the so-called thermophyllic temperature range of 50-57°C. The mesophyllic and thermophyllic ranges derive there names from the type of bacteria that are present at those temperatures. A significant reduction of digestion time can be obtained by converting to thermophyllic digesters, which operate at higher temperatures than the traditional mesophyllic digesters [Grady et al. 1999].

Before potential barrier coatings can be used in wastewater treatment plants, research to investigate their performance at a variety of temperatures and more acidic environments, that are consistent with their use in service conditions, must be performed. The current state of coating evaluation techniques requires a large amount of time in order to bring new coatings into service or to change the intended application of in-service coatings, i.e. operate at a higher temperature [Briand et al. 2003]. Therefore, a more rapid means of evaluating potential coatings is required.

1.4. Electrochemical Monitoring of Coating Performance

In order to monitor the integrity of potential wastewater digester coatings, an electrochemical technique commonly used to study oxides on metals and the integrity of

thin films has been used. In this method the impedance across the thickness of the coating is measured. From an electrical point of view, a perfectly protective coating has an infinite resistance (zero conductance), and is a pure capacitance. As the coating deteriorates, the capacitance properties degrade and conductive paths develop. Once the coating is fully breached, it becomes a conductor of both electrolyte and electrical charges. Under these conditions, any deleterious solution or gas, e.g., sulphuric acid or H_2S, has access to the underlying metal or concrete.

The barrier coatings of interest to us are typically quite thick (of the order of a couple of millimetres) and have a very high electrical resistance, so that small changes in their properties are not easy to capture with traditional direct-current methods because the resistances are above the input resistance of most Ohm meters. However, at frequencies between 0.1 and 10^5 Hz, the coating impedances can be much lower so that measurements can be made. A technique that is known to be sensitive to changes in electrical properties of coatings, films and oxides has therefore been selected [Mansfeld 1990]. This is called electrochemical impedance spectroscopy [Gamry 2007].

Prior to this present study, EIS had not been widely used to evaluate thick barrier coatings. In this technique, a small alternating voltage (10 - 100 mV) is applied across the thickness of the coating, and the current is monitored. This is then repeated for alternating voltage frequencies from 10^{-2} Hz up to 10^5Hz. Analyses of the magnitude of the current, and the phase difference between the current and voltage (see Chapter 2), allows one to derive quantitative information on the resistive and capacitative properties of the coating. In turn, this leads to a quantitative, assessment of the coating's integrity.

1.5. Objectives of the Research

The general objectives of the research described in this thesis is to investigate the potential use of EIS to quantify the performance of barrier coatings proposed for use in wastewater digesters under varying environmental conditions, and also to optimize the chemical conditions and experimental method to obtain an accelerated test procedure. To achieve these objectives a detailed experimental program has been carried out. This included the evaluation of two commercially available barrier coatings using EIS: a Rubberized Epoxy Barrier Coating (REBC) and a PolyUrethane Barrier Coating (PUBC). Note that commercial names will not be used in this thesis.

An additional objective, of the current research is to develop an accelerated test to show if current coatings will work at higher temperatures and under harsher conditions. PUBC has been widely used successfully in mesophyllic digesters. This work has concentrated on the deterioration of barrier coatings due to their exposure to acidic solutions, and has not investigated deterioration due to gases, e.g., H_2S.

The REBC is a 100% solids rubberized epoxy (see Figure 1-4). It was originally developed to protect concrete floors in the cell houses of copper mines. During the mining of copper, concrete floors of cell houses may become exposed to sulphuric acid, in concentrations as high as 2 mol/l, and with a temperature range of 40-60°C [Pletcher et al. 1990]. REBC also has good abrasion properties and flexibility. It was believed that the REBC had the potential to perform well in thermophyllic digesters, in which the exposure to acidic solutions and temperature ranges are similar to the conditions that are present in the cell houses. This hypothesis was tested in the current research.

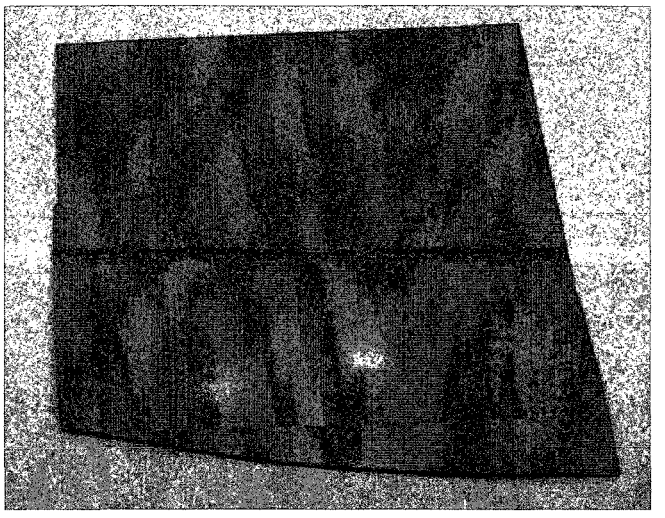

Figure 1-4 A typical REBC sample.

The PUBC is a solvent-free aromatic polyurethane barrier coating that is widely used in mesophyllic digesters (see Figure 1-5). In addition to this application, it is also used to protect concrete or steel in potable water treatment and storage tanks, and for tank linings, pipeline coatings, and coatings in marine vessels and offshore structures. The manufacturer of the PUBC does not recommend its use for concentrated acids, aromatic hydrocarbons, ketones, or chlorinated solvents. The PUBC has 100% solids per volume. This coating is suitable for application on both steel and concrete, and has a long track record of successful operation in mesophyllic temperature ranges.

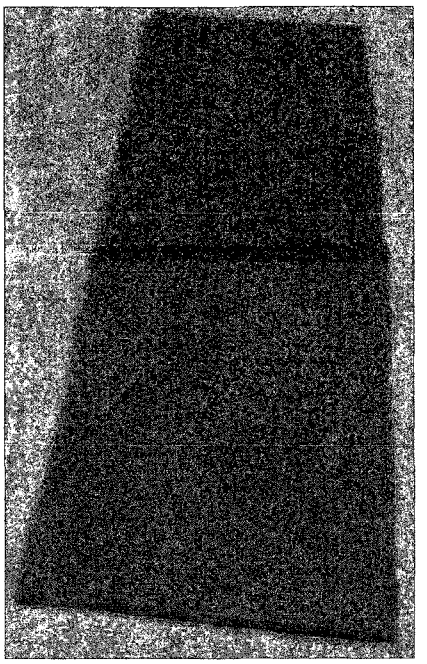

Figure 1-5 A typical PUBC sample.

1.6. Organization of the Thesis

This thesis has 8 chapters.

Chapter 1 contains an introduction to the wastewater treatment process. Also included in this chapter are the problem definition, the objectives and the general methodology of the research.

In Chapter 2, an introduction to EIS is provided.

The literature review is presented in Chapter 3. This review focuses on the conventional testing procedures of coatings, the deterioration mechanisms of coatings in wastewater treatment plants, and the use of EIS in the evaluation of coatings.

In Chapter 4, the preliminary testing program is presented.

The experimental setup and testing regime for the REBC and the PUBC is discussed in Chapter 5.

Chapters 6 and 7 detail the electrochemical cell experiments that study the effect of temperature on the REBC and the PUBC.

Conclusions are presented in Chapter 8.

1.7. Methodology

The main experimental method used in this research is EIS. More technical information on EIS is provided in Chapter 2. The research was carried out in three main stages:

1) Preliminary experiments: The main objective of this stage was to determine if EIS was a feasible tool to characterize the protective properties of barrier coatings, and if so, to optimize EIS parameters and characterize EIS signatures of damaged coatings. Preliminary experiments were carried out at room temperature on the REBC and the PUBC using two setups briefly described below:
    a. *Preliminary metal plate tests:* In this setup, EIS scans were taken of each coating sandwiched between two metal plates. The coatings were first exposed to various solutions, removed and dried, then clamped between two metal plates. Using this approach, coatings containing artificial defects, such as pinholes or a pit, were studied to ensure that EIS could detect and measure faults in the coatings, and to characterize the EIS signals. Coatings, with and without artificial defects, were also tested after they were exposed to distilled water or NaCl solution to see if effects of exposure to different solutions could be observed. A number of verification and calibration tests were also conducted.

b. *Preliminary Electrochemical cell tests:* A commercial electrochemical cell (Tait Cell), was used for the majority of tests. The metal plate tests had severe limitations in that they did not permit the continuous monitoring of EIS spectra, with a coating's surface completely exposed to aggressive solutions. In hopes of overcoming this problem, the use of a Tait cell, described in detail later in this thesis, was investigated for its suitability for in-situ testing of coatings. It was found that with this apparatus, a coating could be continuously exposed to an aggressive solution, while repetitive EIS scans were taken. The entire setup could be placed in an environmental chamber so that the effect of temperature on coating performance could also be studied in situ.

2) Continuous Tait cell experiments: After demonstrating that the Tait cell was a good tool for the intended use, the effects of continuous exposure to different aggressive solutions (e.g. different pH levels) and different temperatures on the REBC and the PUBC were investigated. These studies also established the background for the development of an accelerated testing procedure for barrier coatings.

3) Equivalent circuit modelling and analysis: As its name suggests, an "equivalent circuit" is an electrical circuit that emulates the physical and electrical properties of the coatings. As mentioned earlier, a perfect coating starts off as a perfect capacitor. As degradation occurs, a parallel resistive component grows in, as the capacitive properties degrade. Variations of circuit parameters with respect to exposure conditions and time were determined. The outcome has provided

valuable data about the performance of the two coating systems tested in this investigation.

2. Electrochemical Impedance Spectroscopy (EIS)

2.1. Introduction

EIS is the primary experimental method used in the current research. This chapter gives a basic background on EIS that will be used in further discussions and data analyses in this thesis. More detailed discussions of EIS can be obtained from comprehensive references such as Scholtz (ed.) [2002] and Girualt [2004] and Barsoukov and Macdonald [2005].

EIS is an electrochemical technique with a wide range of applications in different fields of science and engineering, including (but not limited to) corrosion science, electrochemistry, biology, sensor development and coating/paint characterization. The main reason behind its popularity is its ability to provide sensitive qualitative and quantitative information about the physical and chemical properties and changes (reactions) in an electrochemical system (e.g. a coating in an electrolyte). EIS involves the application of a small, sinusoidal, alternating current (AC) or voltage to the sample undergoing investigation. The AC perturbation (either voltage or current) is applied over a range of frequencies, and the electrical response of the system is measured and analysed over this range of frequencies. A typical EIS setup requires a three-electrode electrochemical cell, which is equipped with a working electrode, a counter electrode, and a reference electrode (Figure 2-1). The working electrode is where the reaction(s) take place in an electrochemical system, (*i.e.*, it is the material under investigation). The measurements on the working electrode are carried out with respect to a reference electrode which has a stable and well-known electrical potential. To ensure that

unwanted voltage changes related to current changes do not occur on the reference electrode, a counter electrode serves to carry the current required by the working electrode. At the surface of the counter electrode, no processes of interest should occur; therefore the counter electrode is usually a very stable metal.

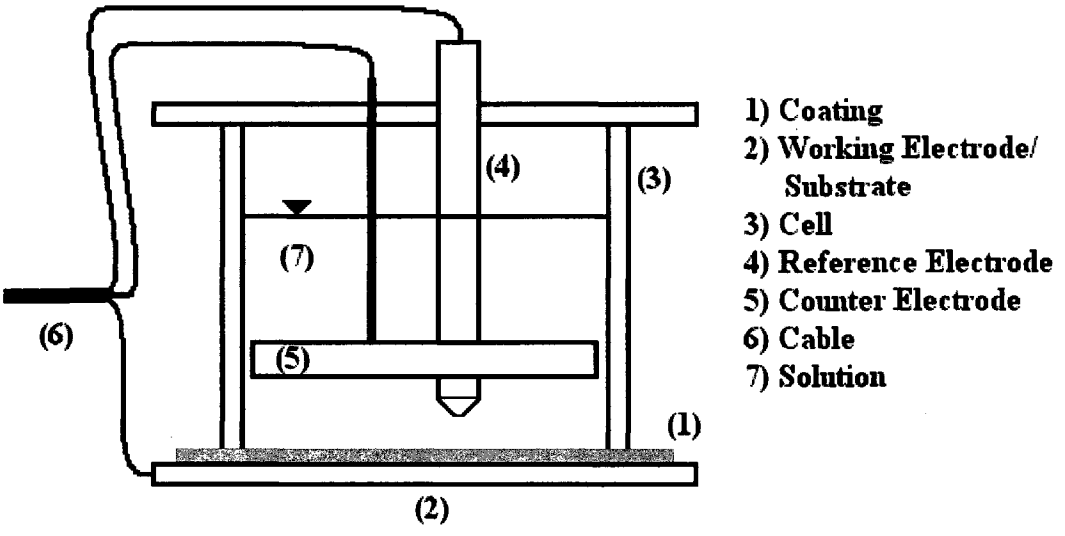

Figure 2-1 Schematic of an electrochemical cell used to carry out EIS measurements on coatings.

EIS experiments are carried out using a potentiostat and additional hardware to apply and measure sinusoidal AC signals. In the present research, a Gamry PC4/ 300 Potentiostat/ Galvanosatat /ZRA from Gamry Instruments [2001] was used to carry out the experiments. The specifications of this system are provided in Appendix A. To enable a single potentiostat to conduct multiple parallel experiments, a Gamry ECM8 Electrochemical Multiplexer, which allows the potentiostat to be connected to eight electrochemical cells at a time, was also used.

The potentiostat and the multiplexer were controlled by Gamry Software (Gamry Framework V4.35); this software allows user scripting to customize the EIS experiments.

The standard scripting was modified from the normal Gamry issue, to enable the software to work at very low currents, and to eliminate problems with gain changes, which originally gave phantom peaks in the EIS spectra (see Appendix A).

2.2. Basic Concept of Impedance

In a DC circuit, the voltage and the current remain constant and are proportional to each other through Ohm's law:

$$I = \frac{E}{R} \qquad 2\text{-}1$$

where I is the current [A], E is the voltage or the potential [V], and R is the electrical resistance [Ω or ohm]. The electrical resistance is the ability of a circuit element to resist the flow of electrical current. The application of Eq. 2.1 and the concept of electrical resistance are limited to pure resistors, which have the following basic properties: (1) Ohm's law is valid at all voltage and current levels, (2) the electrical resistance is not dependent on the frequency of the applied current, (3) the current and voltage signals are in phase with each other, (*i.e.*, changes in them occur simultaneously). Most electrochemical systems contain circuit elements that have more complex properties than can be simulated with ideal resistors. A more general property of the ability of a circuit element to resist the flow of electric current is its impedance, which is not limited by the simplifying properties of electrical resistance.

Electrochemical impedance is usually measured by applying a small oscillating sinusoidal AC potential excitation to an electrochemical cell, and measuring the response of the current; *i.e.*, the corresponding AC current signal containing the excitation frequency and its harmonics. The excitation is kept small, and the current response to a

sinusoidal potential will be sinusoidal at the same frequency but, unless it is a purely resistive system, the peaks in the voltage and current do not occur at the same time. The activating voltage and the response current are characterized by a phase shift as shown in Figure 2-2.

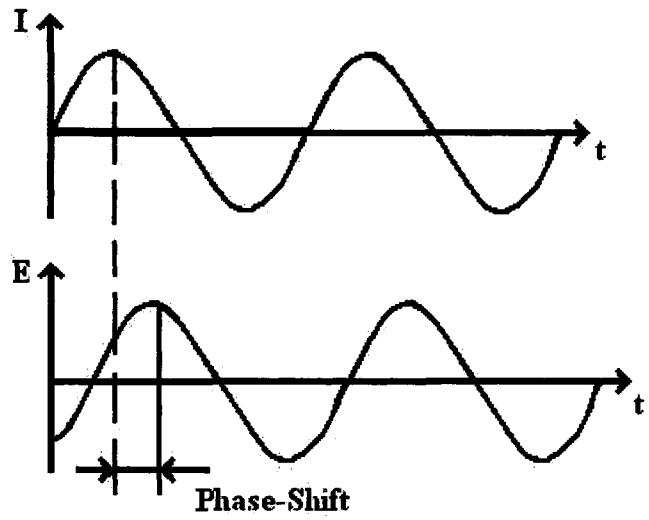

Figure 2-2 A small sinusoidal potential excitation and its current response in an AC system. [Modified from Gamry 2007]

In Figure 2-2 a phase shift can be observed between the voltage and the current such that the voltage is said to lead the current; i.e., the peak voltage occurs before the peak current. It can also be said that current the lags the voltage. The phase angle is measured in degrees and ranges from +180° to -180°. In the case of Figure 2-2, the phase angle would be defined as positive; if the current lags the voltage, the phase angle is considered negative. As an example, the phase angle is -90° for a perfect capacitor.

An AC system can be described in terms of complex arithmetical functions. In this representation, the excitation potential and the response current are given by Eq. 2.2 and Eq. 2.3, respectively.

$$E(t) = E_0 e^{j\omega t} \quad 2\text{-}2$$

$$I(t) = I_0 e^{j\omega t - j\phi} \quad 2\text{-}3$$

where E(t) is the potential at time t, I(t) is the current at time t, E_0 is the amplitude of the voltage, I_0 is the amplitude of the current, ϕ is the phase shift in the current, ω is defined in Eq. 2-4, and $j = \sqrt{-1}$.

$$\omega = 2\pi f \quad 2\text{-}4$$

Using Ohm's law, the impedance can be represented as a complex function:

$$Z = \frac{E(t)}{I(t)} = \frac{E_0 e^{j\omega t}}{I_0 e^{j\omega t - j\phi}} = Z_o e^{j\phi} \quad 2\text{-}5$$

Z_0 is referred to as the magnitude, Z_{mag}, or the modulus, Z_{mod}, of the impedance. These terms are used interchangeably in electrochemistry and in this thesis.

Applying Euler's relationship [Cogdell 1999]:

$$e^{j\phi} = \cos(\phi) + j\sin(\phi) \quad 2\text{-}6$$

The following simplified relationship for impedance can be obtained.

$$Z = Z_0(\cos(\phi) + j\sin(\phi)) \quad 2\text{-}7$$

The impedance has now resolved into real and imaginary components, (Z_{real} or ReZ), and (Z_{img} or ImZ) given by Eqs. 2-8 and Eq.2-9, respectively:

$$Z_{real} = Z_0 \cos(\phi) \quad 2\text{-}8$$

$$Z_{img} = Z_0 \sin(\phi) \quad 2\text{-}9$$

The units for both of these terms are ohms. The magnitude or modulus of the impedance is defined as:

$$Z_{\text{mod}} = \sqrt{Z_{real}^2 + Z_{img}^2} \qquad 2\text{-}10$$

The phase angle between voltage and current can be calculated from the real and imaginary parts of the impedance because:

$$\tan(\phi) = \frac{Z_{img}}{Z_{real}} \qquad 2\text{-}11$$

2.3. Presentation of the EIS Output

When an EIS measurement of a sample is performed, the impedance of the electrochemical cell is calculated from the applied potential and the response current at various frequencies. From the calculated impedance, four particular quantities can be extracted: the real impedance (Z_{real} or ReZ), the imaginary impedance (Z_{img} or ImZ), the modulus of the impedance (Z_{mod}) and the phase angle (ϕ). What is also needed is a method of presenting the EIS data in a convenient manner. For this purpose, there are two presentations that are most commonly used: the Nyquist plot, and the Bode plot. In the Nyquist plots presented in this thesis, the real impedance is plotted against the negative of the imaginary impedance; Figure 2-3 contains a sample of a Nyquist plot. As illustrated in the plot, the Nyquist plot does not provide any explicit information regarding the frequencies of the measured data points. In most electrochemical systems, the impedance increases as the frequency decreases; therefore the low frequency data points are usually on the right side of the Nyquist plot, and the high frequency points are usually on the left. Figure 2-4 is a sample Nyquist plot of a simulated EIS scan.

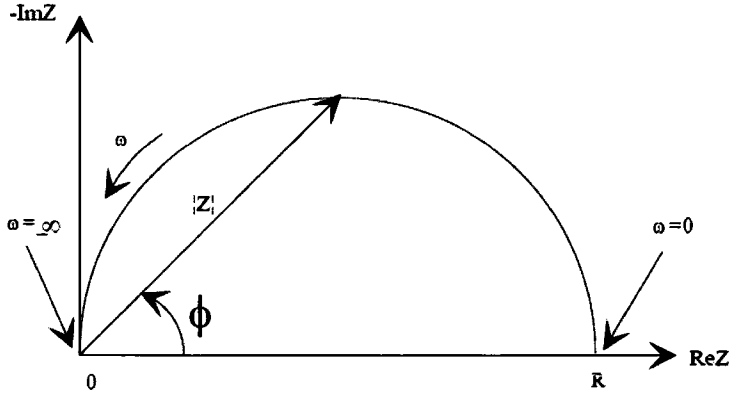

Figure 2-3 A typical Nyquist plot of an EIS scan.

[modified from[Gamry Instruments 2007]

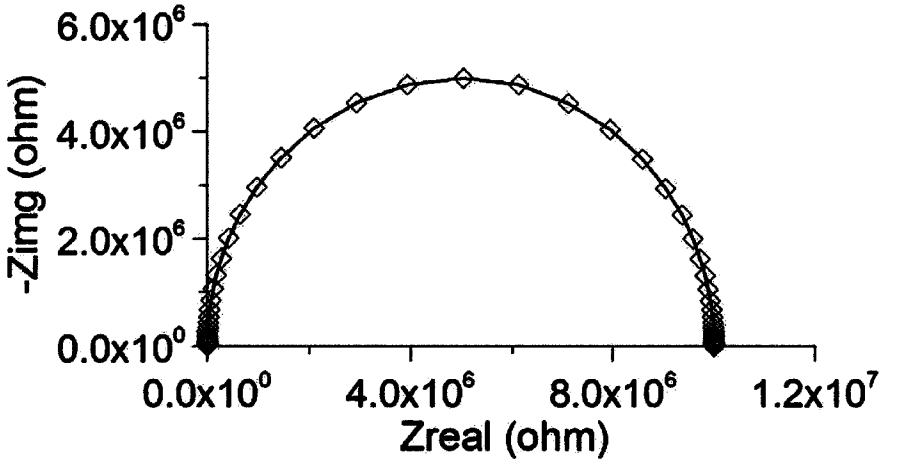

Figure 2-4 Sample Nyquist plot of an EIS scan.

The other standard method of displaying the data from an EIS measurement is in a Bode plot. A Bode plot has the frequency in a log scale along the horizontal axis; while on the left vertical axis the modulus of the impedance is plotted on a log scale. A second vertical axis displaying the magnitude of the phase angle is on the right side. Figure 2-5 is a sample Bode plot of a simulated EIS scan.

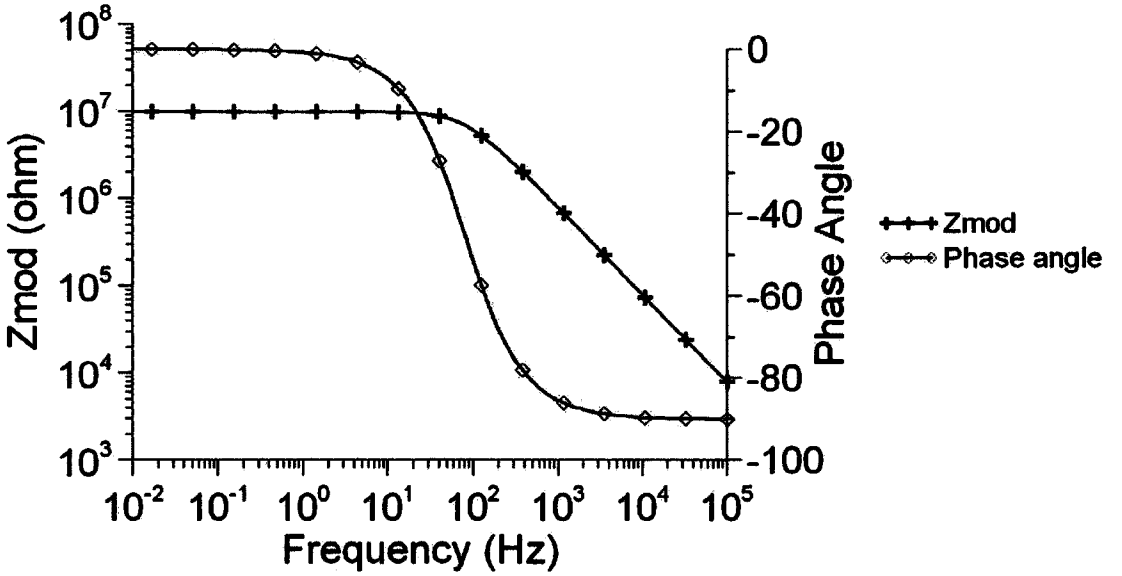

Figure 2-5 Sample Bode plot of an EIS scan.

In general, both the Nyquist and Bode plots only give the results of a single EIS scan, however, it may be desirable to show the variations of the EIS spectrum with respect to time. In this work, this is useful for displaying how the impedance of a coating evolves with time. In these time plots, the horizontal axis is the time, while one of the four EIS parameters (i.e. the modulus of the impedance, the real impedance, the imaginary impedance or the phase angle) is plotted on the vertical axis. The data for several different frequencies can also be plotted on the same graph. A sample of this type of plot for Z_{mod} is illustrated in Figure 2-6. In this thesis only plots of the modulus of the impedance, and of the phase angle will be presented in this manner.

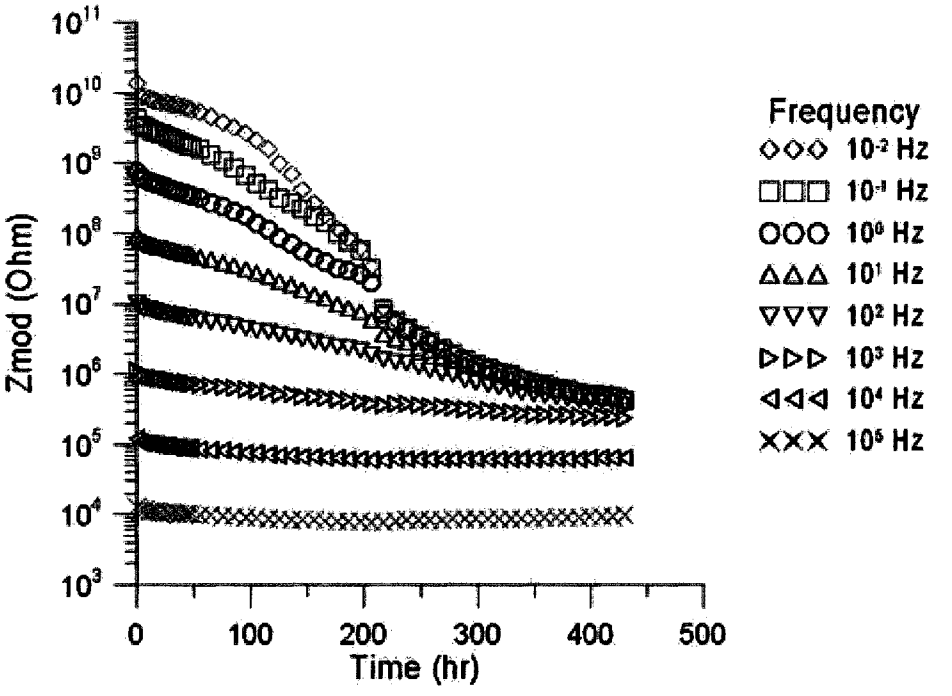

Figure 2-6 Sample Z_{mod} vs time plot at different frequencies.

2.4. Equivalent Circuit Modelling

The interpretation of EIS results can be challenging even after the data are presented using Nyquist and Bode plots. A widely used method of EIS data modelling is Equivalent Circuit Analysis (ECA), in which the goal is to create an equivalent electrical circuit that simulates the physical characteristics of the electrochemical cell being tested. In the equivalent circuit model, the physical characteristics can be represented by a finite number of linear circuit elements (e.g., resistors, capacitors, inductors, and constant phase elements - CPEs). The measured data are fitted to the assumed model to obtain the magnitudes of these circuit elements. Different circuit elements are used to represent different physical attributes of the sample under test. It is possible to derive quantitative information on the thickness, porosity and integrity of a coating. Provided that the model is physically representative of the actual measured system, the variation of the model

components can be tracked with respect to time so that changes in the physical system can be quantified as a function of time.

To understand circuit representations, a basic understanding about the circuit elements is required. A resistor is a two-node circuit element that opposes an electric current (I) by producing a voltage drop (V) between its terminals in accordance with Ohm's law ($V = IR$) and is defined by its resistance, R (ohm). The impedance of a resistor does not depend on the frequency and has only a real component, hence:

$$Z = R \tag{2-12}$$

Since an imaginary component for this impedance does not exist, the current through a resistor is always in phase with the voltage. Figure 2-7 is the circuit-element representation used for modeling a resistor in an equivalent circuit.

Figure 2-7 Circuit-element representation for a resistor.

A capacitor is a passive circuit element that can store energy in the electric field across a dielectric (low-conductivity or insulating) material between a pair of conductors (or plates, as shown in Figure 2-8). The process of storing energy in the capacitor is known as "charging" and involves the separation of electric charges, which build up on each plate, with equal magnitude but opposite polarity. A capacitor's ability to store charge is measured by its capacitance, C, which is measured in Farads (F). The capacitance of a parallel plate capacitor can be calculated using:

$$C = \varepsilon \frac{A}{d} \tag{2-13}$$

where A and d are the area and the separation of the plates respectively, and ε is the dielectric constant (or relative static permittivity) of the material between the parallel

plates. The latter has a value of 1 for a vacuum, 80.1 for water at 20°C, and 4-8 for organic coatings [Gamry 2006].

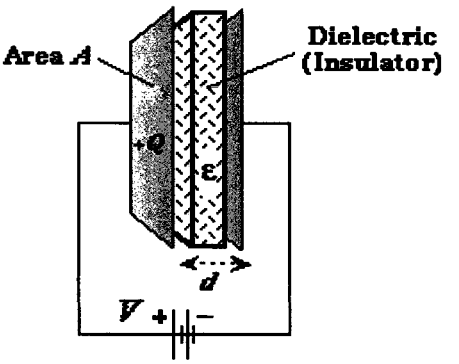

Figure 2-8 Parallel plate capacitor. [Vawter 2008]

A perfect capacitor will cause the voltage to lag behind the current by 90°, or have a phase angle of -90°. The impedance of a capacitor is inversely proportional to the frequency of the AC system and can be written as:

$$Z = \frac{1}{j\omega C} \qquad 2\text{-}14$$

The circuit-element representation of a capacitor is shown in Figure 2-9.

Figure 2-9 Circuit-element representation for a capacitor.

It is unusual to see materials that behave like perfect capacitors; in most real-world cases the behaviour is non ideal. Surface roughness, porosity, non-uniform thickness of the material being tested, and non-uniform current distribution across the dielectric material are some of the possible reasons for this non-ideal behaviour [Barsoukov et al. 2005]. A constant phase element (CPE) is a type of imperfect circuit element (not a

resistor, capacitor or inductor), somewhat like a non-ideal capacitor, that is often used to model these cases.

The impedance of a CPE is given by:

$$Z = \frac{1}{Q(j\omega)^p} \tag{2-15}$$

When the exponent, p, is equal to 1, the CPE is equivalent to a perfect capacitor ($Q = C$), when it is -1 it is equivalent to an inductor, and when it is zero it is equivalent to a resistance. When diffusion limits the current flow, it has a value of 0.5; this is called a Warburg element. For real systems containing an imperfect layer of material, it is usually between 0.5 and 1. When p is close to 1.0, the CPE resembles an imperfect capacitor. The phase angle of a CPE is constant and between 0 and -90° at all frequencies. The phase angle will be as follows:

$$\phi_{CPE} = \frac{-p\pi}{2} \tag{2-16}$$

The proof of the phase angle value of a CPE is shown below:

$$e^{j\frac{\pi}{2}} = \cos(\frac{\pi}{2}) + j\sin(\frac{\pi}{2}) = j$$

$$\therefore j^p = e^{jp\frac{\pi}{2}}$$

$$Z = \frac{1}{Q(j\omega)^p} = \frac{1}{Q\omega^p} e^{-jp\frac{\pi}{2}}$$

$$Z = \cos(-\frac{\pi}{2}p)\frac{1}{Q\omega^p} + j\sin(-\frac{\pi}{2}p)\frac{1}{Q\omega^p} \tag{2-17}$$

$$\tan\phi = \frac{Zimg}{Zreal} = \frac{\sin(-\frac{\pi}{2}p)\frac{1}{Q\omega^p}}{\cos(-\frac{\pi}{2}p)\frac{1}{Q\omega^p}}$$

$$\therefore \phi_{CPE} = \frac{-p\pi}{2}$$

Figure 2-10 displays one of the circuit-element representations for a CPE.

Figure 2-10 Circuit-element representation for a CPE.

Circuit elements, such as resistors and capacitors, can be brought together in a number of combinations to develop equivalent circuits that are representative of the electrochemical system under investigation. Different equivalent electric circuits can be constructed from elements in series or in parallel or from combinations of series and parallel elements.

When combining circuit elements in series, the equivalent impedance is simply the sum of the impedances that are in series; this can be seen in the example given in Figure 2-11. For this system, which consists of a resistor and capacitor in series, the impedance is calculated as:

$$Z = R + \frac{1}{j\omega C} \qquad 2\text{-}18$$

Figure 2-11 A resistor and capacitor in series.

When combining circuit elements in parallel, the inverse of the equivalent impedance is the sum of the inverse of the impedance for each element; this can be seen in the example given in Figure 2-12. For this system, which consists of a resistor and capacitor in parallel, the impedance is calculated as:

$$\frac{1}{Z} = \frac{1}{R} + \frac{1}{\frac{1}{j\omega C}} \qquad 2\text{-}19$$

$$Z = \frac{R\left(\frac{1}{\omega C}\right)^2 - jR^2\left(\frac{1}{\omega C}\right)}{R^2 + \left(\frac{1}{\omega C}\right)^2} \qquad 2\text{-}20$$

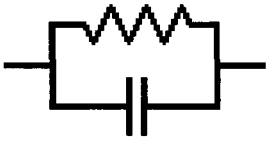

Figure 2-12 A resistor and capacitor in parallel.

2.5. Study of Barrier Coatings using EIS

A good coating acts as a perfect barrier between the environment and the substrate being protected. It is like a perfect insulator that prevents any chemical species (i.e. current) from passing through it from the environment to the vulnerable substrate [Khanna (ed.) 2008]. A perfect barrier coating behaves like a perfect capacitor with no resistance element. Charge builds up upon its surface but cannot pass through it. On the other hand, a bad barrier coating, containing cracks, holes or pores, becomes conductive when exposed to an aggressive medium, and allows chemically undesirable liquid or gas to access the vulnerable underlying surface. EIS can be used to establish quantitatively the integrity and performance of a barrier coating, by measuring its impedance at different frequencies and by analyzing the data using equivalent circuit modelling.

A typical EIS cell for testing a coating is illustrated in Figure 2-1. This shows the coating on a substrate (e.g., a metal plate) exposed to an aggressive solution. In this setup, the coating can be regarded as being an insulating dielectric sandwiched between

the conducting solution and the conducting substrate, analogous a parallel plate capacitor. The counter and reference electrodes are placed near the surface of the coating, which is the working electrode. These three electrodes are then connected to an EIS system, which automatically scans the system's response over the desired range of frequencies, and creates an EIS spectrum. The Bode and Nyquist plots can be plotted, and the changes in impedance parameters (i.e. Z_{real}, Z_{img}, Z_{mod} and ϕ) can be monitored over time. In addition to these approaches, the data can be fitted to equivalent circuit models, which can be used to interpret and quantify the physical properties and efficacy of the coating, and can be used to model its deterioration with time.

The equivalent circuit models that are used in this research are discussed later in this thesis. Only an introductory discussion of the main concepts of the modelling process is provided here.

One of the simplest equivalent circuits to model a purely capacitive coating is illustrated in Figure 2-13. This model consists of a resistor in series with a capacitor; the resistor represents the solution resistance of the electrochemical cell, while the capacitor represents the coating as a whole. Because the solution resistance is small and the impedance caused by the capacitor is large at low frequencies, the phase angle of the system will be at -90°, and the magnitude of the impedance will be a straight line with a negative slope when plotted in a Bode plot, Figure 2-14. If the solution resistance were larger than the impedance caused by the capacitor there would be a horizontal line at the high frequency end of the Bode plot at the value of the resistor. This model describes the behaviour of a good barrier coating. Note that when the capacitance is very small, the

impedance is very large, so that the resistance may not be observable, or may it be so small that it cannot be accurately determined.

Figure 2-13 Resistor and capacitor in series.

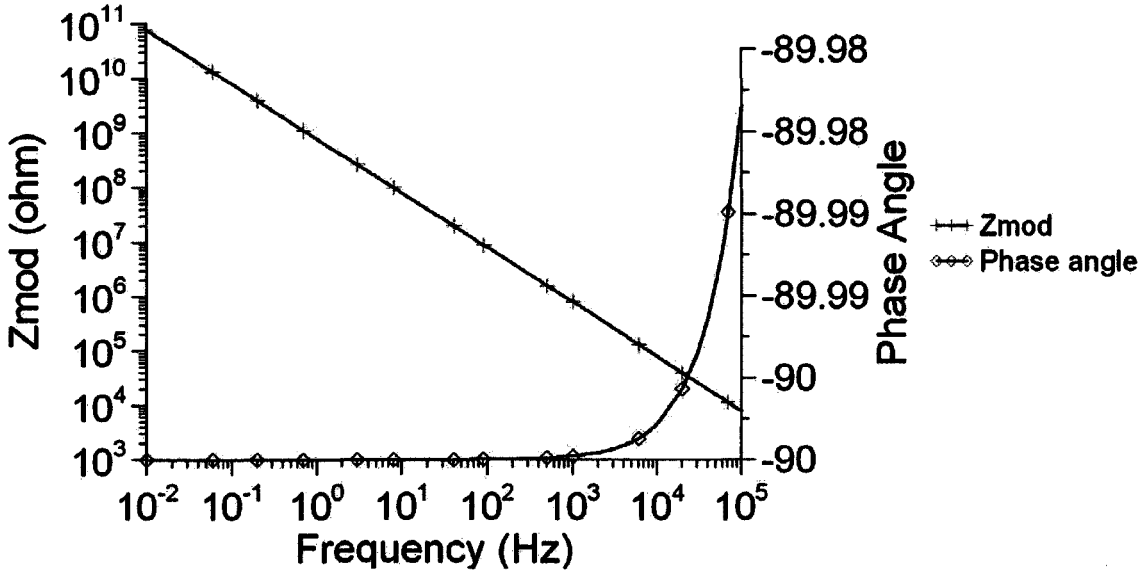

Figure 2-14 Bode plot of a 200 pF capacitor in series with a 3 ohm resistor.

As coatings degrade, they may show an increasingly complex behaviour [Loveday et al. 2004, Dehri 2000, Ozcan et al. 2002, Masadeh 2005]. A model for a failed coating, that allows ions and solution to come into contact with the metal substrate, is illustrated in Figure 2-15. In one of the interpretations of this model, Rs represents the solution resistance of the electrochemical cell, while C_c is the capacitance of the coating. R_{po} is the resistance of ionic conduction paths (pores) that traverse the coating. This is often referred to as pore resistance. An assumption is then made that the coating has partially delaminated from the metal substrate and that the delaminated area is filled with the solution. This model then requires a double layer capacitance, C_{dl}, and either a charge-

transfer reaction element, represented by the charge transfer resistance (R_{ct}), or an element for the resistive corrosion product layer on the metal plate, represented by the polarization resistance (R_p).

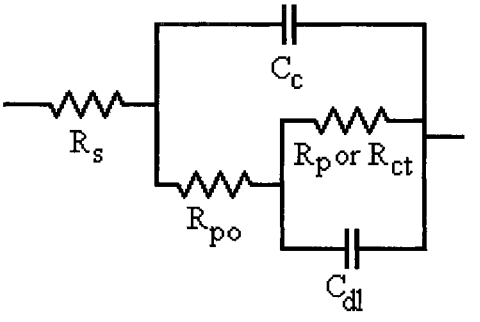

Figure 2-15 Deteriorated coating on metal substrate. [O'Donoghue et al. 2003]

Although equivalent circuit modelling is widely used to interpret EIS data, the physical meaning of each component in a circuit model, even in the simple damaged coating model described above, is subject to debate. Equivalent circuit modelling can be quite subjective. It is very important that the modeller establishes a good physical representation of the real world, with useful parameters that can give a good indication of a coating's performance. The simple models described above do not work in every case; Chapter 3 contains a literature review where many different circuit models are presented. If the physics or chemistry of the system is different, or multiple layers are involved, it is often necessary to tailor an old model or create a new model to interpret the data. One must always remember that a model which gives an excellent fit to the data is not a good model unless it is a good representation of the real physical system. Nearly always, there is more than one circuit configuration that can simulate an EIS spectrum. The modeller must determine which model best provides the explanation closest to reality.

2.6. Summary

A coating's efficacy is a measure of the coating's ability to protect the substrate. In aqueous systems, a good coating protects the substrate by stopping the flow of ions and chemical species. EIS is a technique that measures the electrical impedance of an electrochemical system, and it can measure how well the coating protects the substrate.

This chapter included:

- an introduction to EIS;
- some background on the concept of impedance in AC systems;
- a review of the standard methods of presentation of EIS data; and
- a discussion and presentation of how data can be quantitatively interpreted by employing simulated equivalent circuit models of the physical system.

3. Literature Review

3.1. Introduction

This chapter presents a literature review on the conventional testing procedures of coatings, the deterioration mechanisms of coatings in wastewater treatment plants, and the use of EIS in the evaluation of coatings.

3.2. Conventional Testing Methods of Coatings

The Society for Protective Coatings (SSPC) classifies the tests that can be performed on coatings in four general categories [SSPC, 2005]: (1) visual inspection, (2) coating thickness tests, (3) holiday detection tests, (4) adhesion tests. Most of these tests, provide qualitative or semi-quantitative measures for evaluating coatings; therefore, there is a high degree of variability and uncertainty associated with them.

The visual inspection, in which one looks for visible defects in the coating, is the most practical evaluation technique used to evaluate coatings. SSPC has an inspection manual with procedures, techniques, and standards for use in inspecting coatings [Appleman 1998]. Common types of defect indicators are cracks, abrasion, delamination, blisters, chalking (i.e., powdering), fading (of the colour of the coating), pinhole formation and swelling. Despite its practical nature, this approach can be quite subjective, and its reliability highly depends on the qualifications and the expertise of the person carrying out the inspection.

One of the most commonly used coating thickness determination tests is the Tooke Gauge test as per ASTM D 4138 [2007]. The Tooke Gauge test is a destructive test that

is used for measuring the thickness of a coating, mostly applied on non-metallic substrates like concrete, and it involves the cutting of an angular groove into the coating down to the substrate and taking measurements across the cut under a magnifying lens. The coating thickness is then calculated using basic trigonometry.

If direct access to the edge of a coating sample is available, and the substrate thickness is known, then the coating thickness can be measured directly by using a micrometer.

Another method of determining the coating thickness uses an ultrasonic thickness gage and is described in ASTM D 6132 [2008]; this method is non-destructive. In this method, an ultrasonic pulse is sent through the coating sample, and using the speed of sound in the coating and the echo, the thickness of the coating can be measured.

To test for the presence of holidays, discontinuities or pin-holes on coatings that are applied to metallic surfaces holiday detectors are widely used. The standard used to test for holidays is ASTM D 5162 [2008]. For the holiday detector to function, an electrical connection to the substrate is required. A large electric potential is applied to the coating surface (1.5-25 KV), by means of a moving metal electrode. As the electrode is moved around the coating surface, any holiday in the coating will result in a short circuit between the substrate and the electrode; this triggers an alarm indicating the location of the pin-hole. [Khanna 2008].

There are a number of adhesion tests that can be performed on coatings. One method, called the tape method as per ASTM D 3359A [2008], involves cutting the coating in the shape of an "X", applying a piece of tape across the cut, and pulling the

tape off at a 180° angle. The adhesion of the coating to the substrate is then determined by comparing the damage caused by the tape removal to standard figures.

Another approach in the same standard, ASTM D 3359B [2008], involves cutting 6 lines separated by various distances depending on the thickness of the coating, and then cutting another set of 6 lines that form a cross-hatched pattern. After cutting the pattern, tape is applied, and then removed. Again, the adhesion of the coating to the substrate is determined by comparing the damage to standard figures shown in Figure 3-1.

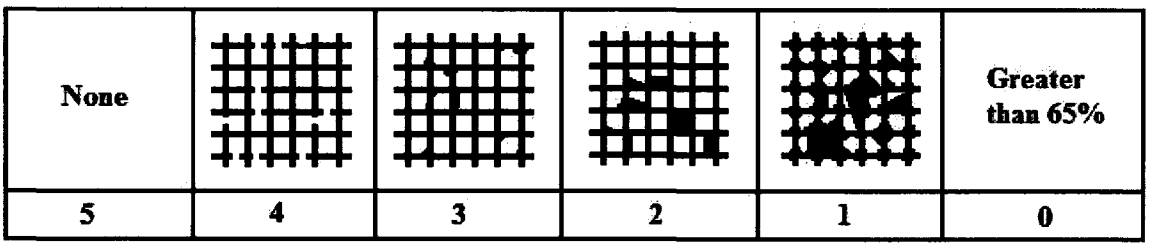

Figure 3-1 Template used for evaluating results of ASTM D 3359B [2008].

A similar test is defined in ASTM D 6677 [2007]. In this approach, an "X" (Figure 3-2) is cut into the coating; a rating is then given to the coating based on how easy the coating is chipped off using the tip of the knife.

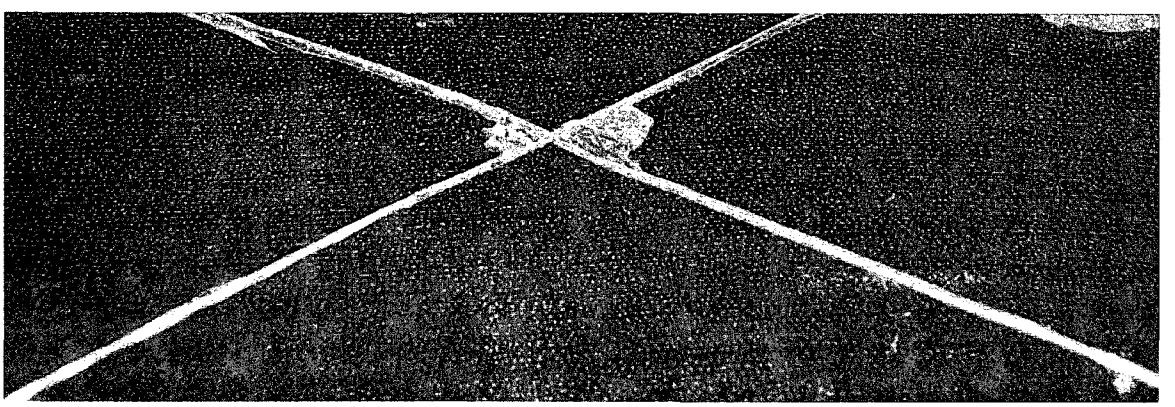

Figure 3-2 Image showing ASTM D 6677 [2007].

ASTM D 4541 [2002] describes the pull-off test. In this test a metal dolly is glued to the surface of the coating, and once the glue has dried, the metal dolly is pulled off

perpendicular to the substrate. The force required to pull-off the metal dolly is then recorded. There are three potential modes of failure for the pull-off test: glue failure, cohesive failure (split of a layer of the coating system), and adhesive failure (failure at the junction of substrate and coating or between layers of the coating).

There are many other similar methods to evaluate the performance of coatings. The brief review provided here of the common testing methods is intended to provide a general idea about the qualitative nature of these approaches.

3.3. Deterioration of Coatings in Wastewater Treatment Plants

Estoup et al. [1997] investigated coatings in a number of operating waste water treatment digesters after 4 years of service. The each of the digesters had a volume of 5000 m^3 and operated at 35°C to process anaerobically domestic waste from an urban setting. The main form of damage observed was cracking in the coatings along the seam between the cover of the digester and the digester wall. Behind the damaged coating section, evidence was found of concrete deterioration, which was attributed to the reaction of the biologically produced sulphuric acid with the hydration products of concrete.

Although anaerobic digesters work in the absence of oxygen; oxygen can leak into the digester from the expansion joints, movable parts, or faults in the cover, so that localized oxygen-rich areas may exist under the cover and above the sludge line. The reaction of oxygen with hydrogen sulphide which is produced by Eq 1-1 and 1-2, in the digester produces sulphuric acid, which reacts with calcium compounds in the concrete, such as $Ca(OH)_2$, to produce gypsum [Drever 1988, Thomson 2000]. The formation of

gypsum in the concrete can lead to the deterioration of the mechanical properties of concrete, cracking, and eventual failure of the structure [Crites and Tchobanoglous 1998].

Oriol et al. [2007] describe a project in which the primary treatment facilities of a wastewater treatment plant were evaluated and rehabilitated in 2004. The plant, which was constructed 1974 and underwent renovations/expansions in 1982, 1987, 1989, had a capacity to treat 17.9 million gallons of average dry weather flow (the average amount of water flowing through the digester during dry weather) per day. It was reported that different types of coatings, including PVC, coal tar and epoxy, had been used in the structure. Oriol et al. state that coatings were in place at the time of the study, however they had all deteriorated, and in some parts, bare concrete and reinforcing steel were exposed. Most deterioration was in the form of cracking and blistering of the coatings, especially around the expansion joints. The authors were also able to determine that the exposed concrete had lost between ¼″ to 1″ of thickness due to exposure to sulphuric acid; the loss of concrete cover also lead to the exposure of the reinforcing steel to the aggressive environment and its eventual corrosion.

A number of researchers have carried out laboratory experiments to simulate the in-service conditions of wastewater pipes. Most of these studies were long-term exposure tests and used the previously discussed conventional methods to evaluate the performance of the coatings. Due to their long duration these laboratory studies do not provide rapid ways of evaluating coatings.

Liu et al. [2001] performed tests on the performance of a polyester coating bonded to concrete cylinders that were exposed to sulphuric acid conditions. The authors also tested the coating for potential use in a rehabilitated structure. Two sets of tests were

performed: the "dry test", in which the coating was applied to the specimen in as-received condition, and the "wet test", in which the coating was applied after the concrete was wetted in a hydraulic pressure chamber. The wetted concrete was used to simulate the rehabilitation project, in which parts of the concrete infrastructure would already be wet.

The concrete samples were exposed to deionised water, or 3% sulphuric acid, inside a closed bottle. The bottle was filled with the solution so that bottom half of the concrete sample was exposed to the solution, while the top half was exposed to the vapour phase of the test solution. The concrete samples also had two artificial pinholes drilled into the samples, with a diameters of 3, 6 or 13 mm (Figure 3-3).

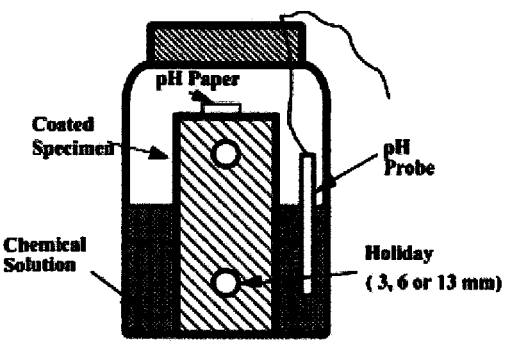

Figure 3-3 Schematic of test setup. [Lui et al. 2001]

The uncoated concrete samples failed after 7 days of exposure to 3% sulphuric acid. The dry-coated samples started to fail after 200 days; 50% of the samples failed after 300 days. While the wet-coated samples started to fail after 500 days, with 50% of the samples failing after 700 days. For the coated samples, failure was defined as a crack in the coating that exceeded 25 mm in length, when exposed to 3% sulphuric acid. The samples with pinholes, generally, experienced a greater mass loss then the samples without pinholes, although the size of the pinholes did not appear to be a factor.

Most common types of damage observed on the coating were blisters and cracking at the sites surrounding the holiday (see Figure 3-4a and b). In addition, it was observed that concrete experienced deterioration at the edge of the concrete cylinder (Figure 3-4c); the proposed cause of this type of damage was the reaction of sulphuric acid with the hydration products of concrete [Neville 1981].

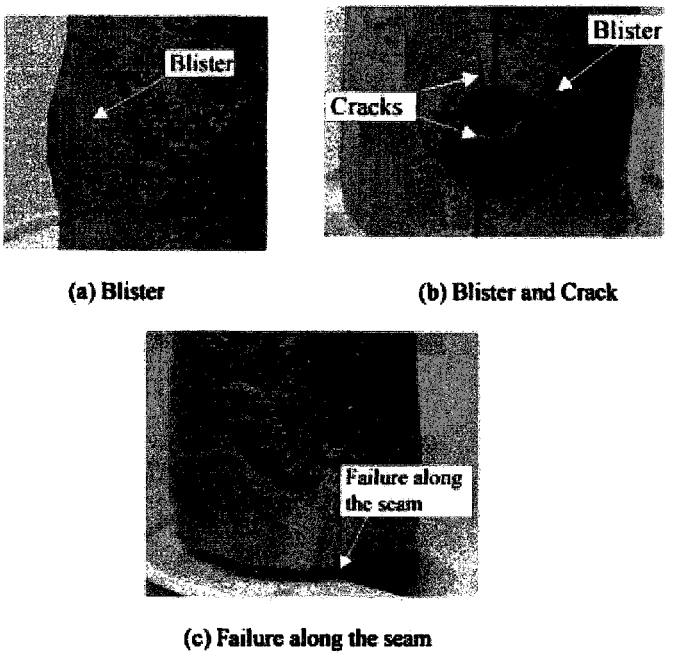

(a) Blister (b) Blister and Crack

(c) Failure along the seam

Figure 3-4 Coating failure observed in concrete cylinders. [Lui et al. 2001]

In addition to the acid exposure test, several of the coated specimens were subjected to bond strength tests using a modified version of ASTM D 4541 [2002]. Again, the concrete specimens were coated in the dry and wetted state. For both sets of samples the bond strengths were below 1.4 MPa, while the failure typically occurred at the coating/concrete interface. The wetted samples did exhibit higher bond strengths after 1160 days.

The authors concluded that in the acid exposure test, the samples with pinholes performed the worst. That the coating bonded better to the wetted concrete samples than

the dry coated samples. It was suggested that the coating being tested would therefore be better suited for coating in-service structures.

Lui et al. [2004] performed a similar experiment on two epoxy coatings applied to clay bricks, called Epoxy 1 and Epoxy 2. The clay bricks were coated in either a wetted condition, to simulate a rehabilitation setting, or with no pre-treatment. The samples were then placed in a bottle, see Figure 3-3, and exposed to a de-ionised water solution or 3% sulphuric acid solution. Two artificial pinholes were drilled into the samples after coating, the diameter of the pin holes was either 3, 6, or 13 mm. Bond strength testing was also performed using a modification of ASTM D 4541 [2002].

Over time, solution enters the uncoated bricks, and this leads to an increase in the mass of the samples. The uncoated clay bricks reached 90% of their ultimate solution saturation mass after 50 days. The specimens with pinholes experienced a greater mass gain from solution ingress through the pin holes then the samples without. The effect of the pinhole size was inconclusive. The mass gains of the coated clay bricks with the two epoxy coatings were similar when exposed to de-ionised water. The dry-coated clay bricks of both epoxies had a greater mass gain then the wet-coated samples.

The surface conditions played a significant role in the water uptake of Epoxy 2 when exposed to 3% sulphuric acid, with the wet coated sample having a mass increase of 6.8% compared to 0.36% for the dry coated sample. The mass gain for Epoxy 1 was similar for the wet-coated and dry-coated samples exposed to 3% sulphuric acid, approximately 5% after 2000 days.

The results of the bond strength for Epoxy 1 showed sensitivity to the surface moisture conditions, while Epoxy 2 did not. The failure of the brick coated with Epoxy 2

occurred in the brick, while the brick coated with Epoxy 1 failed in the clay brick, in the coating, and at the bond at various stages of the experiment. The authors concluded that the results of the bond strength test, was not sufficient to determine coating performance, but the coatings had a significant impact on reducing the mass gain of clay bricks exposed to 3% sulphuric acid or de-ionised water.

Vipulanandan et al. (2005) performed full-scale bond tests on two polyurethane coatings over five years. In these tests, 900 mm diameter "wet" and "dry" concrete pipes were coated with the polyurethane coatings; the "dry" pipes were coated as received, while the "wet" pipes were inside a chamber filled with water for 2 weeks at a pressure of 105 kPa, in order for water to enter the concrete pipes. After coating, the pipes were placed back in the pressure vessel at 105 kPa. After 5 years, the authors found that polyurethane 1 in its dry application was rated as having a good bond strength while its wet application was rated as having a poor bond strength. For polyurethane 2, hard blisters and delaminations were found in the dry coated sample after 5 years; the wet coated sample performed better.

Vipulanandan et al. (2005) also exposed coated concrete cylinders (in dry and wet conditions) to either de-ionised water or to a 3% sulphuric acid solution. After 5 years, no failures were observed in the dry or wet coated specimens of either coating type in de-ionised water. All samples of dry coated polyurethane 1 failed after 5 years of acid exposure, while half of the wet coated samples failed. None of polyurethane 2 coating samples failed after 5 years, although they experienced higher mass gains and lower bond strengths than polyurethane 1. They found that there was no direct correlation between the chemical resistance of the coatings and the bond strength.

The industrial approach for monitoring the performance of coatings in wastewater digesters incorporates in-situ testing. For this purpose, sample concrete coupons are prepared, and then the coating to be tested is applied (see Figure 1-2). These coupons are placed in a digester under service conditions for approximately two years or longer. The inspection of the coupons after this exposure time (see See Figure 1-3) provides belated information about the performance of the applied coating. Although in-service testing is important, it is considered that two years is too long to have to wait to find out if a coating is working.

There are both practical and economic motivations to reduce the time to evaluate the performance of coatings used in wastewater treatment facilities. Electrochemical impedance spectroscopy is known to be a technique sensitive to changes in electrical properties of coatings, films and oxides; therefore this research focused on the investigation of the potential use of EIS to quantify the performance of barrier coatings proposed for use in wastewater digesters under varying environmental conditions, and also to optimize the chemical conditions and the experimental method so as to obtain an accelerated test procedure.

3.4. The Use of EIS in the Investigation of the Performance of Coatings

EIS has been used for many years. One of the main applications of EIS is for the evaluations of coatings [Mansfeld 1990, Mansfeld 1995, Ozcan et al. 2002, Bierwagen et al. 2005, Fedrizzi et al. 2006, Hinderliter al. 2006]. The barrier coatings used in wastewater digesters are typically quite thick (of the order of a couple of millimetres) and have high electrical impedance, so that small changes in their properties are not easy to

capture. Thus EIS is not generally used to study thick barrier coatings, and hence most of the literature presented here will focus on thin-film coatings.

One of the first studies that used electrical means to determine the quality of a coating was by Bacon et al. [1948]. This study used the coating resistance to indicate the quality of coatings. In this work, the authors tested over 300 samples with variations in substrate conditions, electrolyte solution, and coating properties. All samples were tested until visible signs of deterioration were present, and the resistance of the coatings was measured over time. The authors observed that good protection of the substrate was provided by coatings with a resistance greater then 10^8 Ohms, while poor protection was provided by coatings with a resistance of less then 10^6 Ohms. The authors concluded that the resistance measurements could be used to predict the eventual failure of the coating.

In a series of three papers published in 2004 and 2005, Loveday et al. gave a detailed look at the EIS theory, how EIS can be used to evaluate coatings, and different testing regimes that can be used to evaluate coatings using EIS. The first paper [Loveday et al. 2004 - Part 1] provided a background on EIS, in a similar way provided in Chapter 2 of this thesis. The second paper [Loveday et al. 2004 - Part 2] gave a series of electrical circuit models to be used in the analysis of EIS data. The model given in Figure 3-5 is one of the general models, representing a typical coating on a metal. The physical meaning attributed to each element in the circuit is illustrated in the figure.

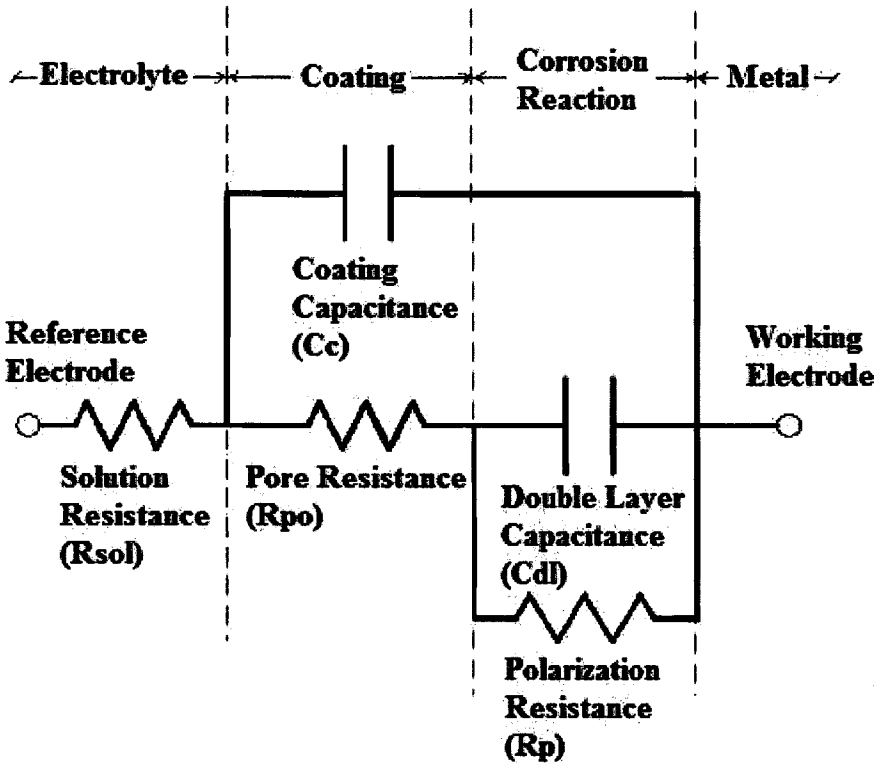

Figure 3-5 Circuit model of an organic coating and the physical significance of each of the elements. [D. Loveday et al. 2004]

Figure 3-6 to Figure 3-9 show the progression of circuit models and simulated Bode and Nyquist plots of a coating being subjected to a corrosive solution [D. Loveday et al. 2004]. In Figure 3-6, the circuit model, and the Bode and Nyquist plots, for an intact coating are presented. It can be seen in this figure that an intact coating behaves like a pure capacitance with straight Zmod line and horizontal phase angle at -90°. In Figure 3-7, the circuit model, and Bode and Nyquist plots, for a coating with solution penetrating the pores are illustrated. It is assumed that water uptake results in low frequency phase angles to rise while the Zmod starts to become horizontal at low frequencies. The Nyquist plot takes the shape of a semicircle. Loveday et al. also note

that, for the case of Figure 3-7, an estimate for the solution uptake can be calculated by the Brasher-Kingsbury equation [Brasher et al. 1954]:

$$V_f = \frac{\log\left(\frac{C_t}{C_o}\right)}{\log \varepsilon_w} \qquad 3\text{-}1$$

where V_f is the volume fraction of water in the coating, C_t is the capacitance of the coating at time t, C_o is the initial coating capacitance, ε_w is the dielectric constant of the solution (approximately 80).

Once the solution reaches the metal substrate, different reactions can occur (e.g. corrosion of the metal surface) and the EIS spectra changes. The model and corresponding plots in Figure 3-8 illustrate these changes. More terms are included in the model: the C_{dl} and R_{po} terms represent processes (e.g. corrosion) on the metal plate surface. These C_{dl} and R_{po} cause changes in the Bode, and Nyquist plots. The Zmod will continue to drop at low frequencies, as the coating degrades and more of the underlying surface is exposed.

Figure 3-9 shows the Bode and Nyquist plots of a completely failed coating, the substrate is actively corroding, and blisters and delamination of the coating may become visible, the low frequency value of the impedance has decreased 5-6 orders of magnitude. The C_{dl} term will increase slightly, with a slight decrease in the C_c. In addition the R_{po} may increase due to corrosion products blocking the pores.

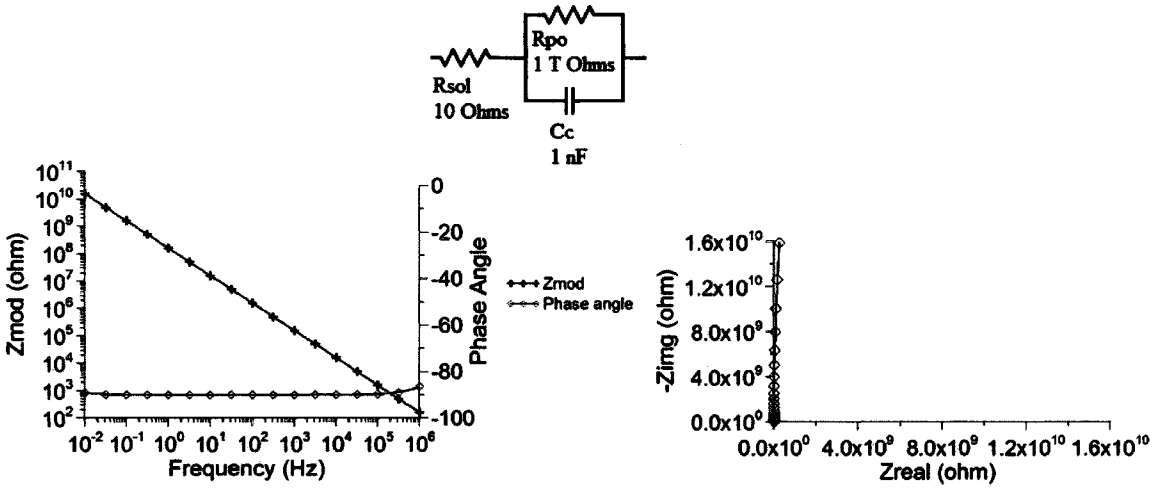

Figure 3-6 Circuit model and Bode and Nyquist plots for an intact coating.

[Modified from D. Loveday et al. 2004]

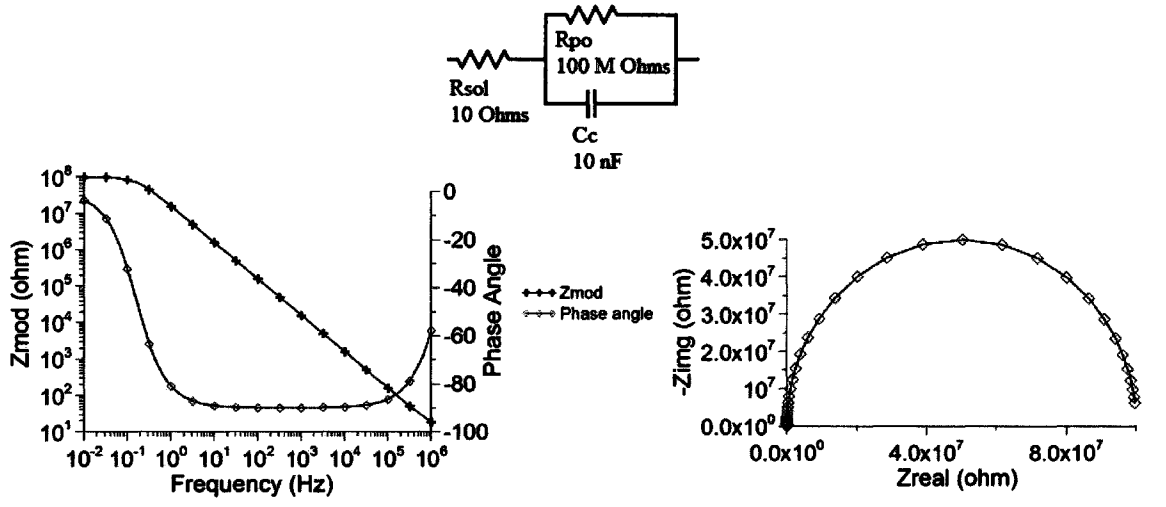

Figure 3-7 Circuit model and Bode and Nyquist plots for a coating with solution penetrating the pores. [Modified from D. Loveday et al. 2004]

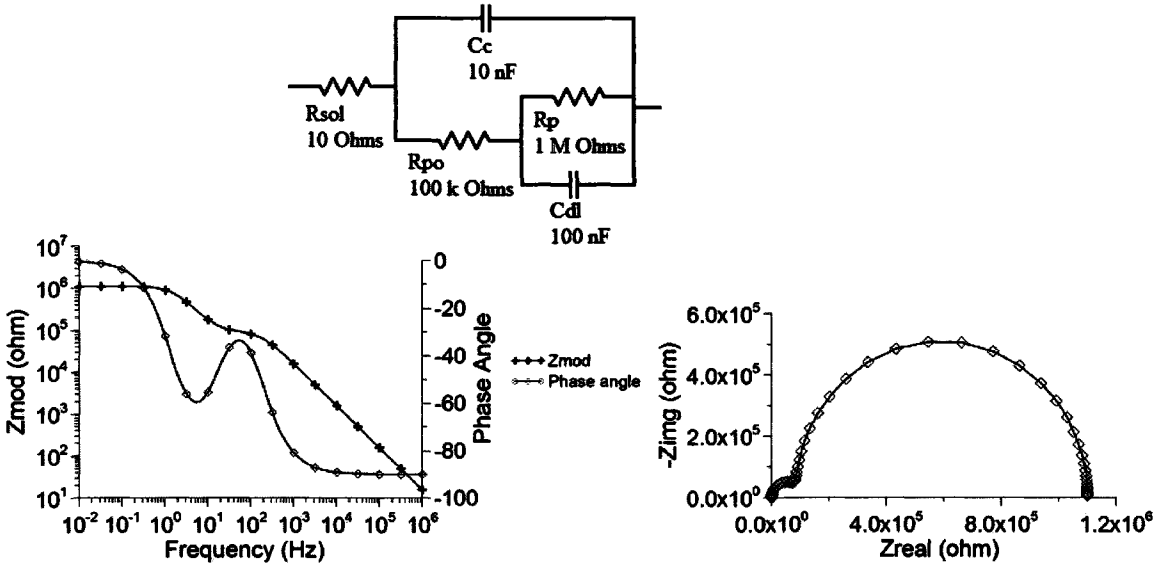

Figure 3-8 Circuit model and Bode and Nyquist plots for a coating with a freely corroding substrate. [Modified from D. Loveday et al. 2004]

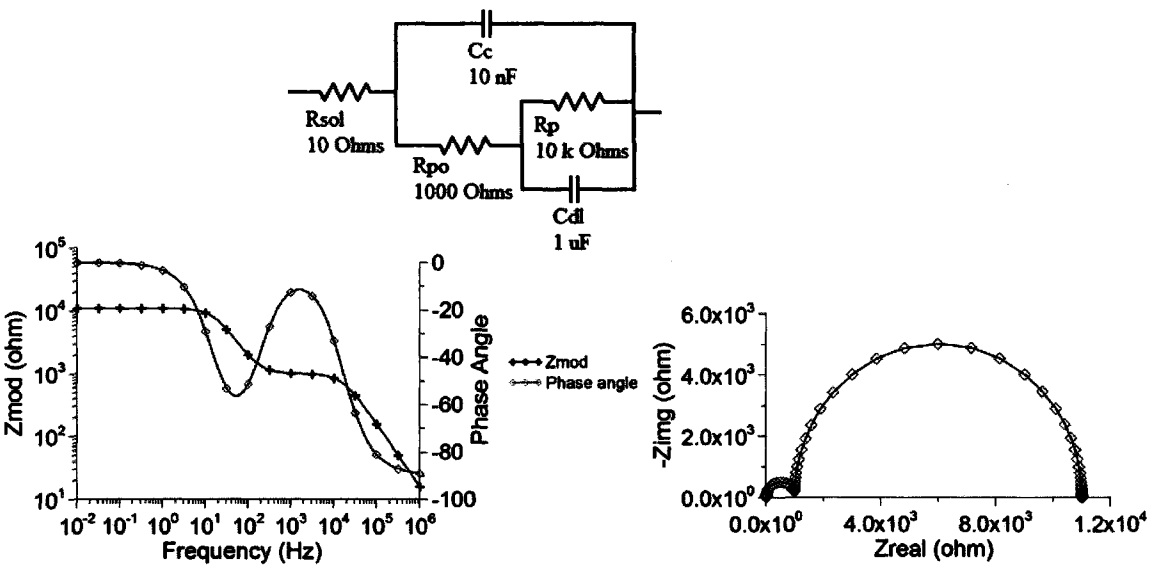

Figure 3-9 Circuit model and Bode and Nyquist plots for a severly damaged coating. [Modified from D. Loveday et al. 2004]

In their third paper Loveday et al. [2005] cite experimental results that show that if the magnitude of the impedance of a coating is greater then 10^9 ohm-cm^2 at a frequency

of 0.1 Hz, then the coating provides "good to excellent" corrosion protection, while if the magnitude of the impedance at the same frequency is below 10^7 ohm-cm^2 the corrosion protection is poor.

A representative selection of EIS studies of coatings will be presented here.

Mišković-Stanković et al. [1996] used EIS, gravimetric liquid absorption, and differential scanning calorimetry (DSC) in order to evaluate two different coatings exposed to various aqueous solutions. The coatings investigated were cathodicaly deposited epoxy resin modified with an amide and an isocyanate. The authors claimed that diffusion was the major mechanism of water uptake and ion penetration into the coating, and that these were the factors affecting the corrosion resistance of their coatings. The EIS data were modeled with the circuit shown in Figure 3-10, where R_{sol} is the resistance of the electrolyte, R_p is the pore resistance of the coating, C_c is the capacitance of the coating, and Q and p are the impedance related to charge transfer reactions at the metal solution interface, represented as a CPE. Figure 3-11 and Figure 3-12 show the results of the EIS analysis displayed over time. The author's state that the plots can be broken into three stages: the first stage where solution enters the coating, is marked by the increase in the C_c and a decrease in the R_p, this occurs almost immediately; the middle stage is the plateau section of the plots, indicating the coating has become saturated and is therefore stable. The last stage is marked by the sudden increase in the C_c and decrease in the R_p. This is caused by corrosion of the substrate and disbondedment of the substrate. Figure 3-13 shows the water uptake data gathered at 25°C; because the absorption increased with a $t^{0.5}$ dependence, which is consistent with a diffusion process [Mišković-Stanković et al. 1996] and a CPE with p = 0.5 behaviour, a

Fickean water absorption coefficient was calculated. The initial change in the results of the EIS analysis corresponded to the amount of time required for the micro pores in the coating to become fully saturated with pure water. This conclusion was confirmed by testing with several different solutions and at different temperatures.

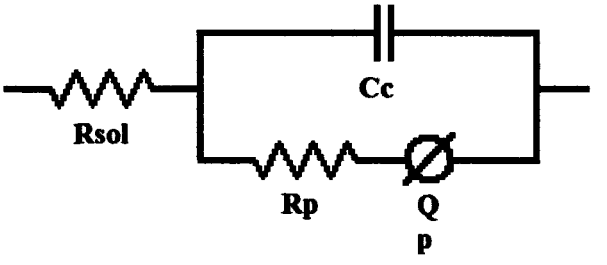

Figure 3-10 Electric circuit model from Mišković-Stanković et al. [1996].

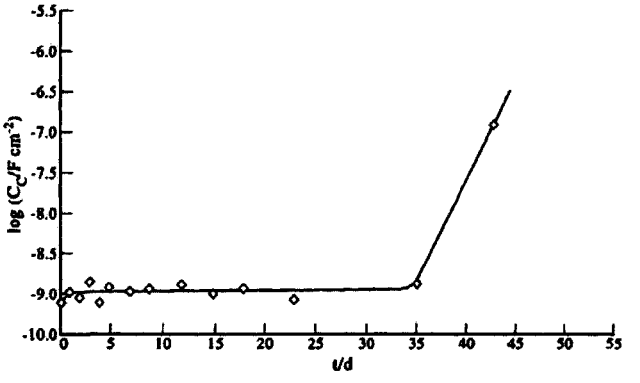

Figure 3-11 The time dependence of coating capacitance for epoxy coating during exposure to 3% NaCl. [Mišković-Stanković et al. 1996]

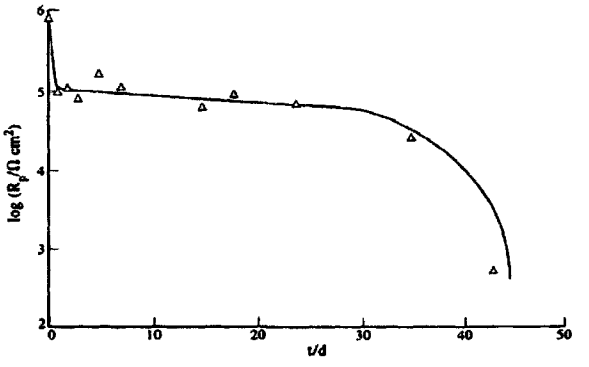

Figure 3-12 The time dependence of pore resistance for epoxy coating during exposure to 3% NaCl. [Mišković-Stanković et al. 1996]

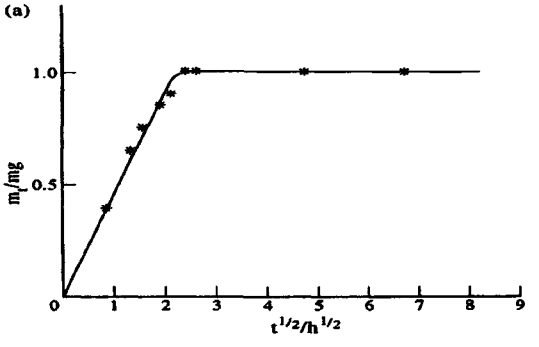

Figure 3-13 A plot of the amount of absorbed water at time t, m_t, against the square root of time. [Mišković-Stanković et al. 1996]

Dehri [2000] used equivalent circuit modeling for the analysis of the performance of polyester coatings that were exposed to concentrated acid rain water. The author stated that a model similar to the one presented in Figure 3-10 would accurately model an intact coating, while Figure 3-14 was proposed for modelling a defective organic coating. In this figure, R_{sol} is the solution resistance, C_c is the coating capacitance, R_{po} is the coating resistance. The terms R_p, R_{ct}, R_{dl}, p and Q represent the circuit elements associated with the activities on the metal surface under the coating. The author concluded that the model in Figure 3-14 could be used to track changes in the performance of the coatings over a 50 day period.

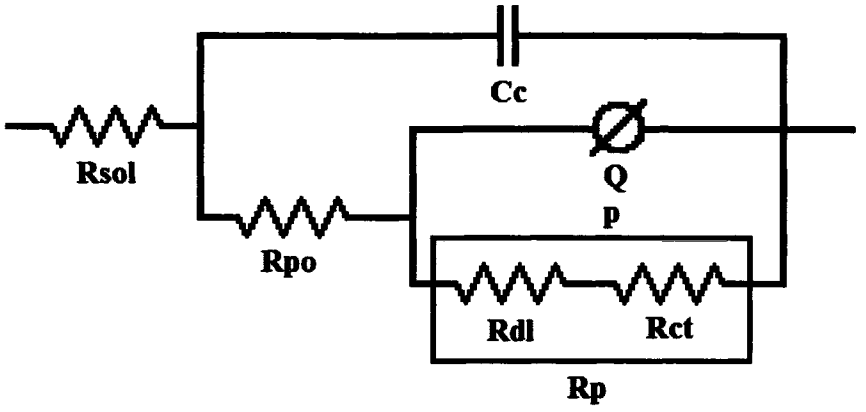

Figure 3-14 Electric circuit model proposed by Dheri [2000] for modeling a defective organic coating.

Kouloumbi et al [2001] investigated an epoxy coating filled with 0, 15, and 30 % iron powder exposed to a corrosive environment. However, instead of a model circuit analysis, the authors analyzed the EIS data using the "breakpoint frequency method". In this method, several features of the coating system can be identified and there is no need for an equivalent circuit model. The breakpoint frequency is identified when the phase angle of the system reaches -45°. At this frequency, the system changes from an insulator to a conductor. If a system has two time constants, such as the one shown in Figure 3-15, then the system should also have two breakpoints ($f_{b,low}$ and $f_{b,high}$), with respect to the lowest phase angle measured, ϕ_{min}. The term $f_{b,high}$ corresponds to changes in the coating characteristics, while $f_{b,low}$ is related to the electrolyte, coating and metal interface. Based on the parameters defined, above an estimation of the ratio of delaminated area to coated metal can be calculated. The behaviour and performance of the coating can be monitored by plotting the f_b values over time. An increase in f_b over time typically means a decrease in the specific resistance of the coating, or an increase in the delaminated area ratio.

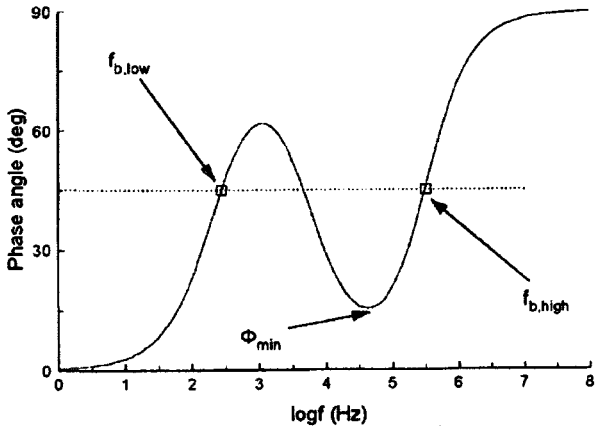

Figure 3-15 Schematic of the various required frequencies for the breakpoint analysis from Kouloumbi et al. [2001].

Yang et al. [2003] used a variety of techniques to evaluate the performance of a polyurethane coating. In their study, coating samples were alternately exposed to UV radiation and water condensation, followed by an exposure in a chamber with cyclic salt fog. Most of the analysis performed in this study was qualitative and was based on Scanning Electron Microscopy (SEM), Energy Dispersive X-Ray analysis (EDX), and Atomic Force Microscopy (AFM). However, the authors also performed an EIS scan in conjunction with these tests. Although the analysis of the EIS data was not detailed, the authors stated that the magnitude of the impedance at a frequency of 0.012 Hz was representative of the coatings' protective property. Table 3-1 shows the criteria used by the authors in evaluating their coatings using EIS. The EIS data collected correlated with the results of the other tests. For one of the coating systems, after 70 weeks of exposure, the pigment and bead-enriched surface had been observed to have been eroded away, the coating was deteriorating, and this corresponded to the point at which the magnitude of the impedance at 0.012 Hz fell below 10^8 Ohms-cm^2.

Table 3-1 Relationship between the magnitude of the impedance and performance of the coating at a frequency of 0.012 Hz. [Yang et al. (2003)]

Z_{mod} @ 0.012 Hz	$10^8 \rightarrow 10^{13}$ Ω cm^2	Excellent protection
Z_{mod} @ 0.012 Hz	$10^6 \rightarrow 10^8$ Ω cm^2	Fair protection
Z_{mod} @ 0.012 Hz	less then 10^4 Ω cm^2	Failed coating

O'Donoghue et al. [2003] showed that EIS can be used to evaluate the performance of two types of epoxy coatings for rapid immersion in water. The coating samples were allowed to cure for varying amounts of time and were exposed to water at two different temperatures. The equivalent circuit model used to model the system is given in Figure 3-16, where R_{sol} is the solution resistance, C_c is the capacitance of the coating (the higher the value the more water present in the coating), R_{po} is the resistance of current traveling through the pore network of the coating (the lower the value, the worse the coatings performance), R_p is the polarization resistance of the substrate (a high value indicates a low steel corrosion rate on the metal plate under the coating), and C_{dl} is the double layer capacitance effect (a value for this capacitor indicates that water has reached the substrate and, the greater the value of C_{dl}, the greater the area of the substrate that is in contact with water). An EIS scan was performed on the coatings at three different periods of exposure, after 192, 528, and 1000 hours. The authors concluded that the EIS technique was able to capture the deterioration of the two different types of coating, and was also able to distinguish between fully and partially cured coatings.

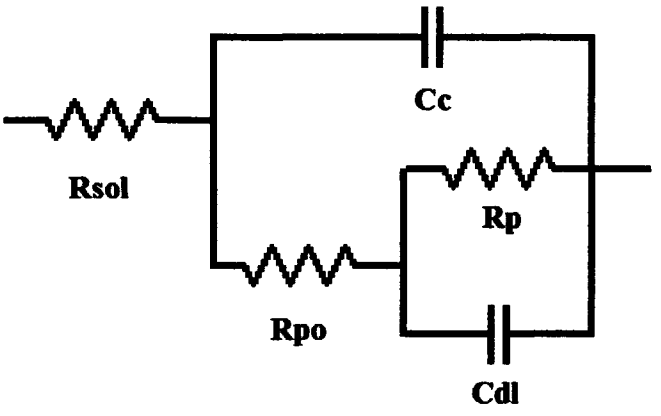

Figure 3-16 Electric circuit model from O'Donoghue et al. [2003].

The model in Figure 3-10 was also used by Souto et al. [2005] in the evaluation of coil coated sheet steel. The process of coil coating steel involves applying a liquid coating to the steel prior to the steel being formed. The samples were exposed to a 3% NaCl solution and polarized to two different potentials. The authors stated that the high frequency component of an EIS spectrum was usually related to the behaviour of the coating itself, while the low frequency was related to the behaviour of the metal substrate and the electrolyte at the bottom of the coating pores. The authors also used the breakpoint frequency, the frequency at which point the phase angle is equal to 45°, to analyse the EIS data. The EIS data were used to follow the delamination of the coating samples.

Masadeh [2005] used a modified version of the model shown in Figure 3-10 to model the behaviour of an epoxy coating exposed to water taken from the Dead Sea at room temperature and at 50°C. The model used by the author is shown in Figure 3-17, where R_s is the solution resistance, C_c is the coating capacitance, R_p is the coating resistance, and W is a diffusion (i.e. Warburg) element, with an impedance given in Eq. 3-2. A Warburg element is a CPE with a CPE with p = 0.5.

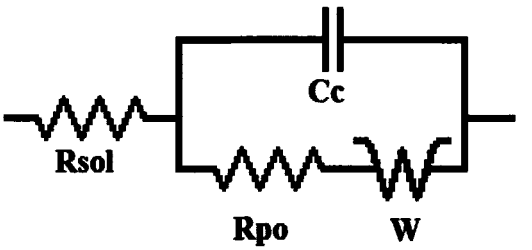

Figure 3-17 Model electric circuit used by Masadeh [2005].

$$Z_W = \frac{1}{W\left(\sqrt{j2\pi f}\right)} \qquad 3\text{-}2$$

The EIS data were used to capture the degradation of the epoxy coating at both temperatures. At 50°C coating degradation was observed after 10 days, while it took 46 days to observe degradation at room temperature. These results were confirmed using SEM images.

3.5. Summary

This chapter has shown that there is an opportunity to improve the current approaches for testing and evaluating barrier coatings for the use in wastewater digesters. Most of the current methods require long exposure times, exceeding in most cases two to three years, and rely mostly on qualitative or semi-quantitative approaches. Although EIS is known to be an effective and accurate technique to investigate coatings, its application to thick barrier coatings with high impedance is not common. Because of the current state of coating evaluation techniques, there is a major gap in required knowledge to bring new coatings into service or to change the intended application of in-service coatings in a timely fashion. The need for an accelerated and accurate method for evaluating the performance of barrier coatings is addressed in this thesis.

4. Preliminary EIS Testing Using Metal Plates and Dry Cells

4.1. Introduction

This chapter presents the preliminary investigations that demonstrated the feasibility and efficacy of EIS in probing the protective properties of barrier coatings. Following the optimizing of EIS scan settings and experimental setups, EIS signatures of deliberately damaged coatings were investigated. These preliminary tests were performed at room temperature and in *dry* conditions (*in air*) on the REBC and the PUBC samples that were sandwiched between two metal plates. The only electrolyte in the system is in the coating. Using this method, coatings containing artificial defects, *viz.*, pinholes or pits, were studied to determine if EIS could detect and measure faults in coatings, and to see how the EIS scans of faulty coatings differed from those of intact coatings. Coatings, with and without artificial defects, were studied after they had been exposed to distilled water or NaCl solution, then their surface was dried with wipes, before running scans in a dry cell setup. This demonstrated how adsorption of solutions of different conductivity could affect the EIS spectra. A number of verification and calibration tests were also conducted to strengthen the observations. The final experiment in this series investigated the effects of prior exposure to acid on the dry cell EIS spectra.

4.2. Experimental Setup

The EIS scans for the preliminary tests were performed on coating samples sandwiched between two metal plates; this creates a parallel plate capacitor, the coating

sample being the dielectric between the electrodes. A schematic representation of a parallel plate capacitor was illustrated in Figure 2-8.

Most experiments were carried out using 10 cm x 10 cm mild steel plates. Additional tests used 10 cm x 10 cm stainless steel (type 304) plates to determine if the plate composition or rusty spots on the surface might affect measurements. Results conclusively verified that they did not. The dimensions of the coating samples are provided in Table 4-1.

Table 4-1 The Dimensions of the Coatings.

	REBC		PUBC	
Property	**Average***	**Std. Dev.***	**Average***	**Std. Dev.***
Width (cm)	7.7	0.1	7.7	0.1
Length (cm)	5.1	0.1	5.1	0.1
Thickness (mm)	1.1	0.1	1.9	0.2
Mass (g)	5.77	0.61	8.21	0.89

(*) The average values and standard deviations were calculated from the measurements on all coating specimens tested in the preliminary study. The thickness measurements were carried out at three locations and averaged for each sample.

In order to minimize the electrical and magnetic noise from external sources, all EIS scans were performed inside a Faraday cage. A Faraday cage is an electrically grounded metal box that prevents external electromagnetic fields from interfering with measurements performed inside the box.

The EIS scans in this chapter were carried out in dry conditions, and it was not possible to do in-situ testing of the coating samples. In following chapters, in-situ testing using a Tait Cell is described. For the dry cell tests, the coating samples were exposed to the solutions before testing, removed from the environment, patted dry, and then sandwiched between the two metal plates that comprised the electrodes.

The cables from the potentiostat were then connected to the electrodes via spot welded connections and alligator clips. The working-electrode cable was connected to

one of the metal plates, and the counter-electrode and reference-electrode cables to the other plate.

Depending on the test, the cell was disassembled and samples were returned to the solution environment for longer exposures, before repeating an EIS scan.

The free potential of the system was measured for 100 s prior to the start of each experiment, to make sure that the system had reached a stable state, and the EIS scan was then performed at an impressed DC potential of zero volts versus the reference electrode.

The settings used for each EIS scan were as follows:

- Starting frequency of the EIS scan: 10^5 Hz;
- Final frequency of the EIS scan: 10^{-2} Hz;
- Number of EIS measurements per decade of frequency: 10 (i.e. 70 EIS measurements in total for each scan);
- Amplitude of the AC voltage: 100 mV (RMS);

4.3. Testing of Experimental Setup

This section includes tests to assess and optimize the experimental setup, and to assess the reproducibility of the EIS scans.

4.3.1. EIS Scan without Cables

It was attempted to initiate an EIS scan with no cables connected to the potentiostat, but the potentiostat was unable to perform an EIS scan without a cable attached. This result confirmed that the potentiostat had no internal parallel contribution to EIS measurements.

4.3.2. EIS Scan of the Cables

The cables that link the potentiostat to the parallel plates were connected to the potentiostat, and the working electrode lead, reference electrode lead, and counter electrode lead were connected together. With this configuration, the potentiostat was able perform EIS scans, and actually measured the capacitance of the cables.

To investigate the effectiveness of using aluminum foil as additional Faraday shielding, these tests were conducted with and without aluminum foil wrapped around the cables. Some noise at the lowest frequencies was observed with the wrapped cable, but the tests showed that the aluminum foil made no significant change to the data. The EIS scans of the cable, with and without aluminum foil wrapping, fit almost perfectly to equivalent electrical circuits consisting of only a single capacitor. The capacitance values for the unwrapped and wrapped cables obtained from modelling were 2.3 pF and 1.8 pF, respectively, with a miniscule error of 0.2% (Figure 4-1). Although, there is noise evident in the low frequency scans of Figure 4-1, there is no noise in subsequent scans when a sample is present to be measured (Figure 4-4).

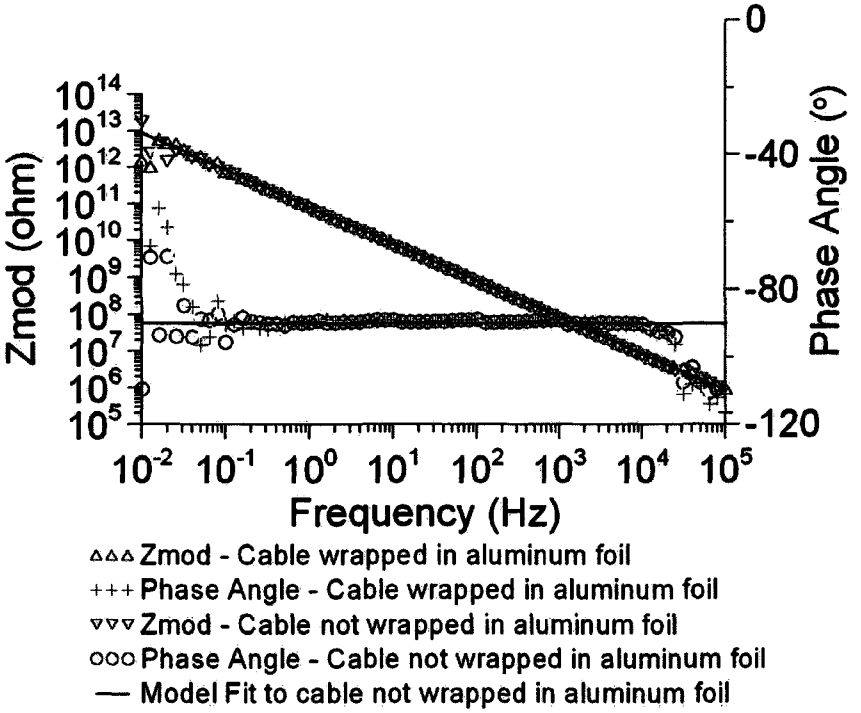

Figure 4-1 Bode plot of the cable with and without aluminum foil wrapping.

4.3.3. EIS Scan of the Parallel Plate Electrodes with Air between Them

For this test, the cables were connected to the electrode plates with a 1.5 mm air gap between the plates, maintained using small pieces of the PUBC as separators at the corners of the plates. Basically this setup allowed the EIS measurement of an air-filled capacitor. The Bode and Nyquist plots are shown in Figure 4-2 and Figure 4-3.

These plots are excellent fits to an electric circuit consisting of a capacitor (C = 85 ± 0.2 pF) in parallel with a very high-valued leakage resistor (R = 407 ± 11 GΩ). For this geometry, air has a capacitance of 10 pF, so most of the capacitance is associated with the PUBC separators.

Small discontinuities/peaks in the phase angle are artefacts of the Gamry software. These did not interfere with the measurements and analyses.

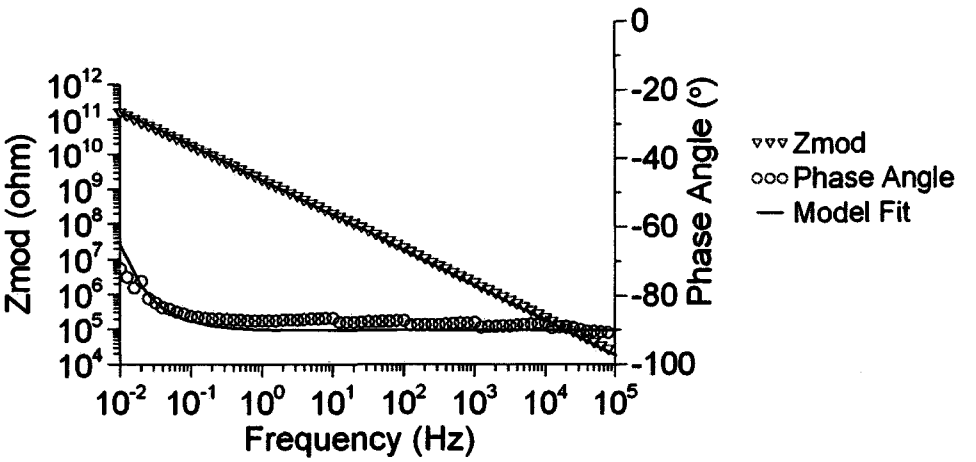

Figure 4-2 Bode plot of metal plates separated by air and PUBC separators. The small peaks in the phase angle every decade in frequency ≥ 10 Hz are artefacts of the Gamry potentiostat's software.

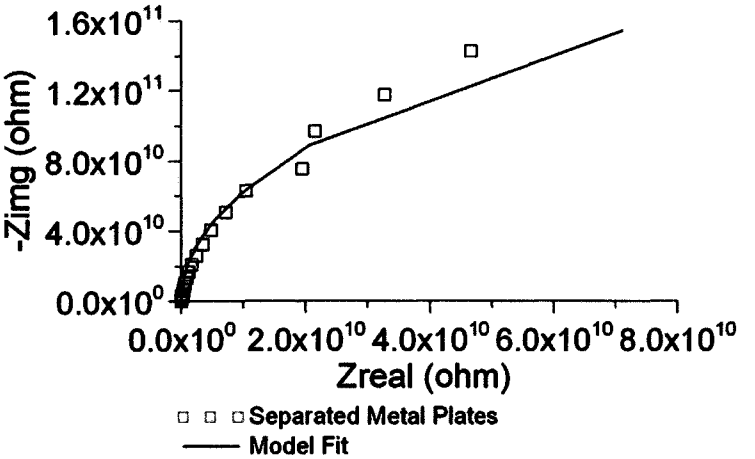

Figure 4-3 Nyquist plot of metal plates separated by air. The discontinuity at Zreal = $2x10^{10}$ ohm is an artefact of the Gamry software.

4.3.4. Reproducibility and Changing Electrode Metals

In order to check whether the nature of the electrode material was important, repeated EIS scans of the same PUBC sample were done with either mild steel or

stainless steel plates, some of the mild steel plates had rust spots. After each scan the entire experimental setup was disassembled and reassembled for the next EIS scan.

These scans showed excellent reproducibility. Results for both mild steel and stainless steel plates are shown in Figure 4-4 and Figure 4-5. Note that the Nyquist plots (Figure 4-5.) always accentuate the low level noise seen at low frequencies in the Bode plot (Figure 4-4).

Both plots clearly show that the plate type did not affect the results.

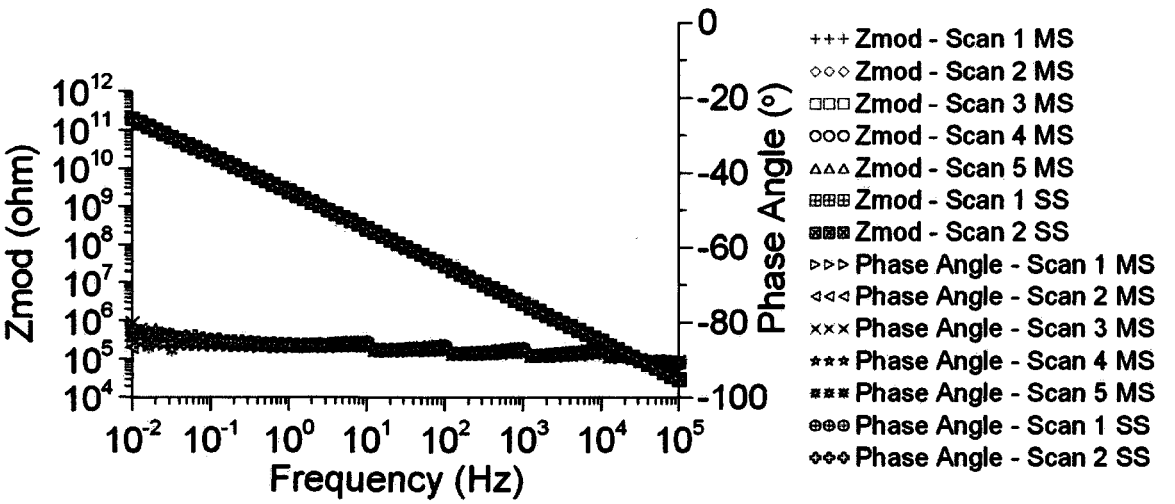

Figure 4-4 Bode plots of seven EIS scans done on a PUBC sample, 5 scans with Mild Steel (MS) metal plates, 2 scans with Stainless Steel (SS) metal plates.

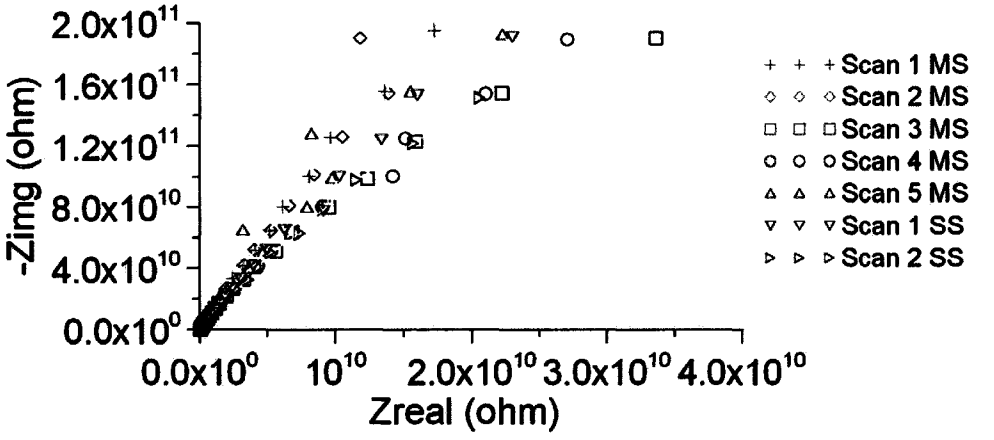

Figure 4-5 Nyquist plots of seven EIS scans done on a PUBC sample, 5 scans with Mild Steel (MS) metal plates, 2 scans with Stainless Steel (SS) metal plates.

The tests to assess the experimental setup were considered successful, and showed that the impedance associated with the potentiostat, cables and electrodes were measurable, but insignificant compared to those of the coatings.

4.3.5. Sample Variations

EIS scans of six samples from each coating, REBC and PUBC, were performed. The results of these scans served as baseline for the experiments in the following sections and chapters. There is clearly a significant sample dependent scatter in the data.

The data clearly illustrate that the PUBC and the REBC behave in remarkably different manners. The Bode and Nyquist plots are shown in Figure 4-6 and Figure 4-7, respectively, for the PUBC samples; and in Figure 4-8 and Figure 4-9, respectively, for the REBC samples. Comparison of the Bode plots for the two different coatings show that low frequency Zmod values of the PUBC samples are considerably higher (approximately by two orders of magnitude) than those of the REBC samples. The PUBC is a better electrical barrier than the REBC, and has only one out-of-phase

element, which is a slightly imperfect capacitor. On the other hand, the REBC is a significantly more complex dielectric with at least two distinctly different dielectric responses, indicated by the inflections in the phase angle plots (Figure 4-8). This indicates two different pathways through the REBC dielectric.

Although there were significant sample-to-sample variations in the data for both coatings, the reproducibility was very good, meaning that although the EIS scans of coatings might have different starting points, the changes and degradation of individual coatings can be tracked. This is illustrated in the following sections in this chapter.

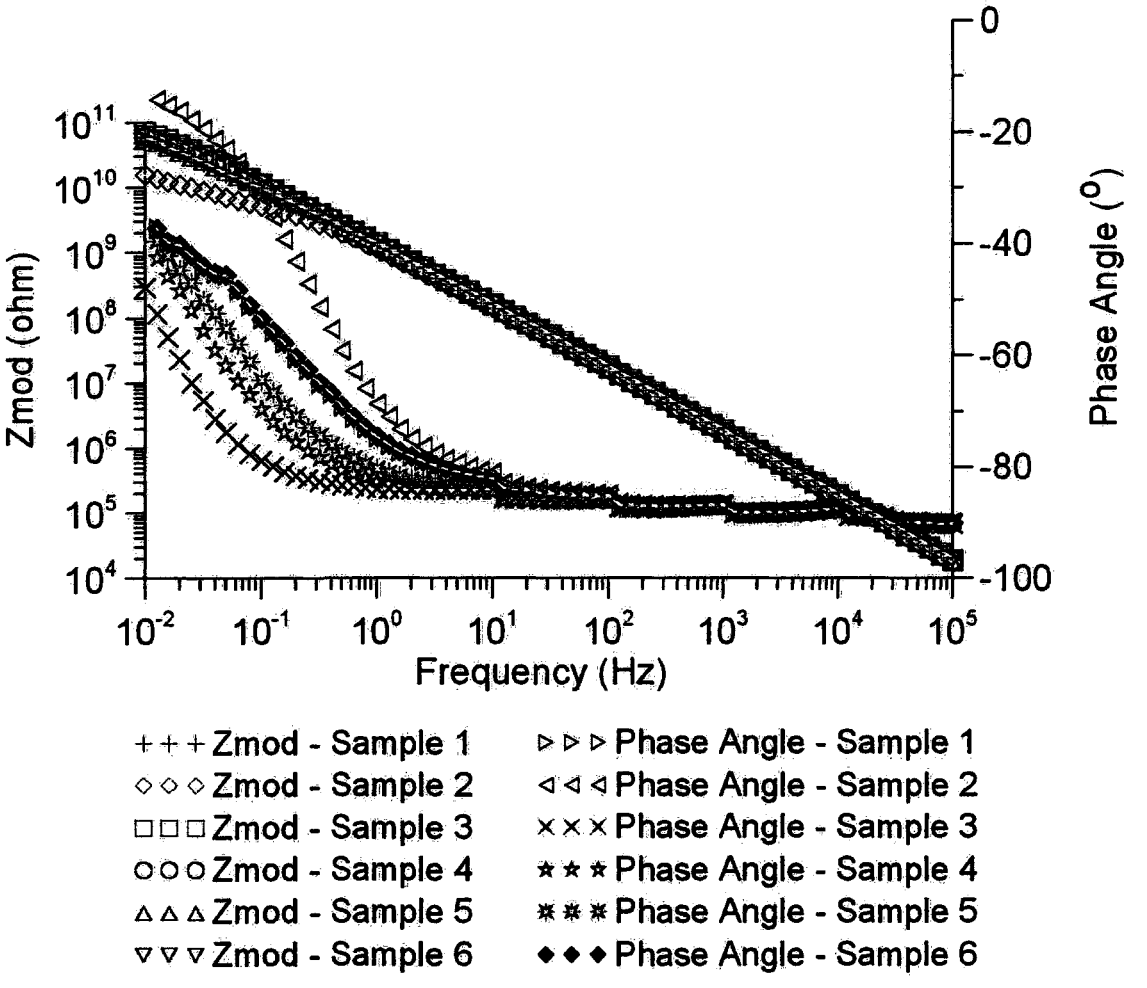

Figure 4-6 Variability in Bode plots for different PUBC samples.

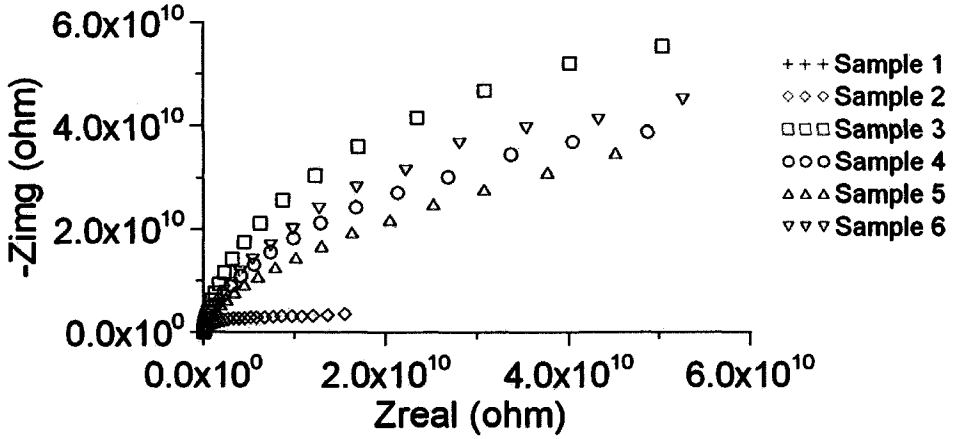

Figure 4-7 Variability in Nyquist plots for different PUBC samples.

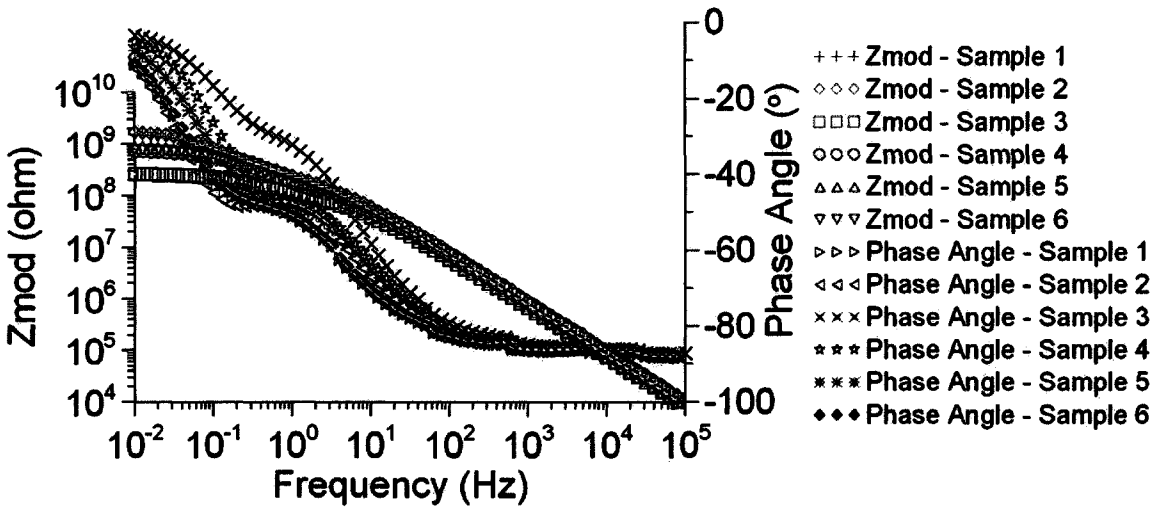

Figure 4-8 Variability in Bode plots for different REBC samples. Note the inflections in the phase angle plots.

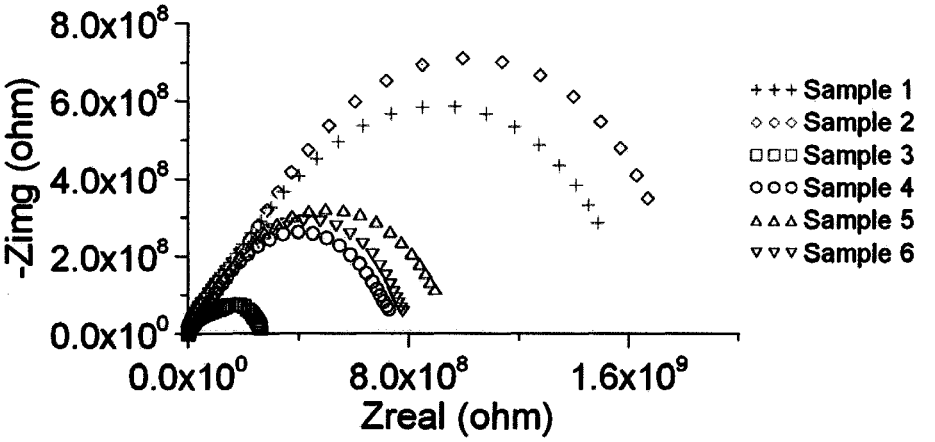

Figure 4-9 Variability in Nyquist plots for different REBC samples.

4.4. Deliberately Damaged Coatings

In order to see if EIS could detect flaws or imperfections in coatings, a number of experiments were performed using coatings that had been deliberately damaged. Two types of imperfections were investigated: a pinhole and a pit.

4.4.1. Effect of a Pinhole on EIS Spectra

A single pinhole was placed in each of two PUBC samples and two REBC samples from Section 4.3.5. The pinhole was created by forcing a needle with a diameter of 1.15 mm through the coating. The samples were then sandwiched between the metal plates and an EIS scan was carried out. Remarkably, the pinhole caused measurable changes in the spectra of both coatings. The phase angle at low frequencies was smaller (see Figure 4-10 for the REBC samples), with a corresponding increase in the imaginary impedance in Nyquist plots (see Figure 4-11 for the REBC samples). In both coating types, the low frequency Zmod increased. In simplistic terms, the coatings became more capacitive at low frequencies, or the resistance of the coatings decreased.

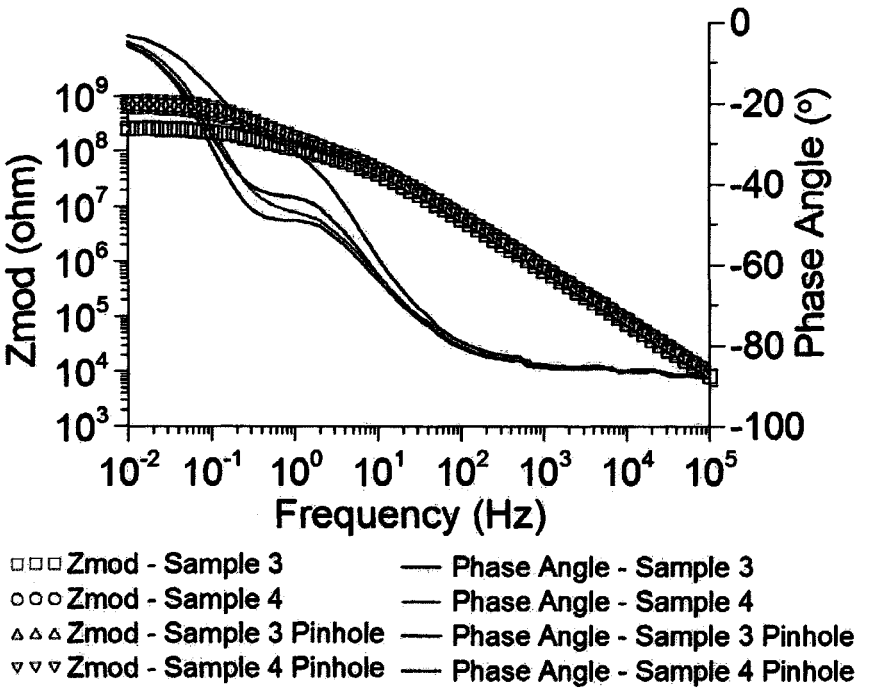

Figure 4-10 Bode plot of the REBC samples before and after artificial pin hole.

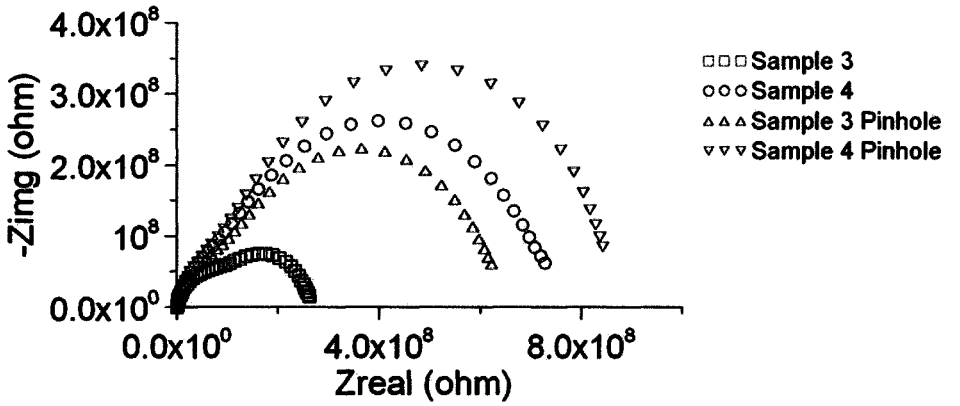

Figure 4-11 Nyquist plot of the REBC samples before and after artificial pin hole.

4.4.2. Effect of Thinned Depressions (Pits) on EIS Spectra.

Depressions, 1cm by 1cm, were cut out of the centre of two PUBC samples and two REBC samples previously studied in Section 4.3.5. The remaining thickness was 1.12, 1.79, 0.68, 0.53 mm out of a starting thickness of 1.71, 2.17, 1.02, 1.06 mm, respectively,

for the two PUBC samples, and the two REBC samples respectively. The samples were then sandwiched between the metal plates, and EIS scans were carried out.

There was no systematic effect of the pits on the EIS spectra of the PUBC samples. In one case the low frequency Zmod increased slightly, while in the other it decreased slightly.

In contrast, dramatic changes were observed in the REBC spectra. These are of the same kind as with the pinhole but even greater. The phase angle at low frequencies was much smaller (see Figure 4-12), with a corresponding increase in the imaginary impedance in Nyquist plots (see Figure 4-13). The coating became more capacitive at low frequencies, and less resistant. Its barrier properties have decreased.

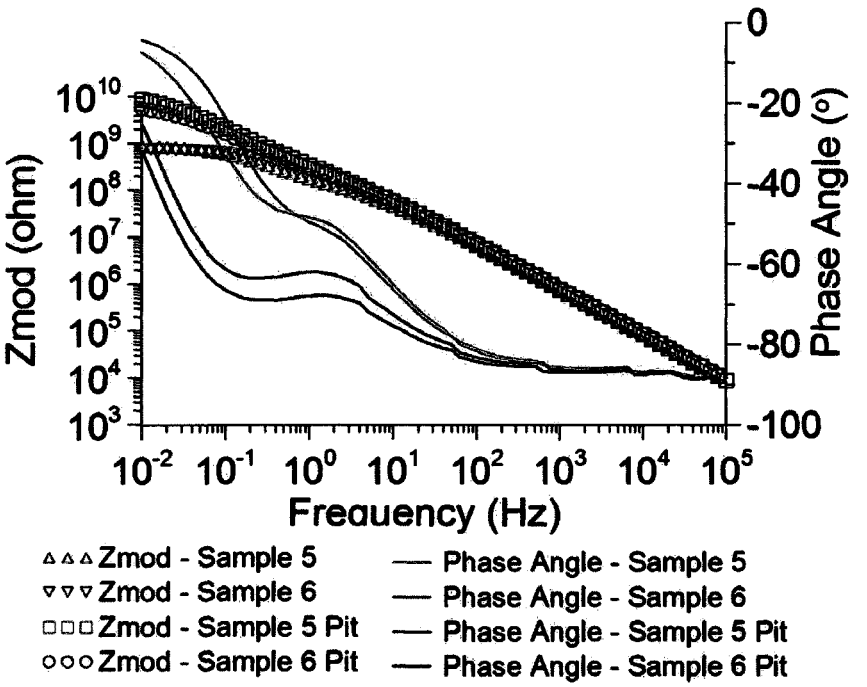

Figure 4-12 Bode plot of the REBC samples before and after cutting depression.

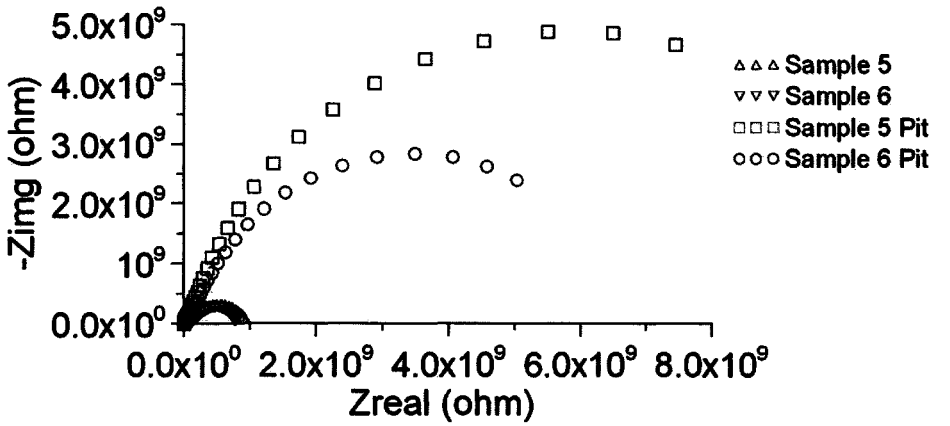

Figure 4-13 Nyquist plot of the REBC samples before and after cutting depression.

4.5. Effects of Exposure to Water and Sodium Chloride Solution

Considerable changes in spectra were observed for samples exposed to water or NaCl. The results obtained from the water are discussed before presenting NaCl results.

4.5.1. Exposure to Water

Both intact coatings, coatings with pinholes, and coatings with artificial depressions (pits) were exposed for a period of 24 hours to distilled water, wiped dry, and then EIS was performed. Both intact and pitted coatings reacted similarly to aqueous exposure. The high frequency responses of the coatings were hardly changed, but there were radical changes in the mid to low-frequency responses.

The PUBC sample behaved like a pure capacitance at low and high frequencies. The low frequency phase angle fell from -40° to close to -90°, while Zmod increased slightly (Figure 4-14).

In the case of the REBC samples, the changes were significant and opposite to those of the PUBC: the phase angle rose to become that of a pure resistor (0°) over the lower half of the frequency spectrum, and the Zmod dropped by a factor of 1000 at low

frequencies. For the first time in the experiments there was also a small but clearly discernable decrease in Zmod at high frequencies (Figure 4-15). The observations are consistent with the formation of a conductive path in parallel with the normal capacitance of the coating. This is probably due to the penetration of distilled water into the pores of the coating.

Experiments with pinholes exposed to water confirmed these results. A PUBC sample with a pinhole gave results very similar to the REBC with no pinhole (c.f. Figure 4-15 and Figure 4-16). The introduction of a pinhole to the REBC gave results little different to the intact coating (Figure 4-17).

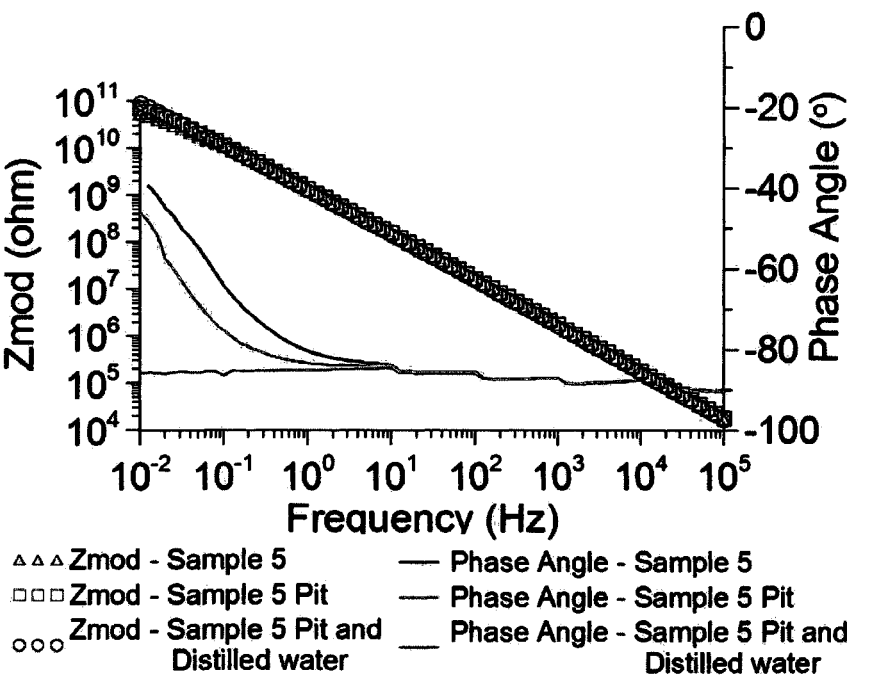

Figure 4-14 Bode plot of three EIS scans of the PUBC sample, dry intact, dry blister, and blister submerged in distilled water for 24 hours.

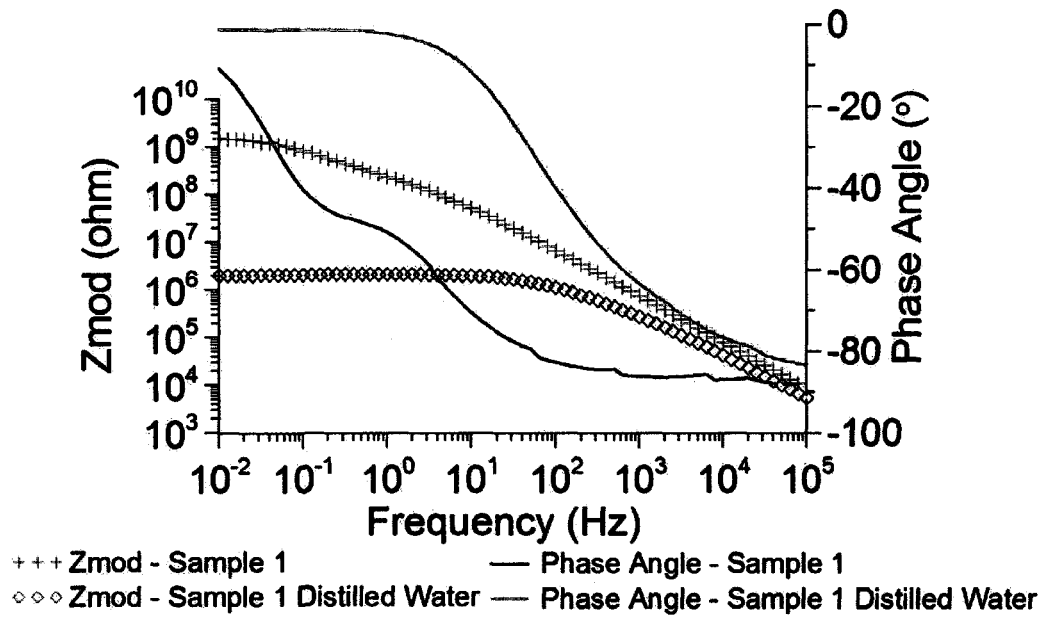

Figure 4-15 Bode plot of the intact REBC samples before and after exposure to distilled water for 24 hrs.

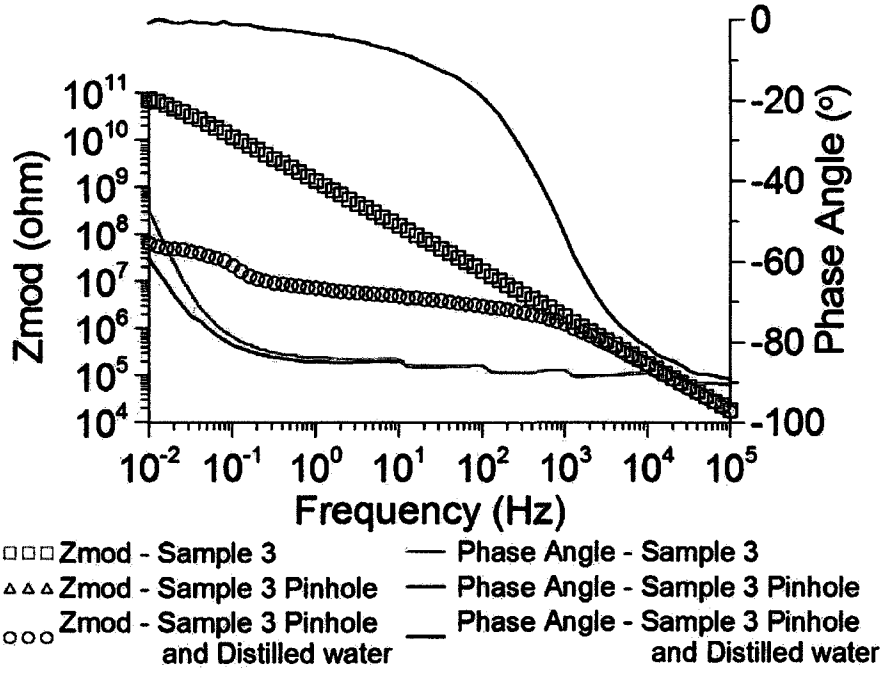

Figure 4-16 Bode plot of the three EIS scans of the PUBC sample: intact, after pin hole, and with pin hole submerged in distilled water for 24 hours.

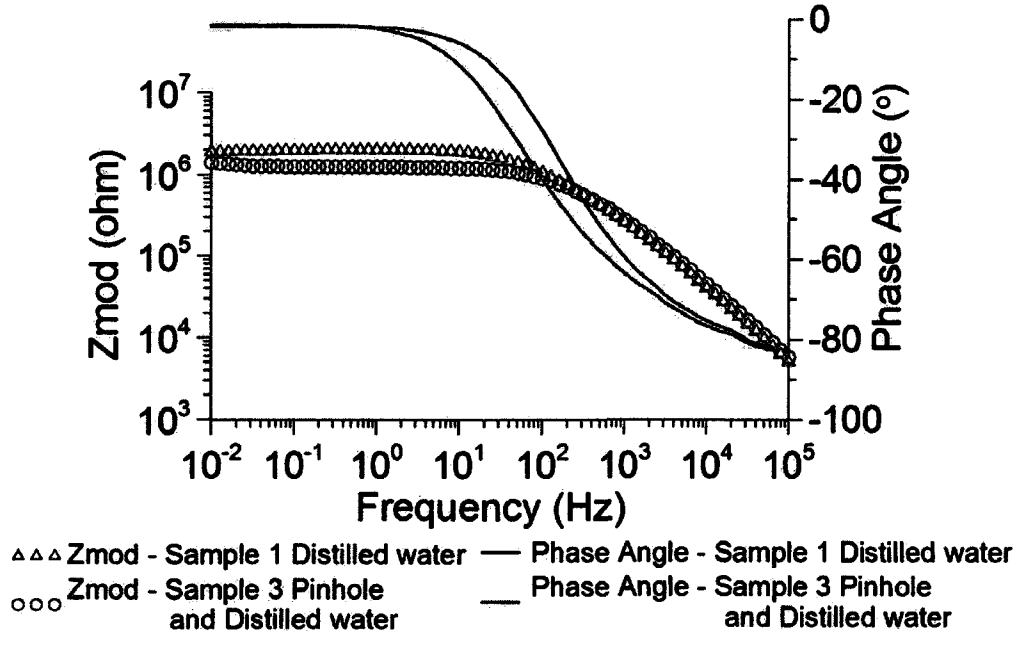

Figure 4-17 Bode plot of the REBC samples submerged in distilled water for 24 hours with and without pin hole.

4.5.2. Exposure to Sodium Chloride Solution

These experiments essentially repeat those in the previous section, but the water has been replaced by a 0.1 M NaCl solution. All the results are qualitatively the same as those observed with water, except that the NaCl solution is a better conductor and so the conductive properties of the coatings are accentuated when compared to those of water. Samples with pits behaved similarly to intact samples. For space considerations pit results are not presented.

As observed with water, after exposure to NaCl, the PUBC sample has a phase angle close to that of a pure capacitor over the whole frequency range (Figure 4-18; c.f. Figure 4-14).

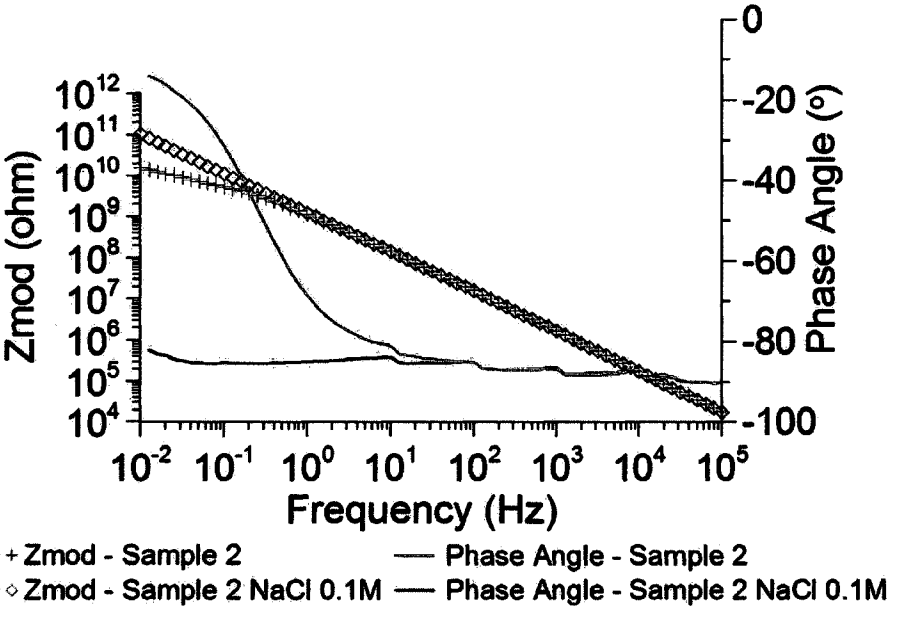

Figure 4-18 Bode plot of the PUBC samples, one scan dry the other submerged in 0.1M NaCl for 24hrs (c.f. Figure 4-14). Note the drop in phase angle at low frequencies.

Exactly as observed with water, after exposure to NaCl solution, the intact REBC sample behaves as though it had a pinhole. The EIS spectra of an intact REBC sample

(Figure 4-19), a REBC sample with a pinhole (Figure 4-20) and a PUBC sample with a pinhole (Figure 4-21) are all very similar.

In these plots the phase angle is close to zero across more than half the frequency spectrum. This indicates that the coating is a resistance (conductor) over this frequency range. The low frequency impedance has dropped by three orders of magnitude, implying an enormous reduction in the effectiveness of the coating as a resistive barrier.

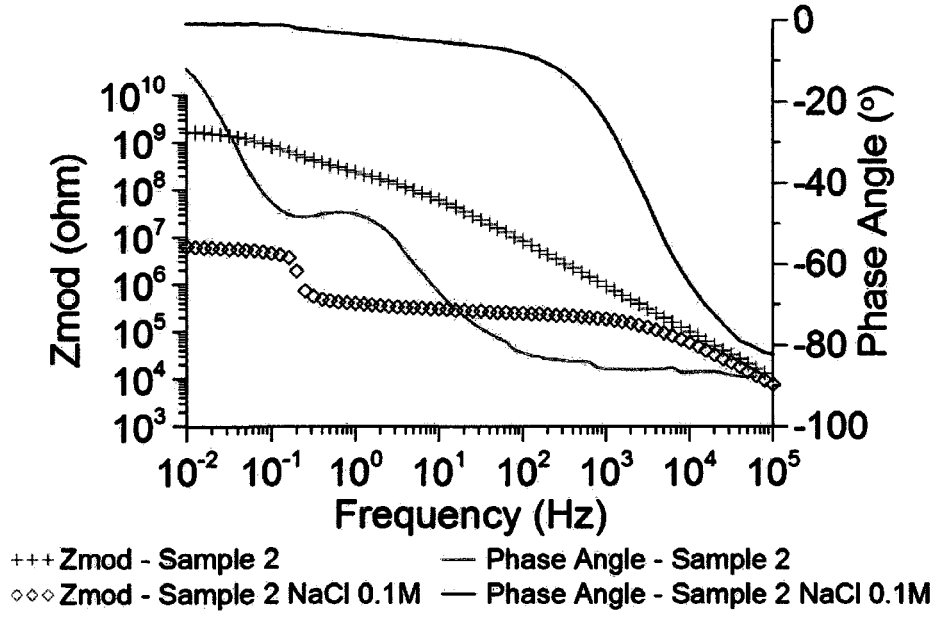

Figure 4-19 Bode plot of the REBC samples, one scan dry the other submerged in 0.1M NaCl for 24hrs.

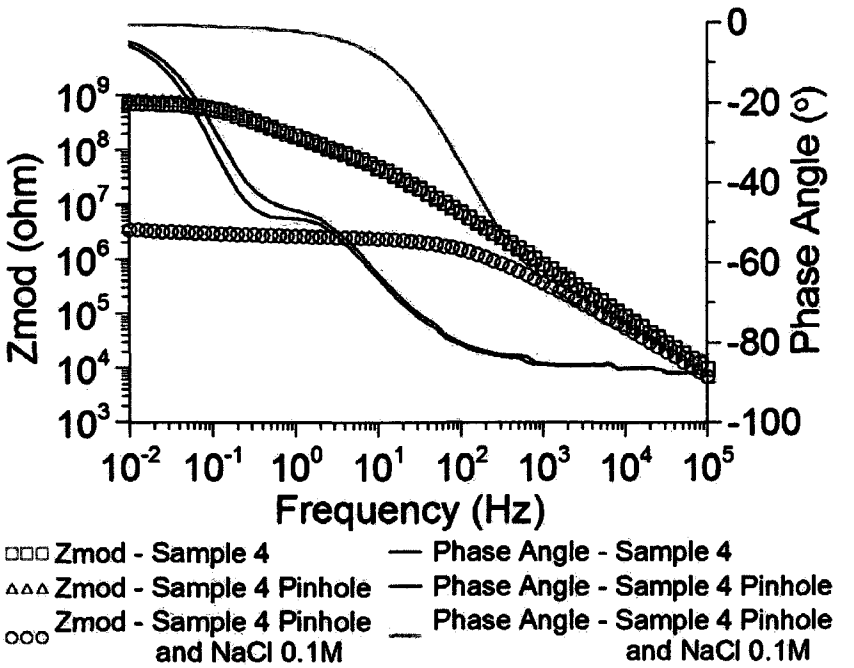

Figure 4-20 Bode plot of three EIS scans of the REBC sample, dry intact, dry pin hole, and pin hole submerged in 0.1M NaCl for 24 hours.

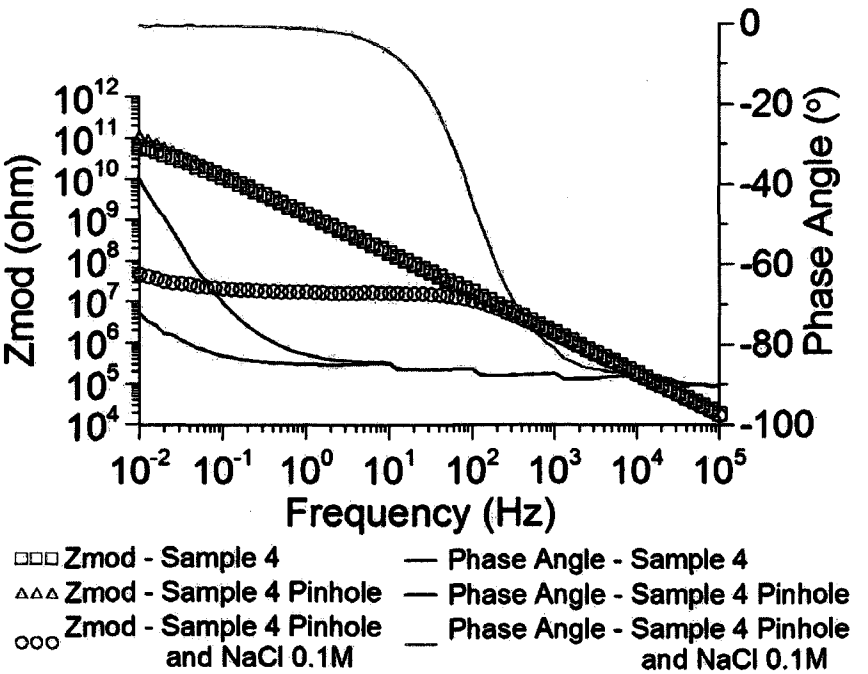

Figure 4-21 Bode plot of three EIS scans of the PUBC sample, dry intact, dry pin hole, and pin hole submerged in 0.1M NaCl for 24 hours.

4.6. Effects of Acid on EIS Spectra

The purpose of this experiment was to assess the response of coatings to various concentrations of sulphuric acid, over a time period of 13 days.

4.6.1 Experimental Details

The mass change of the samples during exposure was monitored. Solutions containing de-ionized water and sulphuric acid were used with the following pH values: neutral, 5, 4, 3, and 2. Five samples of both coatings had nominal dimensions of 7.70 cm by 5.50 cm. The exact dimensions, including thickness and mass were recorded. An EIS scan was performed on each of the dry samples. Samples of the PUBC and the REBC were then placed in containers containing the previously described solutions. The samples were removed from their solutions approximately every 24 hours and were then submerged for 10 seconds in de-ionized water. They were weighed before and after each EIS scan. The temperature, pH, conductivity, and dissolved oxygen concentration of each solution was also recorded. EIS scans were conducted using the method previously described with stainless steel plates.

4.6.2 Results of Experiments with Acid Solutions

Although a large number of experiments were performed using the 2 different coatings, 5 pHs, and daily measurements over 13 days, all data are not presented here in detail.

The lower the pH, the greater was the effect on the EIS spectra, so the data for distilled water and pH 2 will be presented.

Although there were some minor fluctuations in the data for the PUBC, generally the EIS spectra for both coatings steadily progressed with time, so only data for the shortest and longest periods of exposure, viz., time zero and 13 days, will be presented.

The PUBC reacted very similarly to both water and pH 2 sulphuric acid, as can be seen in Figure 4-22. There was no evidence that the acid chemically reacted with the coating. The phase angle shows a rapid increase towards zero at the low to mid frequencies, indicating that the coating is mainly resistive in this region. Overall, there is a dramatic decrease in the magnitude of the impedance at low and mid frequencies. This was also evident in Nyquist plots. It is believed that this is caused by the wetting of the surface and the ingress of electrolyte into the pores of the coating. The differences in the EIS spectra between water and sulphuric acid are thought to reflect the different conductivity, dielectric constant and wetting of the two electrolytes.

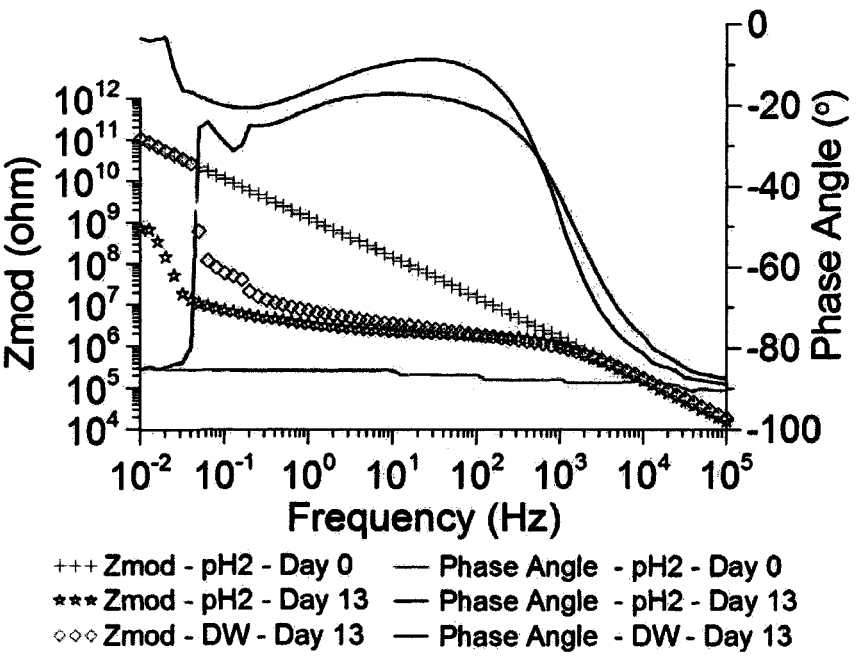

Figure 4-22 PUBC sample in water and pH2 sulphuric acid.

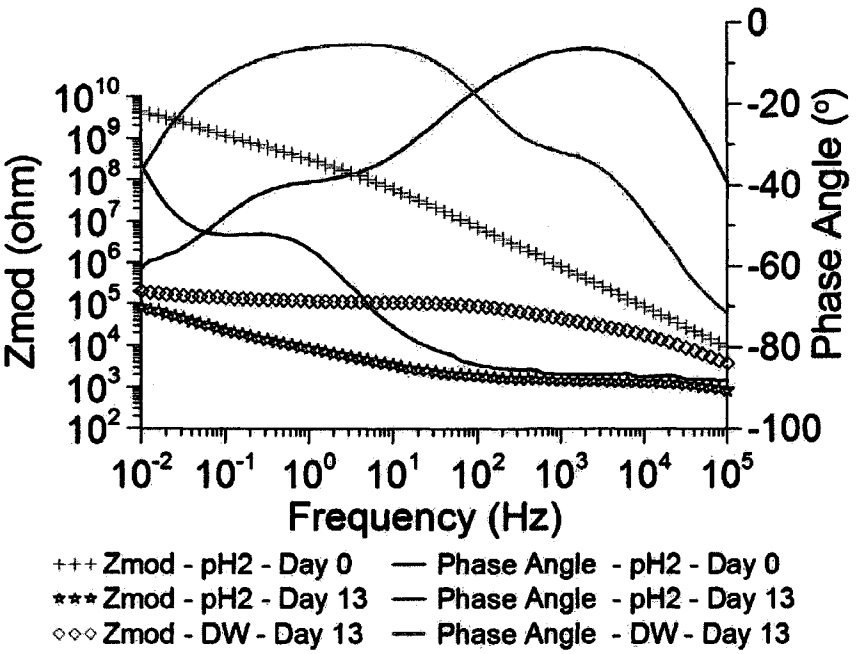

Figure 4-23 REBC sample in water and pH2 sulphuric acid.

The changes in the EIS spectrum of the REBC with time in water and pH 2 sulphuric acid are even greater than those observed with the PUBC. There is an enormous reduction in Zmod. At 10^4 Hz the impedance is only 1 kohm (Figure 4-23), which is a decrease of 5 orders of magnitude. Also there is a large difference between the water and the sulphuric acid spectra, which is believed to reflect differences in the properties of the two electrolytes. All the data to date have suggested that the REBC is much more porous than the PUBC, and the EIS spectra are very sensitive to the electrical properties of the pores' contents.

4.6.3 Mass Gain of Coatings in Water and Acid

Measured weight gains are given in

Table 4-2, and Table 4-3.

Table 4-2 Mass gain of the PUBC sample exposed to various levels of acid concentration.

	De-ionized water	pH = 5	pH = 4	pH = 3	pH = 2
Initial mass (g)	8.71	8.99	8.31	8.09	7.39
% increase in mass relative to initial mass	0.6	0.6	0.6	0.5	0.7

Table 4-3 Mass gain of the REBC samples exposed to various levels of acid concentration.

	De-ionized water	pH = 5	pH = 4	pH = 3	pH = 2
Initial mass (g)	6.23	5.53	5.43	6.09	6.03
% increase in mass relative to initial mass	6	6	7	8	20

It is clear from the data that the PUBC is almost impermeable, while the REBC, in agreement with EIS data, is quite porous, showing mass gains up to 20%. It is also clear that the concentration of the H_2SO_4 has an effect on the REBC samples.

4.7. Summary

The preliminary experiments described in this section showed that the EIS technique can be very useful in assessing the barrier properties of coatings. It can detect flaws such as pinholes (holidays), and responds to different porosities in coatings.

The two coating types tested in this research behave in two completely unique manners. The PUBC sample appeared to be quite impermeable to electrolyte. Its impedance dropped when exposed to liquid, but it still retained good barrier properties. The REBC samples, however, absorbed an appreciable amount of electrolyte, which caused a dramatic reduction in impedance (5 orders of magnitude) compared to the dry coating.

The tests did not show any great differences in EIS spectra for coatings that were thinned in places to make artificial depressions, but no quantitative analysis was done.

Following the success of these preliminary experiments, it was decided to embark on a research program in which the coating samples would be immersed in electrolyte, where in-situ EIS would be done. This obviates the problems and perturbations associated with the dry-cell tests, in which samples had to be removed from solution in order to make EIS measurements. The in-situ immersion tests are described in the following chapters.

5. Tait Cell Experiments

5.1. Introduction

The preliminary metal plate tests had limitations in that they did not permit the continuous monitoring of EIS spectra, with a coating's surface completely exposed to a solution. To overcome this problem, an apparatus, called a Tait cell, was used to carry out repetitive in-situ EIS tests on barrier coatings, without the need to remove the samples from solution. The Tait cell setup also allowed us to test the coatings at elevated temperatures, since it could be placed in a temperature-controlled environmental chamber.

This chapter describes the setup of the Tait cell experiments, which were done to study further the performance of the REBC and the PUBC investigated in Chapter 4. The results of the Tait cell tests will be provided in Chapter 6 and Chapter 7 for the REBC and the PUBC respectively.

5.2. Tait Cell

The Tait cell, shown in Figure 5-1 and Figure 5-2, is an electrochemical cell that can be used to investigate the properties of coatings and paints exposed to aggressive solutions. It is comprised of a glass cylinder with two metal end caps and o-ring seals. The assembly is bolted together forming a leak-tight cell. The Tait cell (Figure 5-1) used in this investigation encloses an interior circular area of 34.6 cm^2. A coating sample was placed on top of a stainless steel (type 304) plate electrode, in between the bottom cap

and the glass cylinder. Two flat rubber o-rings ensured a tight seal between the glass cylinder and the sample, and the glass cylinder and the top end cap.

As illustrated in Figure 5-2, from the top end cap two metal electrodes are suspended: a counter electrode and a reference electrode. The counter electrode has a wide surface area covering almost the entire cross section of the glass cylinder and is placed 10 mm above the surface of the coating (*i.e.*, the working electrode) being tested. The large surface area of the counter electrode is required to provide a uniform current to the entire surface area of the coating placed underneath, ensuring that measurements are accurate and representative of the whole surface of the coating. The reference electrode is suspended through a small hole at the centre of the counter electrode, and its tip is placed 5 mm away from the surface of the coating. Both electrodes are made from Hastelloy [Metals Handbook 1990], which is a special alloy used in highly corrosive environments, where corrosion resistance is required. Hastelloy electrodes are known to perform well in acidic environments and at elevated temperatures. There are several different types of Hastelloy; the type chosen for the Tait cell was C-276 [Metals Handbook 1990].

For an EIS scan to be performed on the coating, an electrical connection between the working electrode and the counter electrode must be established. This was achieved by filling the cell with a conductive solution (around 200 ml) through a screw cap located on the top of the cell. The solutions that have been investigated are all conductive electrolytes. In this setup, the coating can be regarded as being an insulating dielectric sandwiched between the conducting solution and the conducting substrate, in a manner very similar to a parallel plate capacitor. The electrodes were then connected to a

potentiostat so that EIS scans could be carried out to study the effects of the conducting solution on the coating. Since the entire Tait cell system was sealed, it could be placed in an environmental chamber, where the temperature of the environment was controlled.

To carry out the EIS investigations, a Gamry PC4/300 Potentiostat/ Galvanostat/ Zero Resistance Ammeter and Gamry ECM8 Electrochemical Multiplexer were used. The potentiostat and the multiplexer were controlled by Gamry Frameworks V4.35, which uses a program that allows user scripting to customize the EIS experiments. The standard scripting was modified from the normal Gamry issue, to enable the software to work at very low currents, and to eliminate problems with gain changes, which originally gave phantom peaks in the EIS spectra (see Appendix A).

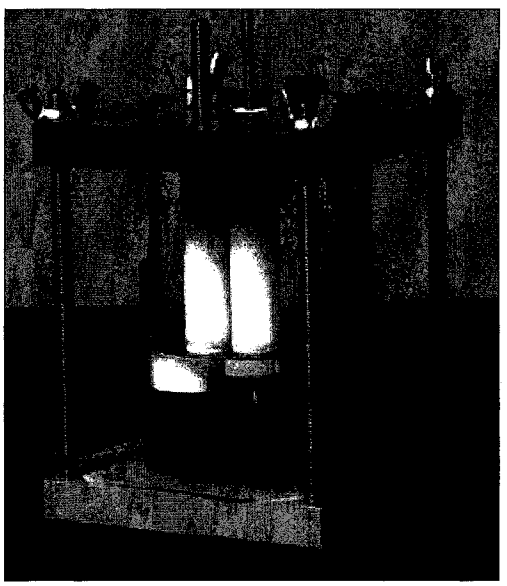

Figure 5-1 The Tait cell used in the current investigation [Princeton Applied Research]

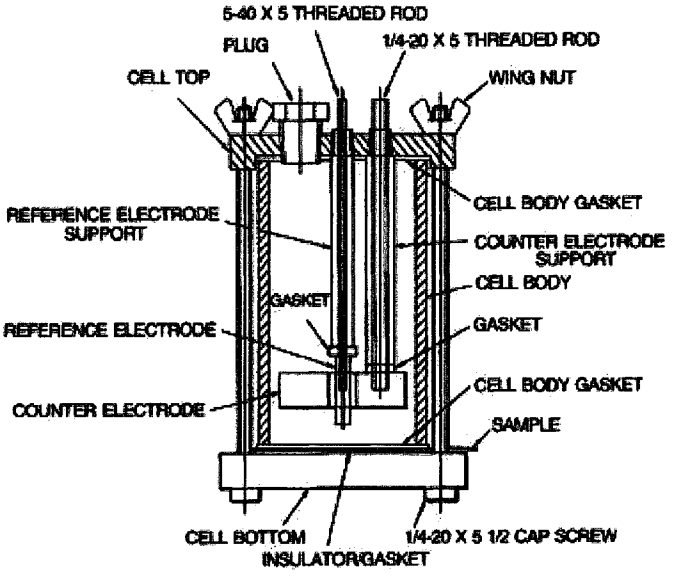

Figure 5-2 Schematic representation of the Tait cell used in the current investigation [Princeton Applied Research]

5.3. Experimental program

Following the preliminary investigations using metal plates with no solution (Chapter 4), a testing program using a Tait cell setup was developed and implemented. Based on the intended application of the coatings, the REBC and the PUBC, it was decided that the coatings should be tested at three temperature levels: 25°C (room temperature), 40°C (the approximate operating temperature of a mesophyllic digester), and 60°C (the approximate operating temperature of a thermophyllic digester). The measurements were carried out in a Faraday cage, and an environmental chamber was used to carry out tests at 40°C and 60°C. The temperatures in all environments were monitored using a probe that collected the temperature data continuously. It was concluded that, throughout the tests, the variations in temperature were within ±2°C in the laboratory (for the tests carried out at room temperature) and ±1°C in the environmental chamber.

Besides the effect of temperature, the effect of different solutions on the protective properties of the two barrier coatings was investigated. These solutions are similar to those used in Chapter 4, but the sulphuric acid concentration was increased by a factor of 10 to pH1. This was done in the hope of speeding up any chemical effects that the acid might have on the coating, and also to amplify the effects of electrolyte in pores seen in Chapter 4.

The following tests were performed:

Test 1: A coating sample was exposed to 0.1 M NaCl solution;

Test 2: The coating from test 1, previously tested in 0.1 M NaCl solution, was exposed to a mixture of 0.1 M NaCl and pH 1 sulphuric acid;

Test 3: A coating was directly exposed to a mixture of 0.1 M NaCl and pH 1 sulphuric acid;

Test 4: A coating was directly exposed to pH 1 sulphuric acid.

Test 1 was performed in order to capture the entry of solution into the coating, while at the same time not damaging the coating, it was also intended to determine how long it would take for a coating to become fully saturated with solution. In order to ensure that the solution used was conductive enough not to cause an effect on the EIS scan, therefore a solution of 0.1 M NaCl was selected.

Test 3 was performed to see the effect of the sulphuric acid on the coating system, to see how the coating would react, and how the solution would enter the coating in comparison to test 1. Because, test 1 would be used for comparison it was decided that the solution for test 3 should also contain 0.1 M NaCl as well.

This led to test 4, which is intended as a duplicate of Test 3 without the 01 M NaCl, in order to assess if the 0.1 M NaCl had an effect on the reaction between the sulphuric acid and the coating system.

Test 2 was performed as complimentary to test 1, and test 3. The test was performed in order to see how the coating would perform when it was exposed to sulphuric acid after it had become fully saturated. The test was performed in order to answer if the acid would rapidly attack the substrate by diffusing along any existing electrolyte paths created in Test 1 or would the acid have to react with the coating prior to coming into contact with the substrate.

Since three Tait cells were available at a time, several tests were carried out simultaneously at a given temperature, and the temperature of the environmental chamber was kept constant until all tests at a given temperature were completed. The pH, conductivity, temperature, and dissolved oxygen concentration of the solutions were measured using a VWR SympHony SP90M5 multimeter before and after each test. No major changes were observed in these parameters.

Using three different temperatures, it was originally planned that 12 tests would be done for each of the two coating types. As discussed later, it was found that the PUBC samples did not show any major change in their properties after long periods of exposure, even at elevated temperatures, so some of the tests were eliminated from the testing program. For example, tests 2 and 4 were not performed on the PUBC samples at room temperature, because test 3 had failed to produce any major evidence of change in the properties of the coating. Test 4 at room temperature was not performed on the REBC

since this coating failed in test 3 after a relatively short period of exposure. Consequently, a total of 16 Tait cell tests, as listed in Table 5-1, were carried out.

Table 5-1 Tait cell experiments performed on the PUBC and the REBC samples.

	Room Temperature	**40°C**	**60°C**
Test 1 0.1M NaCl	REBC PUBC	REBC PUBC	REBC
Test 2 Test1 then 0.1M NaCl + pH1 H_2SO_4	REBC	REBC	REBC
Test 3 0.1M NaCl + pH1 H_2SO_4	REBC PUBC	REBC PUBC	REBC PUBC
Test 4 pH1 H_2SO_4		REBC	REBC

The tests were performed using "free film" coating samples that were not bonded to the metal substrate. To study if bonding to the metal substrate would make any difference in the results, additional tests were conducted on the REBC. In this setup, the manufacturer of the coating prepared the samples by applying the coating on metal plates using their product specifications. These samples, which were bonded to the metal plate, were investigated in test 1 at 40°C and test 3 at 60°C, and the results were then compared to the free film results.

The free potential of the system was measured for 200 s prior to the start of each experiment, to make sure that the system had reached a stable state, and the EIS scan was then performed at an impressed DC potential of zero volts versus the reference electrode. The settings used for each EIS scan were as follows:

- Starting frequency of the EIS scan: 10^5 Hz;
- Final frequency of the EIS scan: 10^{-2} Hz;

- Number of EIS measurements per decade of frequency: 10 (*i.e.*, 70 EIS measurements in total for each scan);
- Amplitude of the AC voltage: 100 mV (RMS);

During the assembly of the Tait cell, prior to the start of each experiment, the following procedure was followed. The stainless steel plate, on which the coating was placed, as well as the counter and reference electrodes, were cleaned prior to use by first washing them with acetone, then with ethanol, and finally rinsing them with de-ionized water. The o-rings, the top and bottom ends of the cell and the glass cylinder were rinsed thoroughly with distilled water. The cell was then assembled. The test solution was poured into the cell using the threaded opening on the top, in a controlled manner so as not to create any air bubbles underneath the counter electrode. The threads of the opening were coated with Teflon tape to prevent gas leakage.

The equivalent-circuit modeling of the EIS data was performed using Gamry Echem Analyst (Version 5.3). These models attempt to use electrical circuit elements in order to emulate the structure of the coating, e.g., layers and pores and cracks etc., in terms of the electrical properties measured by EIS. Using the built-in "circuit designer" feature of the software, several circuits, from simple to more complex ones representing intact and failed coatings, were constructed and used to model the behaviour of the coatings in each test. The selection of the models was guided by previous works of other researchers (see Chapter 3). An effort was made to establish a good physical representation of the real world, with useful parameters that can give a good indication of a coating's performance. To achieve this, it was often necessary to tailor an old model or create a new model to interpret the data. A total of 36 models, with various degrees of

complexity, were investigated while fitting the EIS data for different experiments. The actual models used are presented in Chapter 6 and 7.

When a fit to a model is performed using Gamry Echem Analyst V5.3, a quantity called the "Goodness of Fit" is calculated. This term is a quantitative assessment of the error of the fit. The circuit fit is determined by using a "non-linear least squares" approach. In order to fit a function f(x) to a data set y, the following equation is used:

$$\chi^2 = \sum_{i=1}^{n} \left[\frac{y_i - f(x_i)}{\theta_i} \right]^2 \qquad 5\text{-}1$$

where, θ_i is the standard deviation of each datum. The best fit is achieved by reducing χ^2 to an acceptable value. This term is dependant on the number of data points, n, and as such increasing the number of data points would increase your χ^2. In order to compensate for this Gamry looks at χ^2 per degree of freedom:

$$\frac{\chi^2}{n-m} \qquad 5\text{-}2$$

where m is the number of adjustable parameters in the fit, and (n-m) is the number of degrees of freedom of the system. If the assumed θ_i is correct, then the expression in Eq. 5-2 should be close to one.

In electrochemical experiments involving EIS, an auto-ranging potentiostat is used, so that the current measured is always close to the limit that can be measured for that range. If the assumption is then made that the error on the measurement is a fixed fraction of the full current that can be measured, ε, then the following is true:

$$\theta_i \approx \varepsilon y_i \qquad 5\text{-}3$$

By combining Eq.5-1, 5-2, 5-3, and by weighting each data point by y_i the following is achieved:

$$E^2 = \frac{\sum_{i=1}^{n}\left[\frac{y_i - f(x_i)}{y_i}\right]^2}{n-m} = \frac{\varepsilon^2 \chi^2}{n-m} \qquad 5\text{-}4$$

By minimizing the E^2 term, which is the "goodness of fit" term, the χ^2 is also minimized. The % error is then calculated by taking the square root of E^2 and multiplying by 100 [Research Solutions and Resources 2008].

The goodness of fit of each model to the EIS data was evaluated by the percent error. When a model proved to be successful, in terms of both reproducing the data and corresponding with our physical understanding of the system, an attempt was made to use that model for most, if not all, of the EIS scans of a particular test. This was not always possible, however, because the chemical and physical processes in the coatings evolved with time. When the error of the fit exceeded 15-20%, a different model was tried. The details of the equivalent circuit modelling for each test will be discussed in the following chapters.

6. Tait Cell Test Results for the REBC

6.1. Introduction

This chapter presents the results of the Tait cell experiments that were carried out on the REBC samples. In addition to a qualitative analysis of the Zmod, and phase angle plots, equivalent circuit modelling was also performed.

As explained previously in Chapter 2, surface roughness, porosity, non-uniform thickness of the material being tested, non-uniform penetration of solution into the coating pores, and non-uniform current distribution across the dielectric material are some of the possible reasons why coatings exhibit non-ideal behaviour. A constant phase element (CPE) is a type of circuit impedance arising from inhomogeneous physical properties of the system. The impedance of a CPE is given by (also given in Eq. 2-19):

$$Z = \frac{1}{Q(j\omega)^p} \qquad 6\text{-}1$$

When the exponent, p, is equal to 1, the CPE is equivalent to a perfect capacitor ($Q = C$), and when it is zero it is equivalent to a resistor. When it is -1 it is equivalent to an inductor. For real systems containing an inhomogeneous layer of material, it is usually between 0.5 and 1. When p is close to 1.0, the CPE may be simplistically thought of as a distribution of imperfect capacitors, *i.e.*, capacitors with some resistance or inductance properties, but its phase angle is constant and less negative than -90° at all frequencies.

Equivalent circuit modelling was used to analyze the EIS data in further detail. Figure 6-1shows the general electrical circuit model that was used in this thesis. The definitions of circuit elements used in this model are provided in Table 6-1.

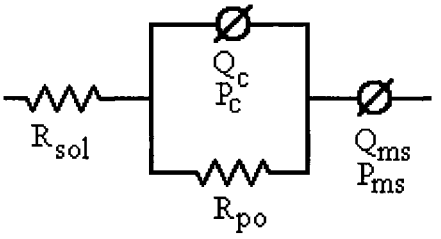

Figure 6-1 General equivalent circuit analysis model.

Table 6-1 Definition of circuit elements.

Model Term	Definition	Units
R_{po}	This is the bulk resistance of the coating, and since conduction occurs by the easiest path, this is the resistance via pores, cracks and similar defects.	ohm
R_{sol}	Solution resistance of the bulk electrolyte	ohm
Q_c	One of the two parameters that define a CPE, which in this case is an impedance representing a distribution of inhomogeneous circuit impedances in the coating (see text discussion and Equation 6-1 above).	$F*s^{-1}*s^p$
P_c	The power factor of the CPE, which defines the out-of-phase nature of the coating, Q_c (see Equation 6-1 above)	
Q_{ms}	One of the two parameters that define a CPE, which in this case is an impedance representing a distribution of inhomogeneous circuit impedances, in the vicinity of the surface of the metal electrode, underlying the coating	$F*s^{-1}*s^p$
P_{ms}	The power factor of the CPE, which defines the out-of-phase nature of the system, Q_{ms}, in the vicinity of the surface of the metal electrode, underlying the coating (see Equation 6-1 above).	

In some cases, as different impedances became more or less important during different stages of exposure in a given Tait cell experiment, modeling was done using variations of the model circuit shown in Figure 6-1. These variations are described below.

In general, equivalent circuit models A, B, and C were identified as the circuits that fit the EIS data most accurately for different stages of the tests, and model D was

used for failed coatings. Model A, as illustrated in Figure 6-2, represents an intact coating immediately after exposure to the solution. This model consists of a solution resistor R_{sol}, in series with a parallel circuit that includes a pore resistor (R_{po}), and a CPE (Q_c and P_c), representing a distributed impedance in the coating.

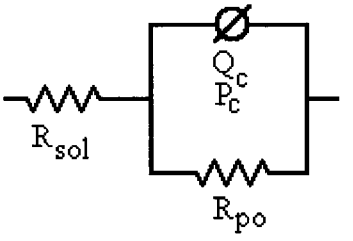

Figure 6-2 Equivalent circuit model A.

Since the solution resistance, R_{sol}, is typically orders of magnitude smaller than R_{po}, it is possible to ignore this term without introducing a significant error. Model B, as illustrated in Figure 6-3, is the equivalent circuit model without the solution resistance term, and it represents the electrical analogy of a coating that is experiencing the ingress of solution into its pores, before the metal plate underneath the coating is wetted by the solution. This model is a parallel circuit that includes a resistor (R_{po}) and a CPE (Q_c and P_c), representing the coating properties.

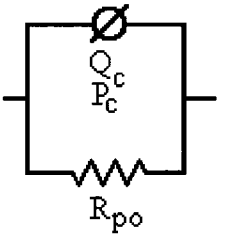

Figure 6-3 Equivalent circuit model B.

Model C (Figure 6-4), differs from model B, because it represents the coating and the metal plate after the solution has passed through the coating and reached the metal plate. The coating is now a leaky dielectric, lying on top of an inhomogeneously wet

electrode. The impedance on the metal surface is modelled as a CPE (Q_{ms} and P_{ms}) in series with the circuit in model B, representing the coating properties. Although all model parameters were evaluated in the equivalent circuit analysis, only the properties of coatings, *i.e.* R_{po}, Q_c and P_c, will be reported here.

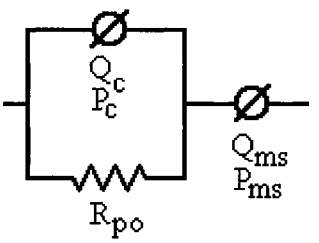

Figure 6-4 Equivalent circuit model C.

Model D (Figure 6-5) was used for seriously breached coatings, where the coating no longer presents a barrier to the liquid. A resistor representing a solution resistance (R_{sol}) is in series with a CPE (Q_{ms} and P_{ms}) representing the complex impedance in the vicinity of the electrode's surface.

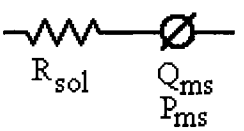

Figure 6-5 Equivalent circuit model D.

6.2. Effects of Temperature and Exposure Solution

Considerable changes in EIS spectra were observed for the REBC samples exposed in a Tait Cell to four different chemical exposure conditions in the tests described in Chapter 5. The results of these tests are presented here.

6.2.1. Test 1: Exposure to 0.1 M NaCl Solution

The EIS scans of the REBC samples exposed to 0.1 M NaCl solution, at all temperatures showed a similar pattern. In general, it was observed that at some time after the initial exposure, the values of the modulus of the impedance (Zmod) at low frequencies decreased rapidly, over several orders of magnitude. Subsequently, Zmod values levelled off, and no further significant change was observed. Figure 6-6 illustrates this behaviour for all three temperatures[1]. The time after which Zmod became stable depended on the temperature of the system. At room temperature, this was observed after around 200 hours of exposure, while for 40°C and 60°C, it occurred after 80 and 20 hours, respectively. As discussed in Chapter 4, the decrease in the modulus of impedance can be explained by the diffusion of NaCl solution into the pores in the REBC. The low frequency impedance dropped by three to five orders of magnitude depending on the experimental temperature, implying a large reduction in the efficacy of the coating as a resistive barrier. It is hypothesised that after the modulus of the impedance became stable and relatively constant, the solution had penetrated the entire thickness of the coating.

[1] In **Figure 6-6**a, an anomalous step change in Zmod for some frequencies at c.200 hours complicated subsequent modeling.

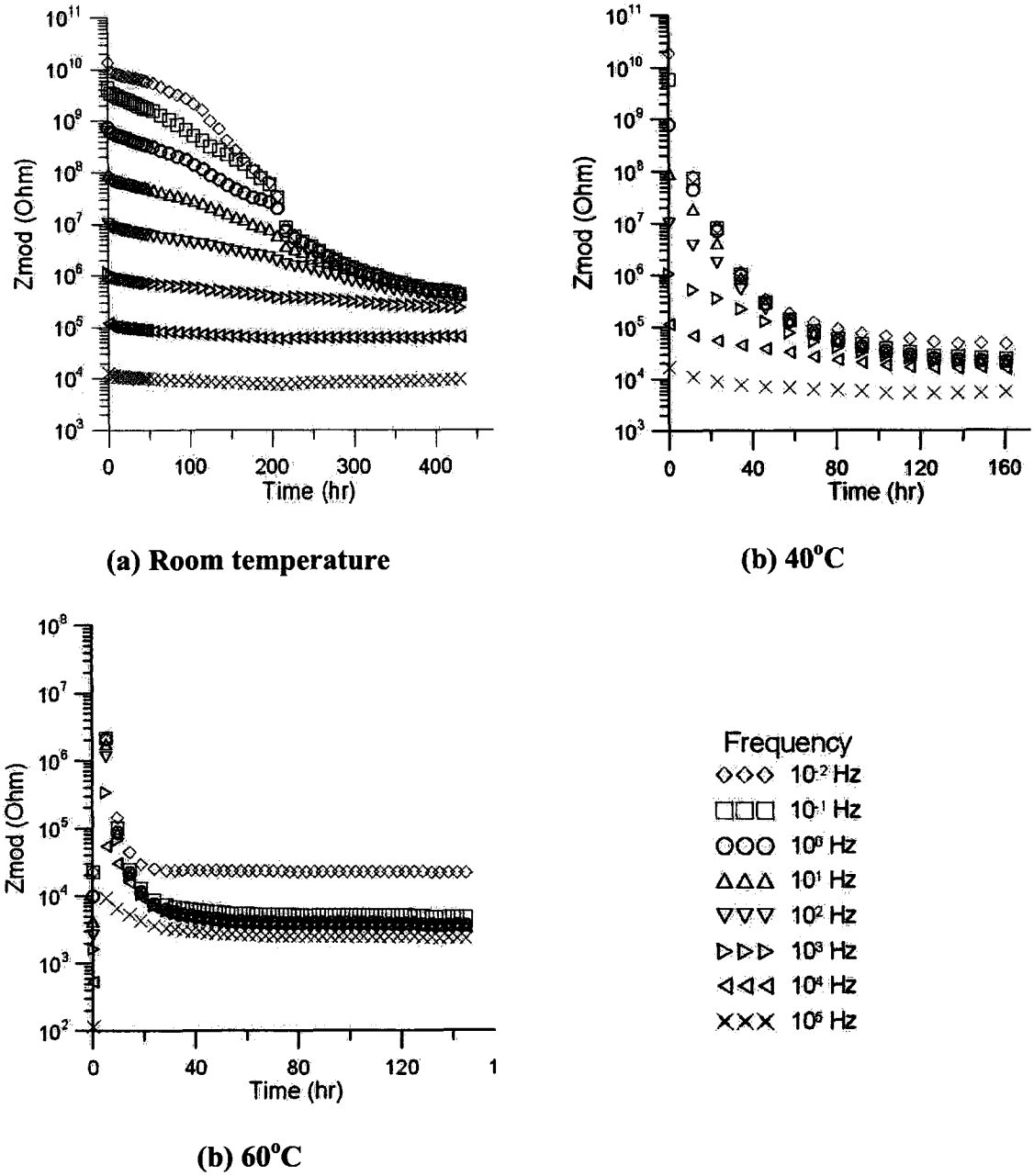

(a) Room temperature

(b) 40°C

(b) 60°C

Figure 6-6 Change with time of the modulus of the impedance of the REBC samples exposed to 0.1 M NaCl solution at various temperatures.

Phase angle measurements, also support these observations. The phase angle increased towards 0^{o} (indicating transformation to a resistor) for all but the highest frequencies and for all temperatures. This increase was fastest at low frequencies, and at higher temperatures, as illustrated in Figure 6-7. At room temperature, after 200 hours of exposure, the phase angles reached 0^{o} at the lowest three frequencies. With increasing temperature, the increase in the phase angle to 0^{o} was significantly faster, presumably indicating faster diffusion of electrolyte into the pores. After a period of time, the coating behaved like a conductor, once again supporting the preliminary experiments, which showed the inefficacy of the REBC samples as a resistive barrier (see Chapter 4).

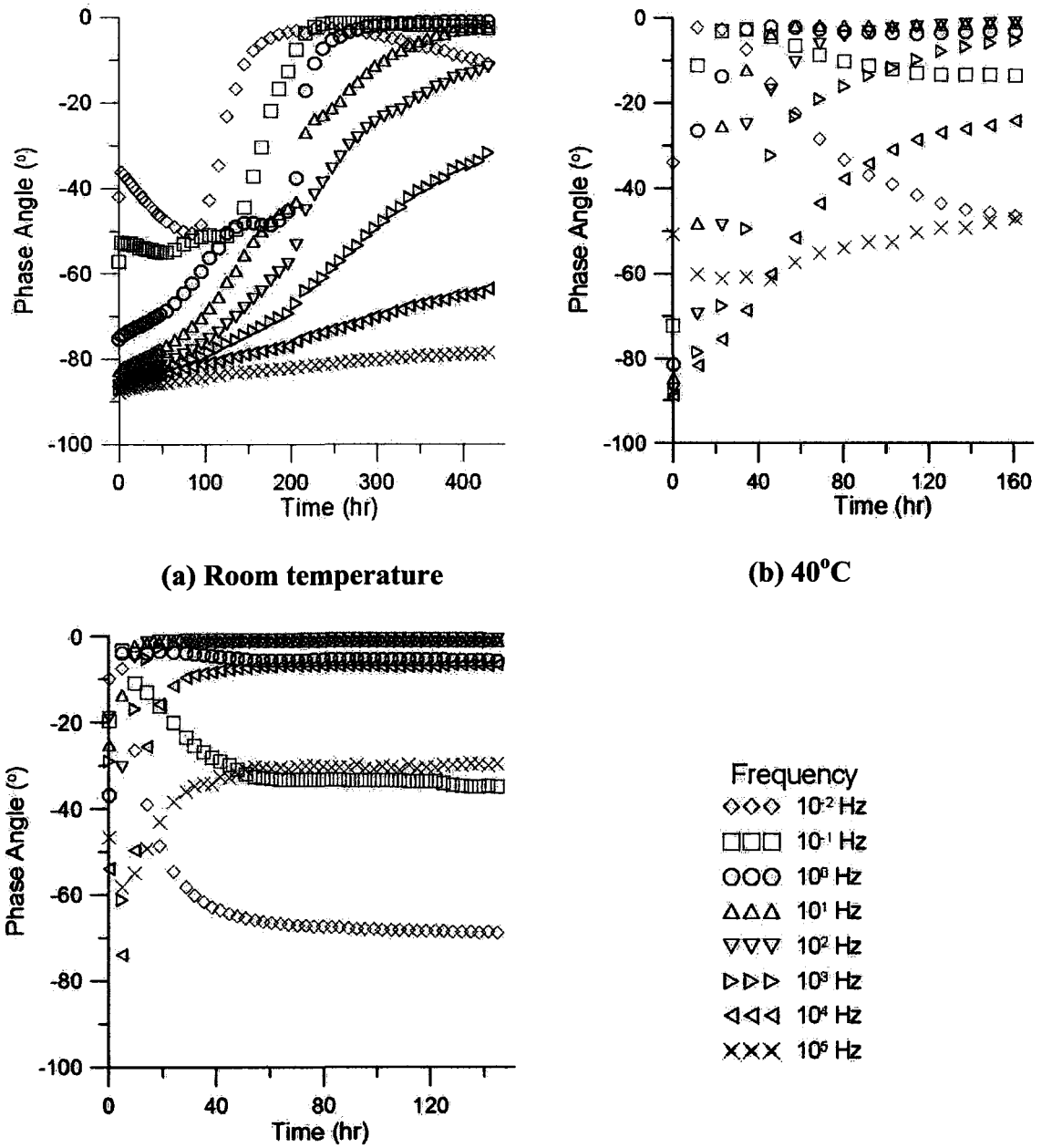

(a) Room temperature

(b) 40°C

(b) 60°C

Figure 6-7 Change with time of the phase angle of the REBC samples exposed to 0.1 M NaCl solution at various temperatures.

Figure 6-8 shows a bode plot, with a typical fit to model C, of an REBC sample exposed to 0.1 M NaCl at 60°C. The particular EIS scan shown is number 95 of 169, and was taken 84 hours after exposure. The marker symbols of the Zmod and the phase angle plots are only shown for every third data point. The model fit performed on the sample is presented in the figure; in this case the model fit was very accurate with a 1.09 % error of the fit (see Chapter 5 for a discussion of fitting and errors). More information on the model fit is provided in

Table **1-2**. The plot clearly shows that, over the majority of the frequencies, the phase angle is very close to 0°, indicating that the sample is mostly resistive at this point in time. The Zmod plot shows a comparatively low value over all frequencies measured.

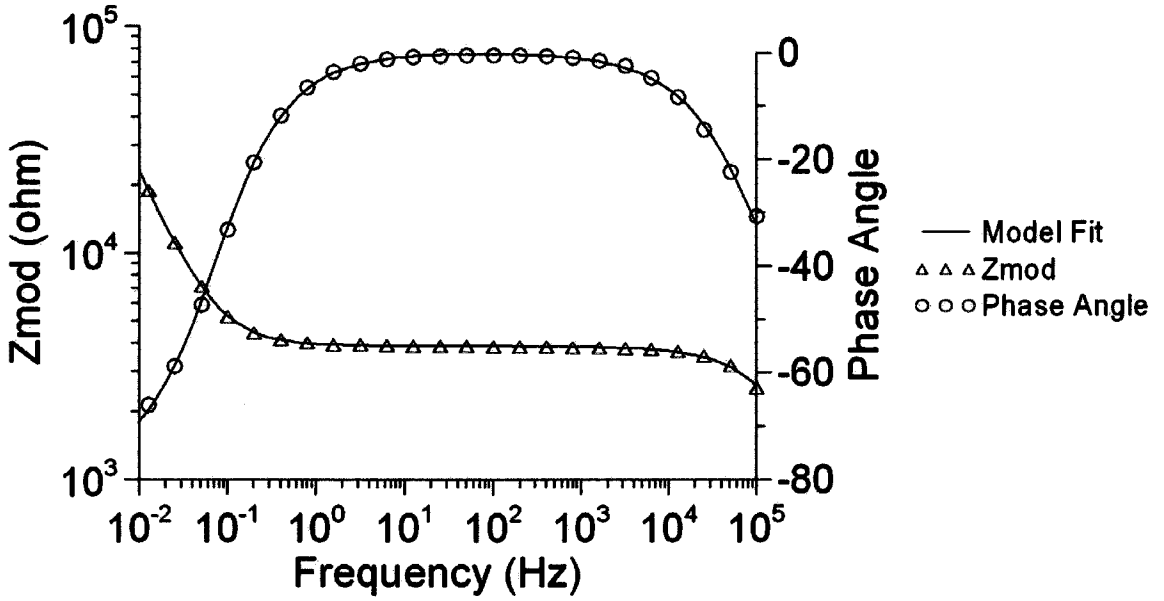

Figure 6-8 A typical Bode plot of an REBC sample exposed to 0.1 M NaCl at 60°C. This fit was done using model C.

Table 6-2 Model fit results of an EIS scan performed after 84 hours of exposure of an REBC sample exposed to 0.1 M NaCl at 60°C.

Parameter	Value	± Error	Units
R_{po}	$3.9x10^{3}$	18.0	ohm
Q_c	$4.8x10^{-9}$	$1.0x10^{-9}$	$F*s^{-1}*s^{p}$
P_c	$8.0x10^{-1}$	$1.7x10^{-2}$	
Q_{ms}	$5.2x10^{-4}$	$7.6x10^{-6}$	$F*s^{-1}*s^{p}$
P_{ms}	$8.7x10^{-1}$	$6.2x10^{-3}$	
Goodness of Fit	$1.2x10^{-4}$		

A summary of the equivalent circuit modelling results for the REBC samples at three temperatures is presented in Table 6-3. The equivalent circuits used to model each case are also identified in the table. In all models, the error of the fit was usually less than 15%; however increases in the error of the fit were occasionally observed at the beginning of the tests and after major changes in the properties of the coating occurred. An example of an error plot with time for the REBC exposed to 0.1 M NaCl at 60°C is presented in Figure 6-9.

Table 6-3 Summary of the equivalent circuit modelling results of the REBC in test 1.

Parameter	60°C	40°C	Room Temperature
Duration of test (hours)	145	171	436
Maximum % Error of Fit	22.5	18.0	27.9
Average % Error of Fit	2.9	8.1	17.0
R_{po} at the start of test (Ohms)	$8.2x10^{7}$	$2.7x10^{10}$	$1.1x10^{10}$
R_{po} at the end of test (Ohms)	$3.6x10^{3}$	$2.1x10^{4}$	$4.1x10^{5}$
Q_c at the start of test	$6.4x10^{-10}$	$2.4\ x10^{-10}$	$2.9\ x10^{-10}$
Q_c at end of test	$5.4\ x10^{-9}$	$6.5\ x10^{-9}$	$2.1x10^{-9}$
Model(s) used	C	A,B,C	B,C

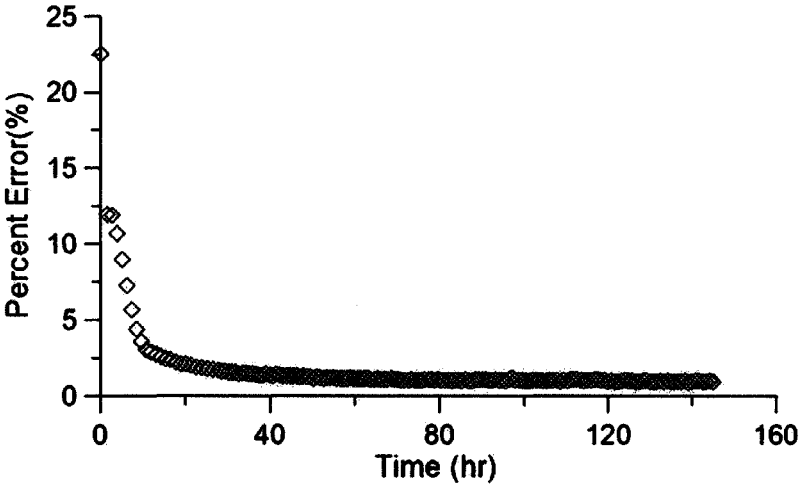

Figure 6-9 Variation with time of the error of the fit for model C applied to the REBC sample exposed to 0.1 M NaCl at 60°C.

The coating properties, R_{po} and Q_c and P_c, are plotted in Figure 6-10[2] and Figure 6-11, respectively. It can be seen from these figures that continued exposure to NaCl solution decreases the R_{po} and increases the Q_c of the REBC samples. The changes are larger at elevated temperatures. For example, R_{po} decreases by four orders of magnitude at 60° and by one order of magnitude at room temperature. This is another indication that solution is entering the pores of the coating, and the higher the temperature, the higher is the mobility of ions. The CPE terms, P_c and Q_c, were previously related to the non uniformity of the coating, in terms of pore depth and electrolyte content. When these values stop changing, this indicates that there are no more physical or chemical changes occurring inside the coating.

[2] The discontinuity in Figure 6-10-a corresponds to an anomalous jump in the data at this time.

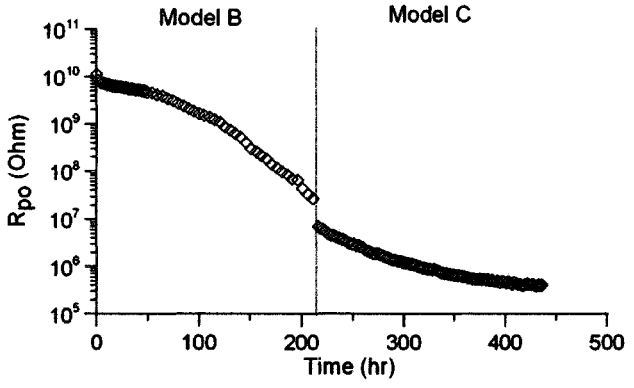

(a) Room temperature[3]

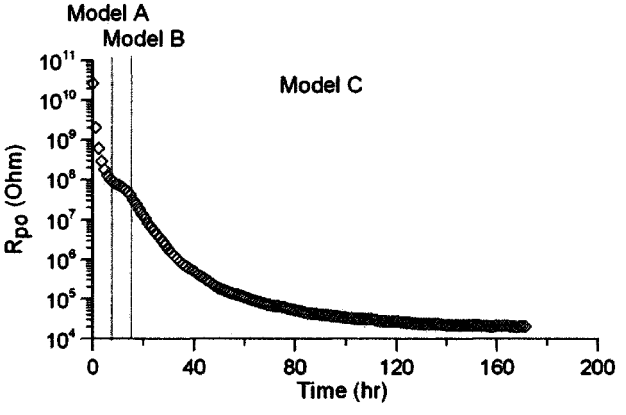

(b) 40°C

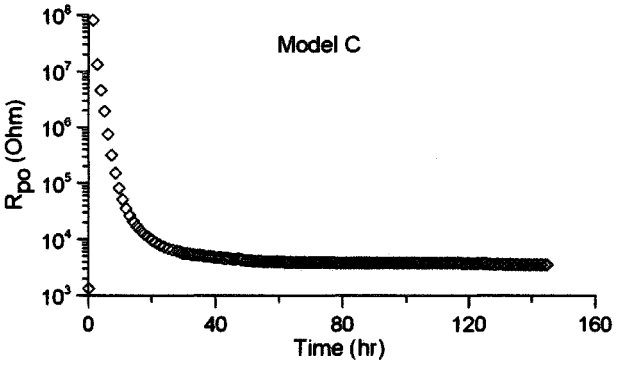

(b) 60°C

Figure 6-10 The change with time in R_{po} of the REBC samples exposed to 0.1 M NaCl solution at various temperatures.

[3] The discontinuity corresponds with an anomalous discontinuity in the data at this time.

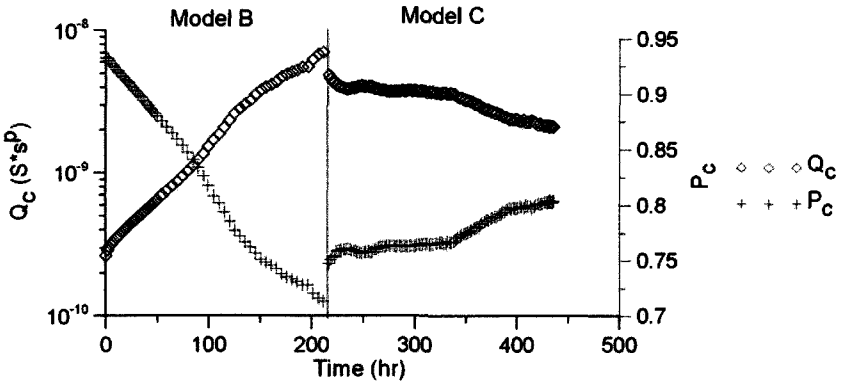

(a) Room temperature[4]

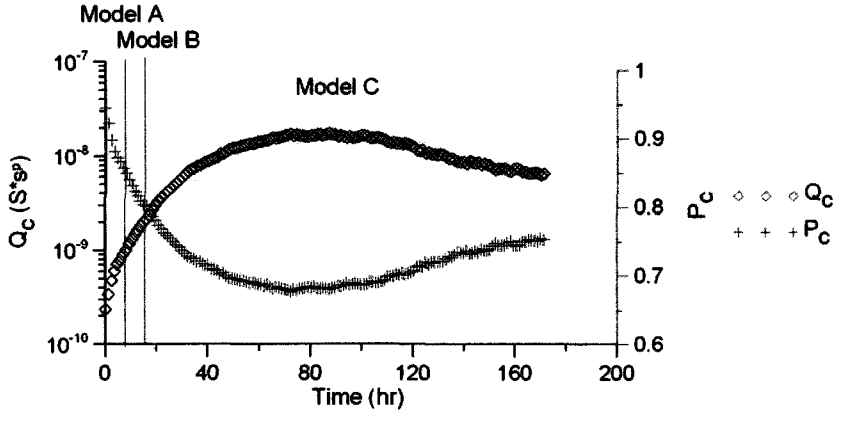

(b) 40°C

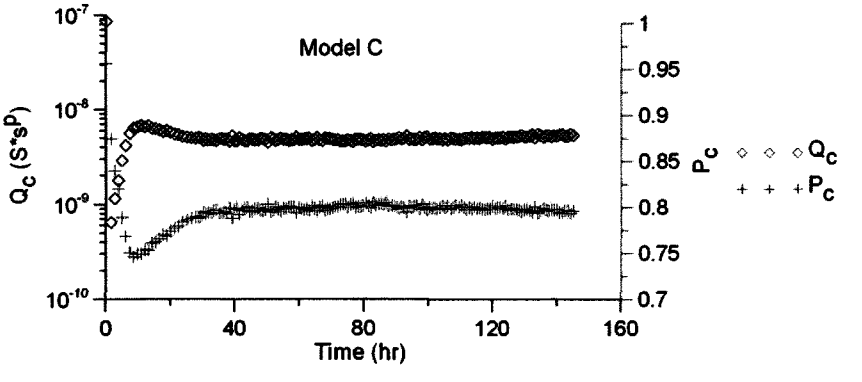

(b) 60°C

Figure 6-11 The change with time in Q_c and P_c of the REBC samples exposed to 0.1 M NaCl solution at various temperatures.

---

[4] The fitting was complicated by an anomalous change in the data close to the point where the models changed. Ideally, the curves would be smoother with a shape similar to that shown in (b) and (c).

6.2.2. Test 2: Coating from Test 1 Exposed to 0.1 M NaCl and then pH 1 H_2SO_4.

In this test, the coating samples from test 1, which had been continuously exposed to a 0.1 M NaCl solution at three different temperatures, were exposed to a new solution that contained 0.1 M NaCl plus sulphuric acid (pH = 1). In these experiments, the coating blistered (Figure 6-12) and ultimately failed (Figure 6-13). The changes in the modulus of the impedance and the phase angle of these REBC samples with time are shown in Figure 6-14 and Figure 6-15, respectively. As expected, the starting values of these parameters are very close to the final values obtained at the end of test 1[5], the exposure to 0.1 M NaCl.

It was observed that the modulus of the impedance and the phase angle remained relatively constant for all test frequencies until the coating samples failed, marked by the discontinuities in the plots. Prior to failure, gas had accumulated under the coatings and caused a blister to form. Gas formation and accumulation was indicative of electrochemical activity on the metal plate surface, and also indicative of complete penetration of the electrolyte through the coating. The REBC samples failed after pressure had built up under the coating, eventually tearing the sample near the o-ring of the Tait cell (Figure 6-12, and Figure 6-13). The time to failure was shorter at elevated temperatures: 84 hours at room temperature, 25 hours at 40°C and 11 hours at 60°C. After failure, as illustrated in Figure 6-14, the Zmod values dropped sharply, by several orders of magnitude for some frequencies.

---

[5] For the test performed at 40°C, the gap in the plots from the first scan until the 17 hour mark was caused by a computer malfunction.

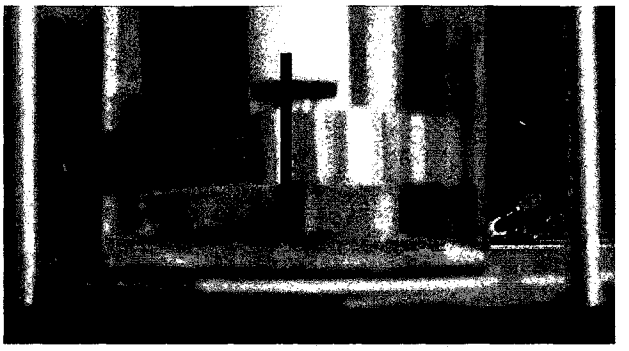

Figure 6-12 Digital image of blister caused by gas formation underneath the REBC during testing.

Figure 6-13 Close up of the REBC after failure, note the gas bubble still visible at the tear in the coating.

The lack of a significant change in the plots of the modulus of the impedance and of the phase angle before the failure of the REBC samples indicates that the sulphuric acid did not noticeably degrade the coating. The acid initiated electrochemical activity on the surface of the metal plate. This implies that the sulphuric acid used the path thru the coating, already forged by the sodium chloride during saturation of the sample in test 1. The REBC samples were no longer protecting the substrate. In fact the NaCl, that already filled the pores from test 1, can act as a salt bridge, transferring charge from the metal electrode under the coating, to the bulk solution containing sulphuric acid above

the coating. It follows that it is not strictly necessary for the sulphuric acid itself to penetrate the coating, in order for there to be an electrochemical reaction at the electrode.

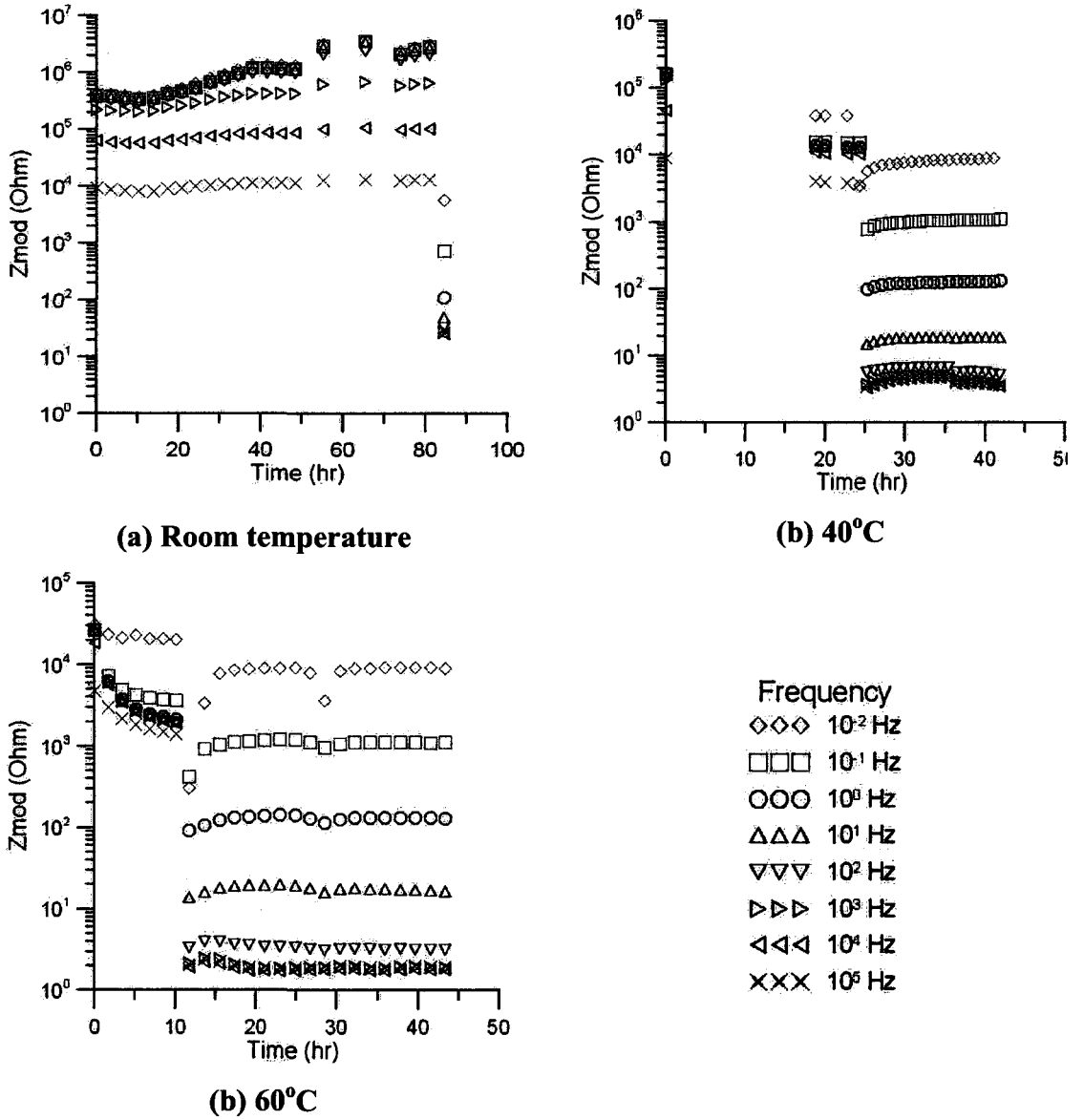

(a) Room temperature

(b) 40°C

(b) 60°C

Figure 6-14 Change with time of the modulus of the impedance of the REBC samples exposed to 0.1 M NaCl then sulphuric acid (pH 1) at various temperatures. Step discontinuities correspond to coating failure.

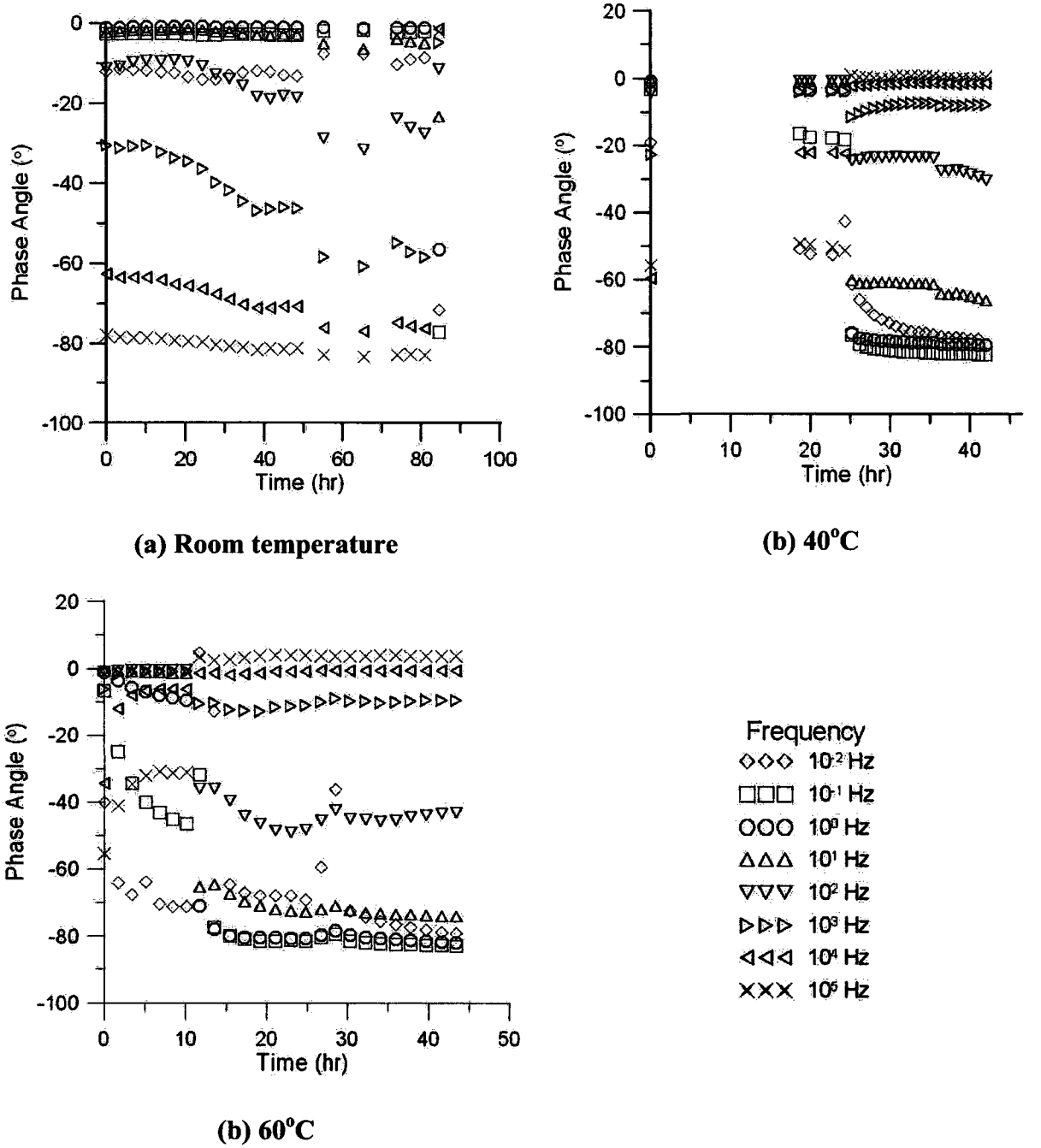

Figure 6-15 Change with time of the phase angle of the REBC samples exposed to 0.1 M NaCl then sulphuric acid (pH 1) at various temperatures. Discontinuities indicate the time when the coating was breached by tearing.

The results of the equivalent circuit modelling are summarized in Table 6-4.

Table 6-4 Summary of the equivalent circuit modelling results of the REBC in test 2.

Parameter	60°C	40°C	Room Temperature
Time to failure (hours)	11	25	84
Maximum % Error of Fit	17.1	12.2	24.3
Average % Error of Fit	6.0	7.4	6.7
R_{po} at the start of test (Ohms)	$2.7x10^{4}$	$1.7 x10^{5}$	$3.6 x10^{5}$
R_{po} at failure (Ohms)	$1.9 x10^{3}$	$1.3 x10^{4}$	$2.6 x10^{6}$
Q_c at the start of test	$4.1 x10^{-9}$	$2.7 x10^{-9}$	$2.2 x10^{-9}$
Q_c at failure	$6.0 x10^{-9}$	$6.1 x10^{-9}$	$8.4 x10^{-10}$
R_{sol} after failure (Ohms)	1.8	5.0	8.7
Model(s) used	C,A	C,D	C,D

At room temperature and at 40°C, equivalent circuit models C (Figure 6-4) and D (Figure 6-5) were identified as the circuits that fit the EIS data most accurately for different stages of the tests. As previously described, model C represents the coating and the metal plate after the NaCl solution has passed through and reached the metal plate; it represents the coating at the beginning of test 2. At 60°C, the failed coating was best modelled using model A (Figure 6-2). Although models A and D provide information on the impedance in the vicinity of the metal surface through Q_{ms} and P_{ms} terms, only the coating properties represented by the R_{po}, Q_c, and P_c terms, are presented here.

In all models, the error of the fit was generally less than 10%, however, increases in the error of the fit were observed after the coating failed. An example of an error plot is presented for the test at room temperature in Figure 6-16.

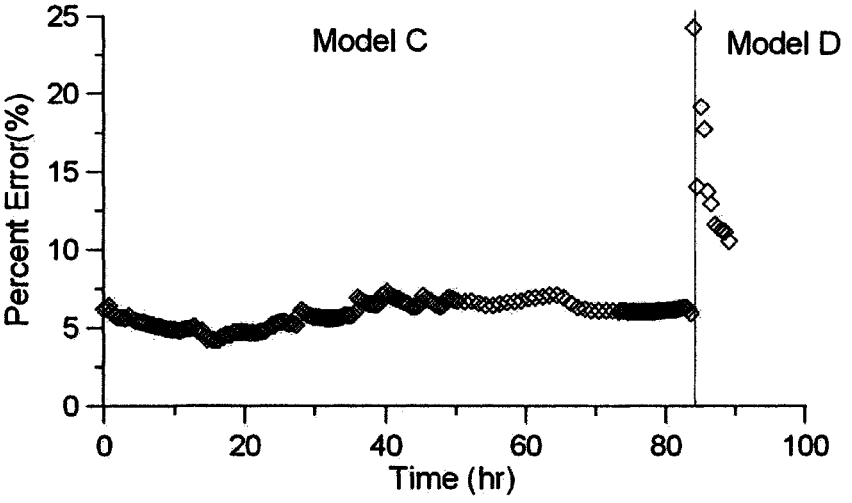

Figure 6-16 Variation with time of the error of the fit for models C and D applied to the REBC sample exposed to 0.1 M NaCl then pH 1 sulphuric acid at room temperature. The change from C to D is when tearing of the coating occurs.

As illustrated in Figure 6-17 at room temperature, the parameter which represents the coating resistance, R_{po}, increased over the course of the test prior to failure. This may arise from the oversimplicity of the model. There are probably unaccounted effects of the gas pressure building up beneath the coating. It is very unlikely that there is a chemical reaction between the sulphuric acid and the coating. At room temperature, as demonstrated in test 1, the rate of penetration of the solution into the coating was relatively slow. At 60°C, where the kinetics of diffusion are faster, the R_{po} term decreased over time.

As illustrated in Figure 6-18, Q_c decreased with time at room temperature, while at 60°C it increased. In the same plots for the 40°C and 60°C tests, the R_{po} term decreased, and the Q_c term increased. The erratic fluctuations of the value of the P_c term in the room temperature test may indicate that the solution had difficulty penetrating into the pores at low temperatures.

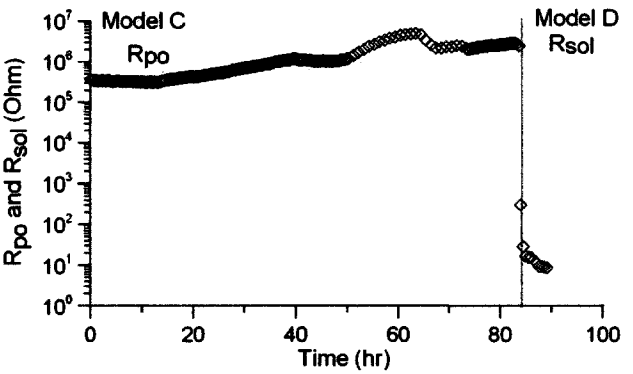

(a) Room temperature

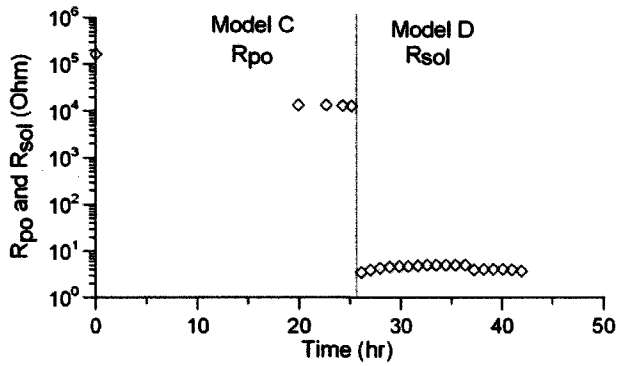

(b) 40°C

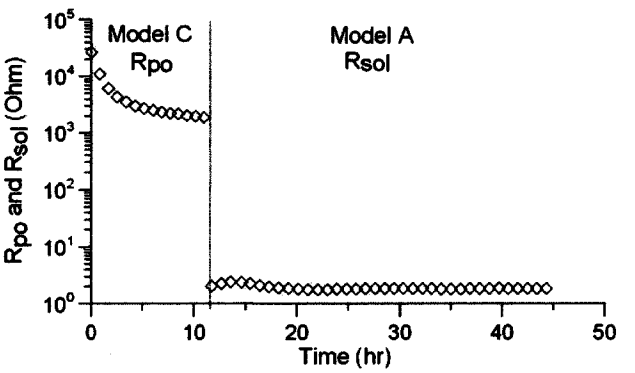

(c) 60°C

Figure 6-17 The change with time in R_{po} for the REBC samples exposed to 0.1 M NaCl then sulphuric acid (pH 1) at various temperatures.

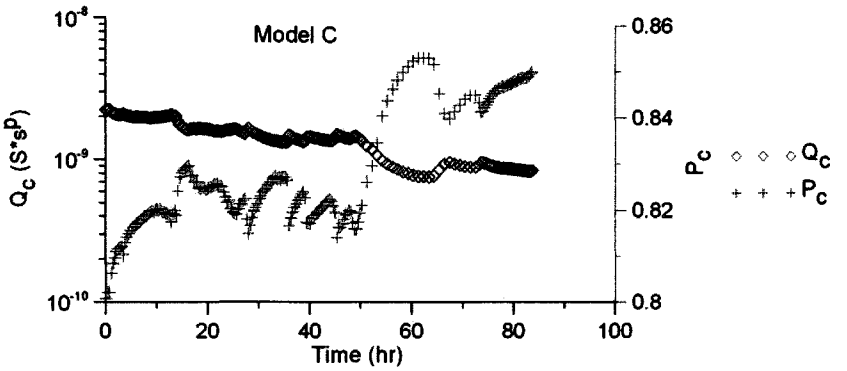

(a) Room temperature

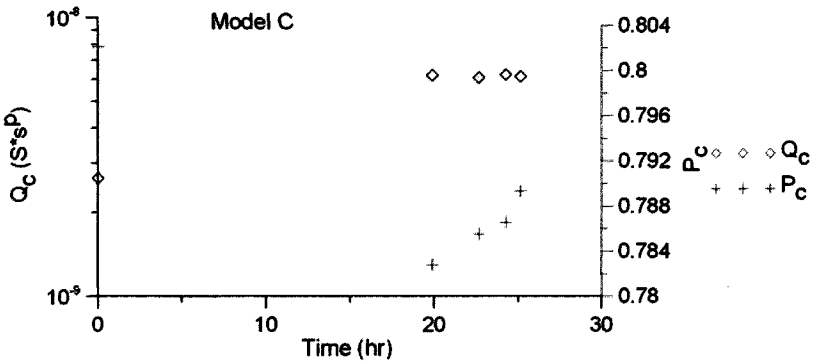

(b) 40°C

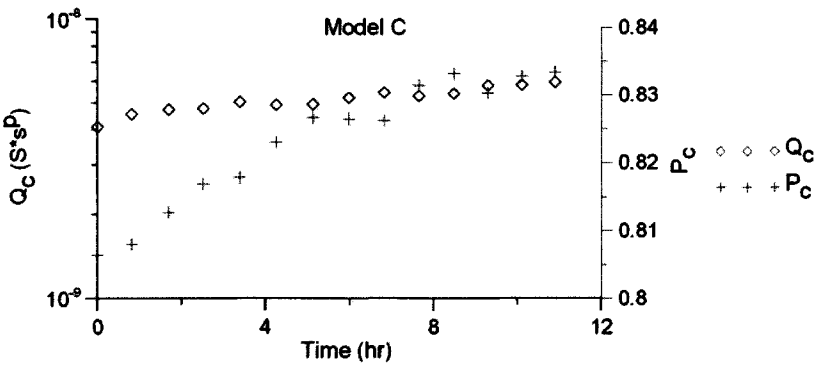

(c) 60°C

Figure 6-18 The change, at various temperatures, in Q_c and P_c of the REBC samples exposed to 0.1 M NaCl then sulphuric acid (pH 1) solution.

6.2.3. Test 3: Coating exposed to 0.1 M NaCl and pH = 1 H_2SO_4

In this test, coatings samples were exposed directly to a solution containing 0.1 M NaCl and sulphuric acid (pH = 1) in a Tait cell. It was observed that the modulus of the impedance at low frequencies decreased by several orders of magnitude starting in the early hours of exposure, while the high frequency values remained relatively constant (Figure 6-19). The behaviour is reminiscent of that observed with the NaCl solution in test 1. After a certain period of exposure time, coatings at all temperatures failed in a similar manner to that observed in test 2, *i.e.*, pressure-induced tearing due to gas formation on the metal plate under the coating. The time to failure was 100 hours at room temperature, 39 hours at 40°C and 21 hours at 60°C. These times are longer than in test 2, but the pores were not already filled with a conductive electrolyte, as was the case in test 2. After the failure of the coatings, all Zmod measurements remained fairly constant.

Phase angle measurements, as illustrated in Figure 6-20, increased towards 0° for most frequencies and for all temperatures, however, this increase was more significant at low frequencies. At room temperature, after 60 hours of exposure, the phase angles at the lowest three frequencies reached 0°. With increasing temperature, the phase angle increased to 0° faster.

The behaviour of the coating samples in test 3 was quite similar to the combined behaviour of the coating observed in tests 1 and 2. For example, at room temperature, when the coating was exposed to NaCl solution only (test 1), a decrease in impedance measurements and an increase in phase angle over a period of 435 hours was observed. When the same coating was exposed to the acidic solution at room temperature (test 2), it

failed after 84 hours of additional exposure. The coating in test 3 at room temperature, which was directly exposed to the mixture of 0.1 M NaCl and pH 1 acidic solution, experienced a decrease in impedance measurements, as well as an increase in phase angle, and failed after 100 hours, which was longer than the failure time in test 2 but significantly shorter than the combined exposure time of tests 1 and 2. Similar behaviour was observed at 40°C and 60°C. Differences between tests 2 and 3 arise from the preloading of the coating samples' pores for test 2 with NaCl in test 1.

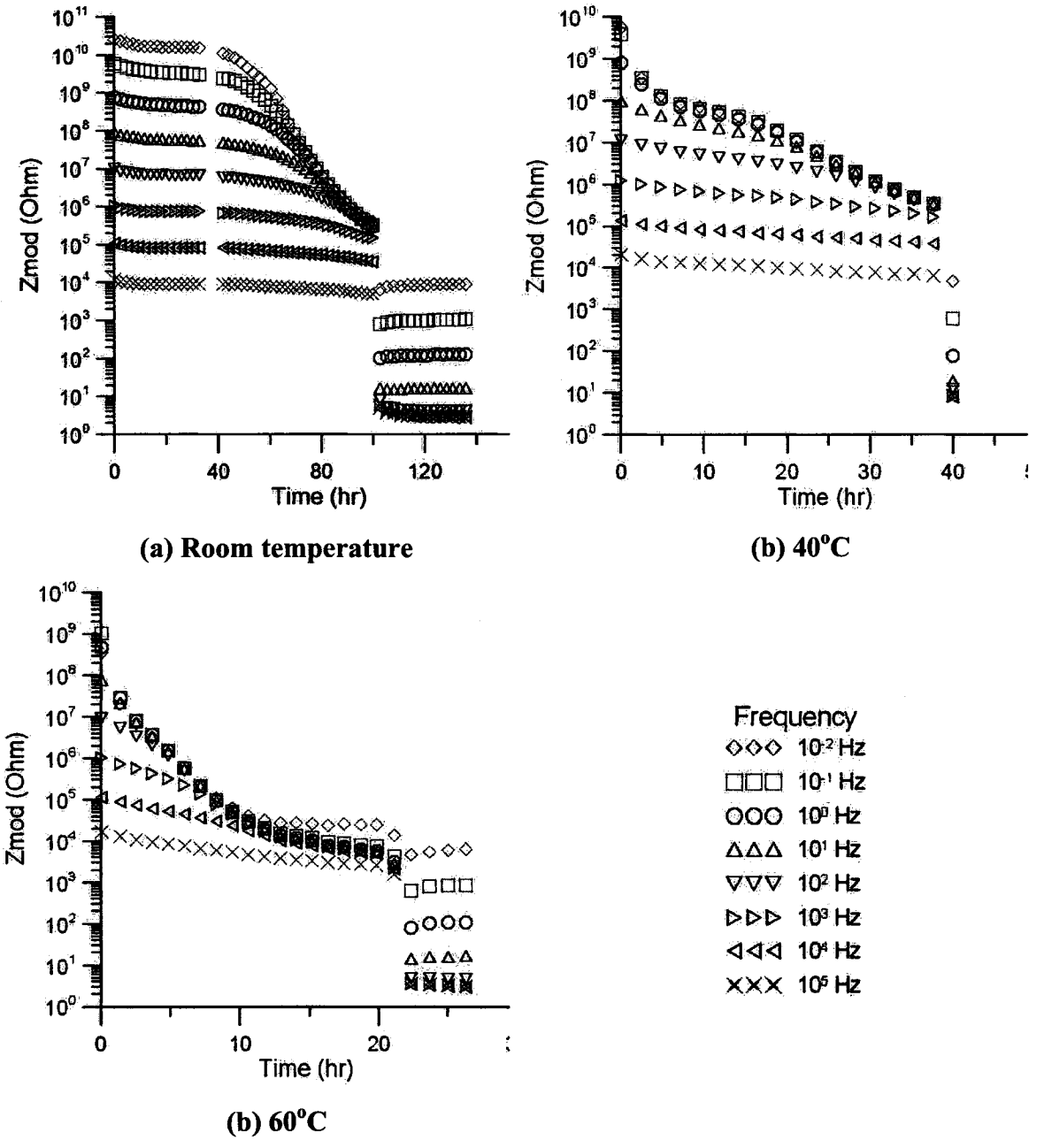

(a) Room temperature

(b) 40°C

(b) 60°C

Figure 6-19 Change with time, at various temperatures, of the modulus of the impedance of the REBC samples exposed to 0.1 M NaCl and sulphuric acid (pH 1) . Discontinuities mark the time of failure of the coating.

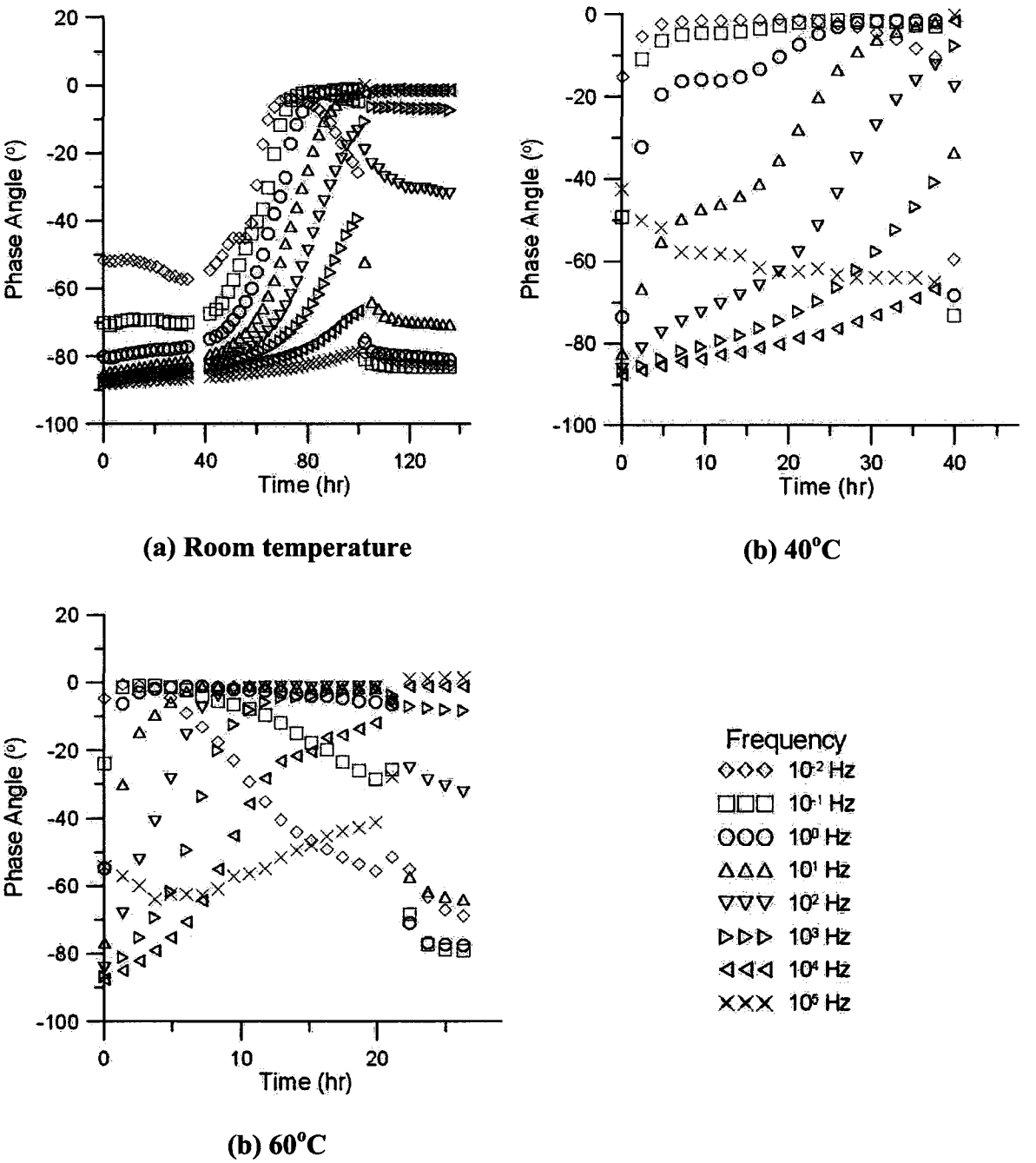

Figure 6-20 Change with time, at various temperatures, of the phase angle of the **REBC samples exposed to 0.1 M NaCl and sulphuric acid (pH 1).**

When compared to direct exposure (i.e., test 3), the saturation of the solution with 0.1 M NaCl solution prior to acid exposure shortened the time to failure by 10 hours at

60°C, 14 hours at 40°C, and by 16 hours at room temperature. These differences in time to failure are a result of the salt-bridge effect with preloaded NaCl solution in the pores.

The results of the equivalent circuit modelling are summarised in Table 6-5. The equivalent circuits used to model each case are also identified in the table. In all models, the error of the fit was generally less than 10%, however, increases in the error of the fit were observed after the coating failed. As illustrated in Figure 6-21, the R_{po} terms at all temperatures had substantial decreases, between 4 and 5 orders of magnitude, prior to the coating failure. This behaviour was similar to the decreases observed in test 1 caused by solution entering the pores of the sample. The behaviour of the Q_c term in test 3 (Figure 6-22) was also very similar to the behaviour seen in test 1. The Q_c term increased at all temperatures, while P_c decreased, as solution entering the coating, magnified the dielectric properties of the coating.

Table 6-5 Summary of the equivalent circuit modelling results of the REBC in test 3

Parameter	60°C	40°C	Room Temperature
Time to failure (hours)	21	39	100
Maximum % Error of Fit	25.0	17.1	23.2
Average % Error of Fit	7.0	9.4	10.8
R_{po} at the start of test (Ohms)	7.7×10^{8}	6.7×10^{9}	3.0×10^{10}
R_{po} at failure (Ohms)	2.7×10^{3}	2.8×10^{5}	2.8×10^{5}
Q_c at the start of test	2.8×10^{-10}	2.4×10^{-10}	2.5×10^{-10}
Q_c at failure	6.7×10^{-9}	4.3×10^{-9}	4.0×10^{-9}
R_{sol} after failure (Ohms)	3.5	10.6	3.1
Model(s) used	C,A	B,C,A	B,C,D

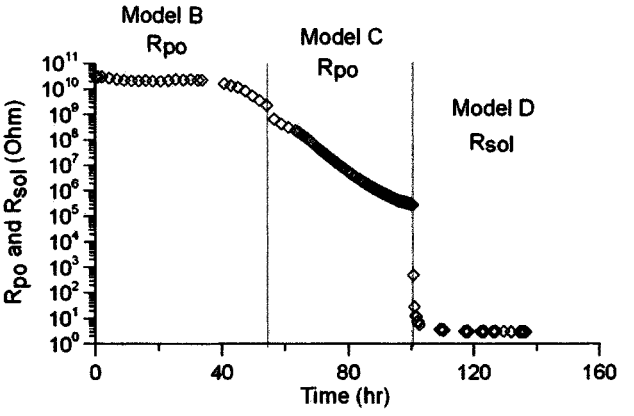

(a) Room temperature

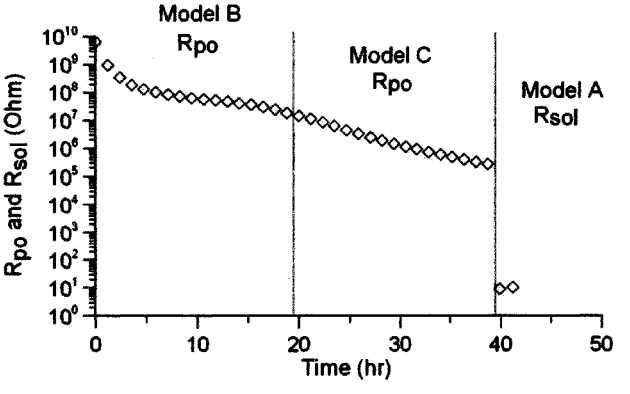

(c) 40°C

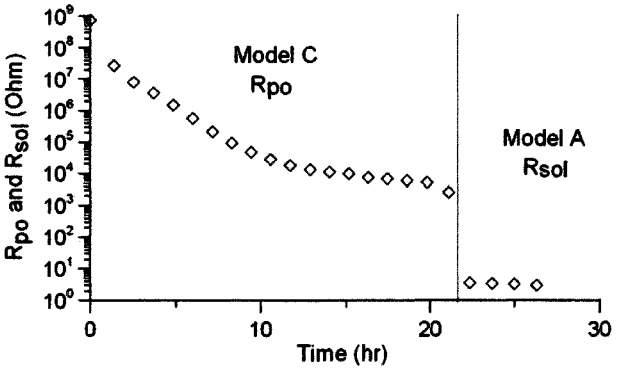

(c) 60°C

Figure 6-21 The change in R_{po} with time, at various temperatures, for the REBC samples exposed to 0.1 M NaCl and sulphuric acid (pH 1).

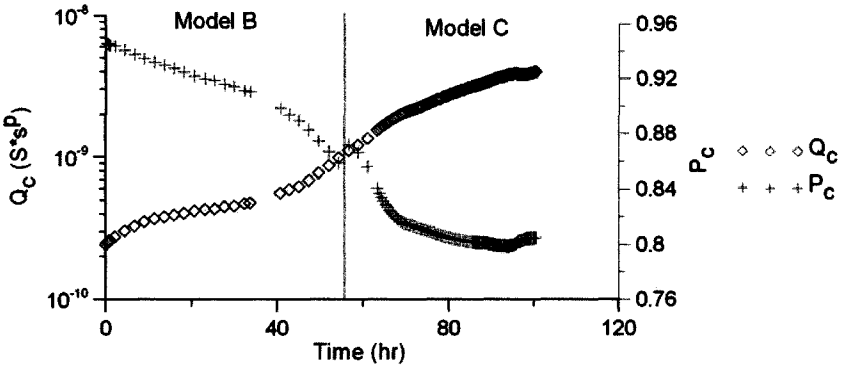

(a) Room temperature

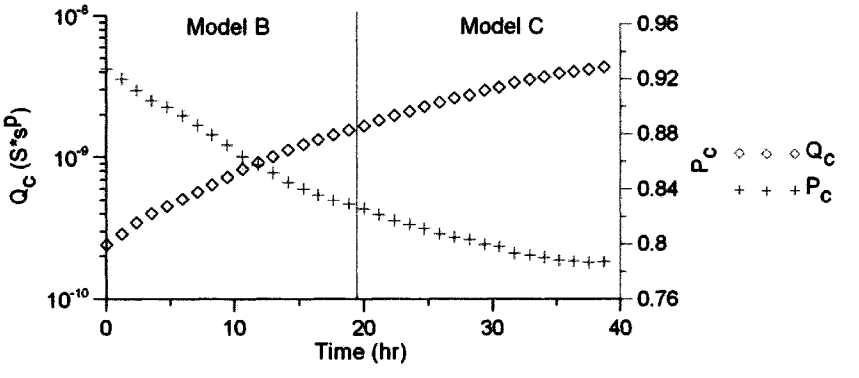

(c) 40°C

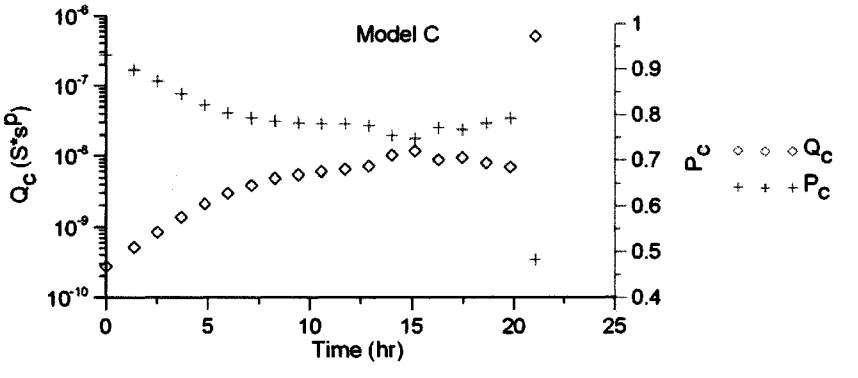

(c) 60°C

Figure 6-22 The change in Q_c and P_c with time, at various temperatures, for the REBC exposed to 0.1 M NaCl and sulphuric acid (pH 1).

6.2.4. Test 4: Coating Exposed Directly to H_2SO_4 at pH 1

In this test coating samples were exposed to a solution of only sulphuric acid at a pH of 1. The tests were performed at temperatures of 40°C and 60°C. A large step change in the data corresponded to failure of the coating. The plots of the modulus of the impedance are illustrated in Figure 6-23. These show the same trends observed in tests 1 and 3: as solution entered the coating there was a rapid decrease in the low frequency modulus of the impedance, accompanied by an increase in the phase angle, as shown in Figure 6-23 and Figure 6-24. The changes in Zmod and phase angle were larger at the higher temperature (60°C).

After a time, coatings at both temperatures failed in a similar manner to that observed in tests 2 and 3, *i.e.*, pressure-induced tearing that followed gas formation between the metal electrode and the coating. The times to failure in this case were 29 hours at 40°C and 7 hours at 60°C; 14 and 10 hours faster at 60°C and 40°C, respectively, than in test 3. The pure sulphuric acid solution was more efficient in causing failure than the mixture of sulphuric acid and sodium chloride. This could be because the sodium chloride is only an indirect path for ion transport to the acid, and/or the sodium chloride decreases the direct access of the acid through the pores.

The equivalent circuit modelling results are summarized in Table 6-6. The equivalent circuits used to model each case are also identified in the table. In all models, the error of the fit was generally less than 10%, however, increases in the error of the fit were observed after the coating failed. As illustrated in Figure 6-25, the variation of the R_{po} term was consistent with the previous tests, decreasing in value as solution entered the coating. Similarly, the Q_c term showed an increase over time at both temperatures as

dielectric effects in the coating were increased when electrolyte entered the pores (Figure 6-26).

Table 6-6 Summary of the equivalent circuit modelling results of the REBC in test 4.

Parameter	60°C	40°C
Time to failure (hours)	7	29
Maximum % Error of Fit	27.4	20.5
Average % Error of Fit	10.0	13.7
R_{po} at the start of test (Ohms)	$1.4x10^{9}$	$8.7x10^{9}$
R_{po} at failure (Ohms)	$3.3x10^{4}$	$4.6x10^{6}$
Q_c at the start of test	$3.6x10^{-10}$	$2.3x10^{-10}$
Q_c at failure	$7.6x10^{-9}$	$3.1x10^{-9}$
R_{sol} after failure (Ohms)	1.9	4.3
Model(s) used	C,A	B,D

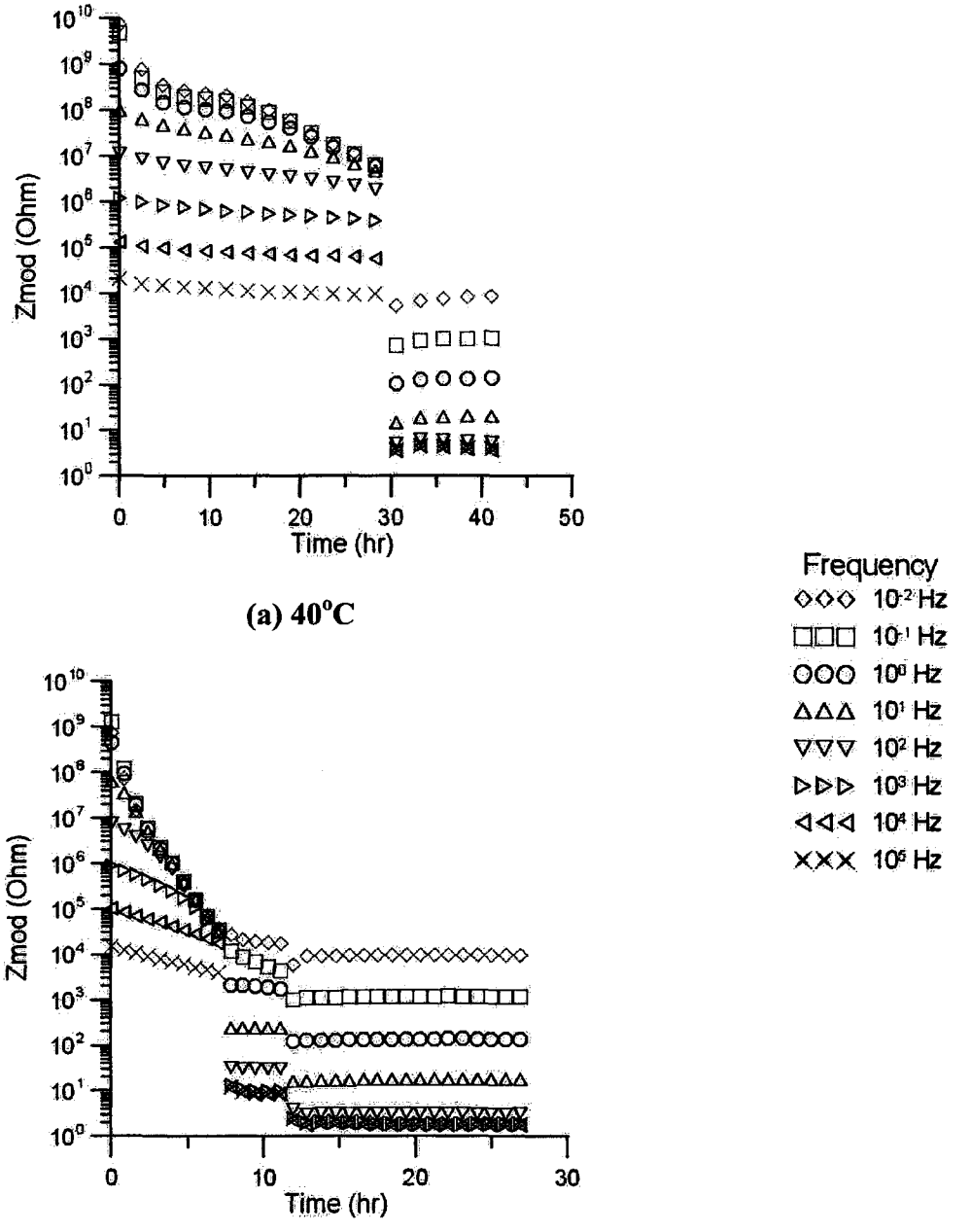

(a) 40°C

(b) 60°C

Figure 6-23 Change with time at various temperatures of the modulus of the impedance for the REBC samples exposed to sulphuric acid (pH 1).

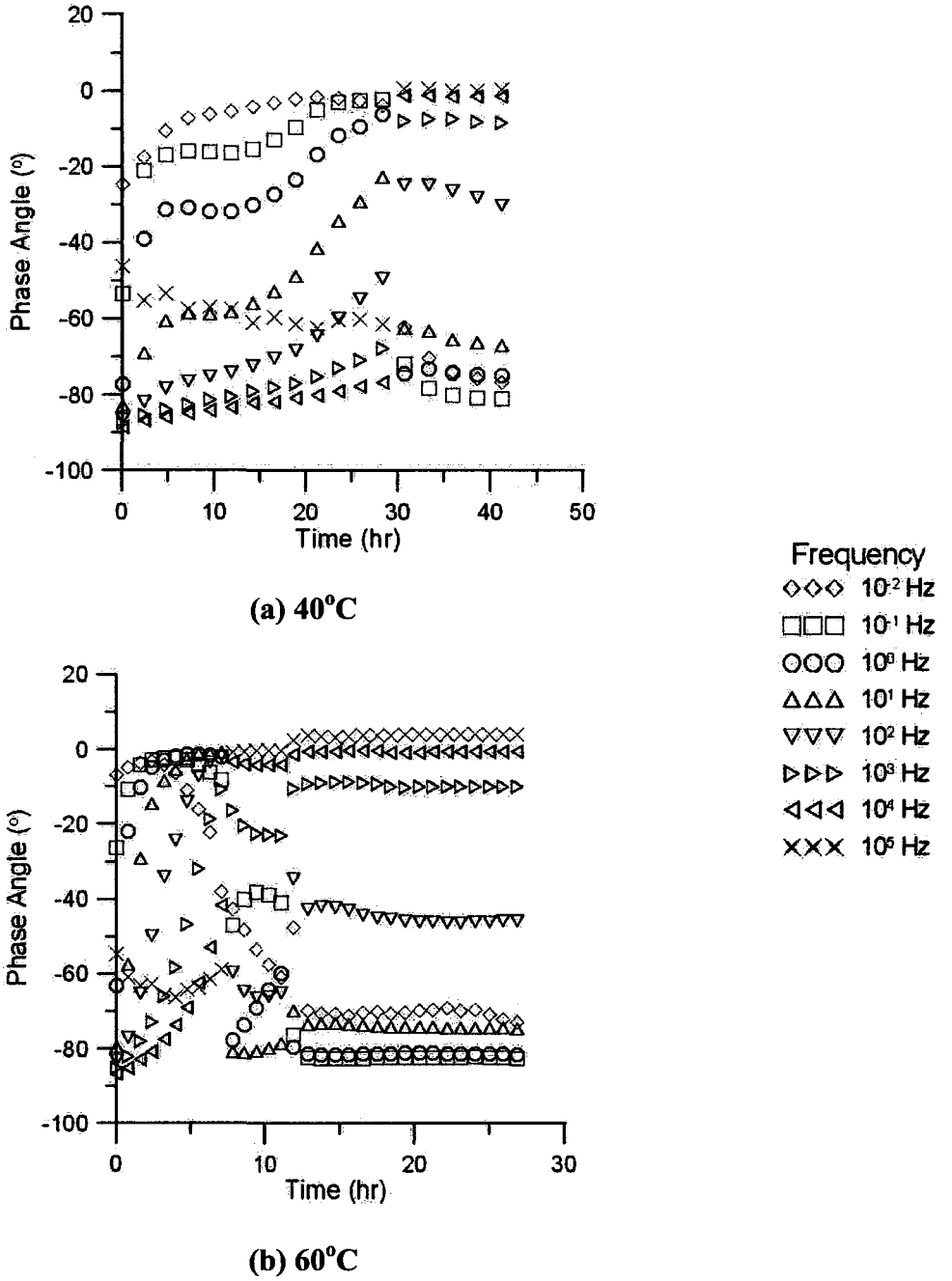

(a) 40°C

(b) 60°C

Figure 6-24 Change with time at various temperatures of the phase angle for the **REBC samples exposed to sulphuric acid (pH 1).**

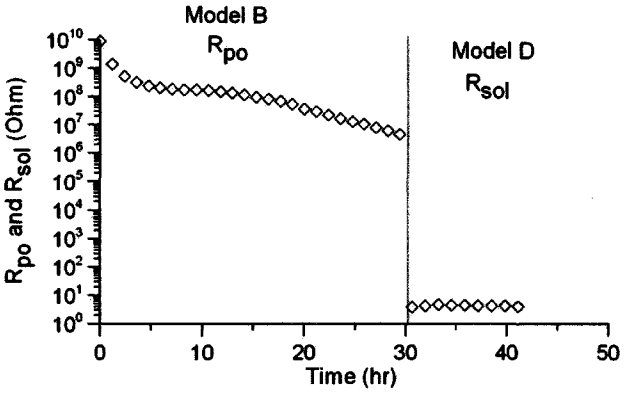

(a) 40°C

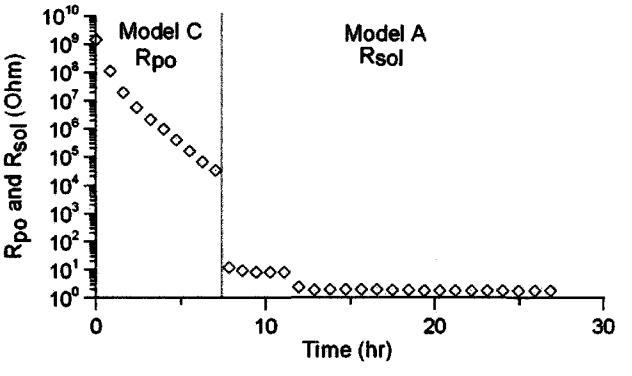

(a) 60°C

Figure 6-25 The change with time at various temperatures in R_{po} for the REBC samples exposed to sulphuric acid (pH 1).

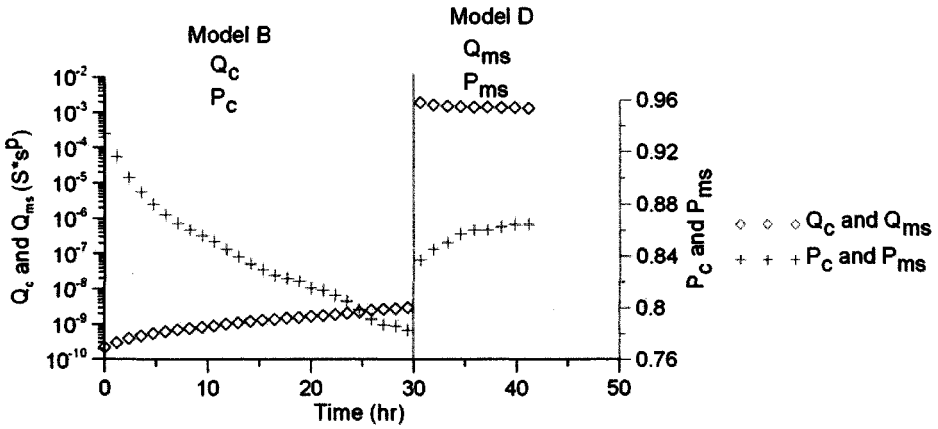

(a) 40°C

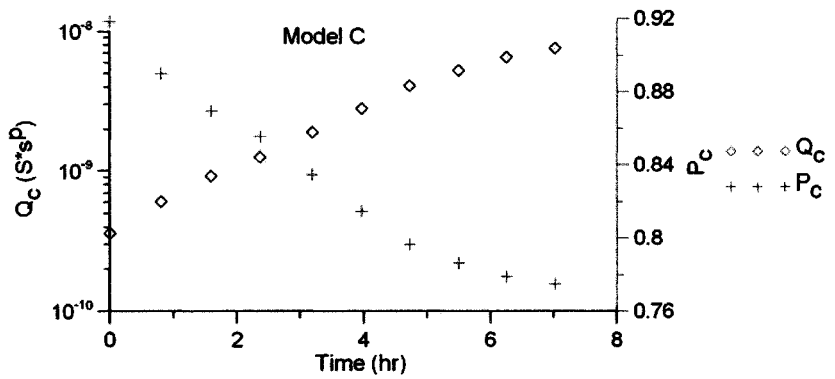

(b) 60°C

Figure 6-26 The change with time at various temperatures in Q_c and P_c for the REBC samples exposed to sulphuric acid (pH 1).

6.3. Effects of Bonding between the Coating and the Base Plate

To study if bonding to the metal substrate would make any difference to the results, additional tests were conducted on the REBC. In this setup, the manufacturer of the coating prepared the samples by applying the coating on metal plates using their product specifications. These samples were investigated in 0.1 M NaCl Solution (test 1) at 40°C

and 0.1 M NaCl plus pH 1 Sulphuric Acid (test 3) at 60°C. The results of the tests are presented here.

6.3.1. Exposure to 0.1 M NaCl Solution (test 1) at 40°C

The thickness of the bonded sample is provided in Table 6-7. Figure 6-27 and Figure 6-28 show respectively the variation of the modulus of the impedance and the phase angle of both the free-film and the bonded coating samples with time. It can be seen that the general behaviour of Zmod and phase angle in both cases are very similar. The modulus of the impedance showed a significant decrease in the low frequencies, indicating the solution was entering the coating. Similarly, the low frequency phase angle climbed towards zero from -90°. In both cases, Zmod values reached a stable level between 10^4 to 10^5 Ohms after 40-60 hours of exposure. Obviously, the rate at which the solution enters the coating is not affected by the substrate conditions.

Table 6-7 Thickness of bonded sample.

	Mean	Standard deviation	Units
Metal thickness	1.37	0.071	mm
Metal and coating thickness	2.40	0.17	mm
Coating thickness	1.03		mm

These observations were also confirmed with equivalent circuit modelling, as illustrated in Figure 6-29 and Figure 6-30. The R_{po} term of the bonded coating behaves in a very similar manner to the R_{po} term of the free film coating. They both have drastic decreases over approximately the same period of time and reach approximately the same value. This indicates that solution is entering the coating regardless of the substrate conditions. Although the shapes of the plots for the variation of Q_c with time were

somewhat different for bonded and free-film coatings (Figure 6-30), it is thought that this difference might be attributed to sample variation.

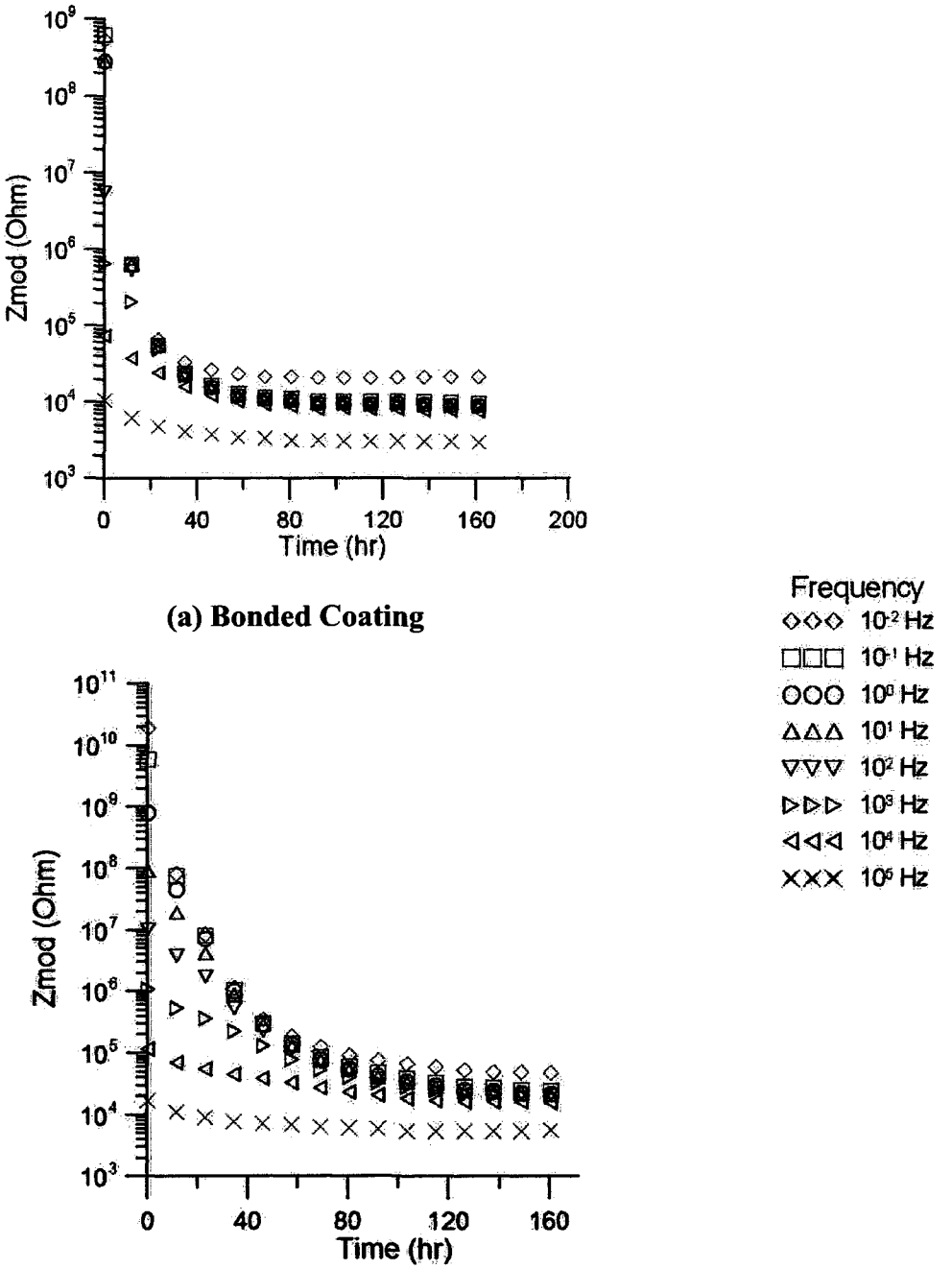

(a) Bonded Coating

(b) Free-film Coating

Figure 6-27 Change of the modulus of the impedance for the REBC, bonded and free-film samples, exposed to 0.1 M NaCl.

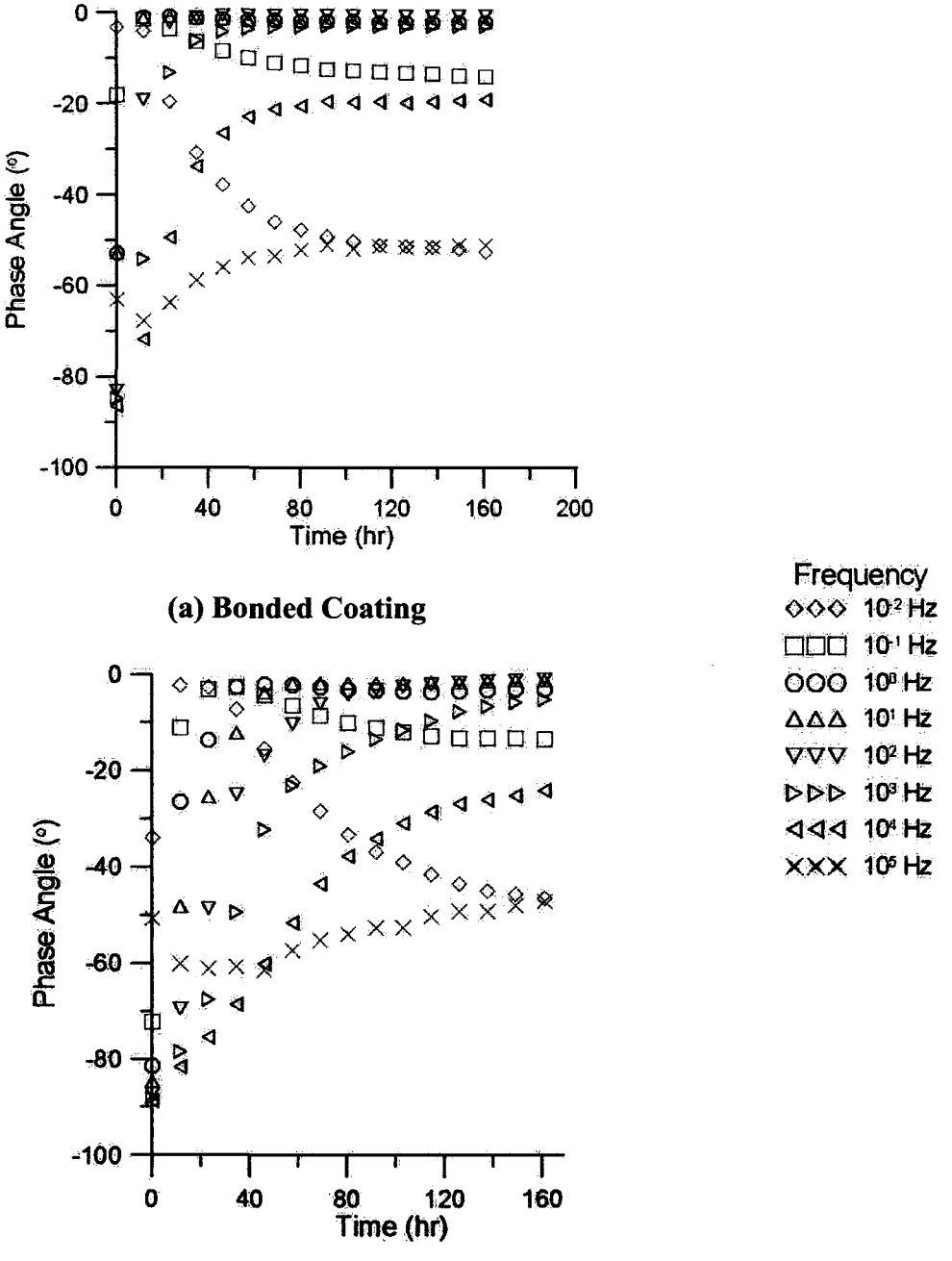

(a) Bonded Coating

(b) Free-film Coating

Figure 6-28 Change of the phase angle for the REBC, bonded and free-film samples, exposed to 0.1 M NaCl.

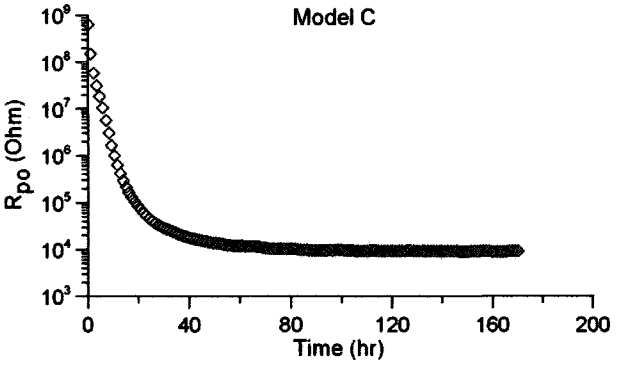

(a) Bonded Coating

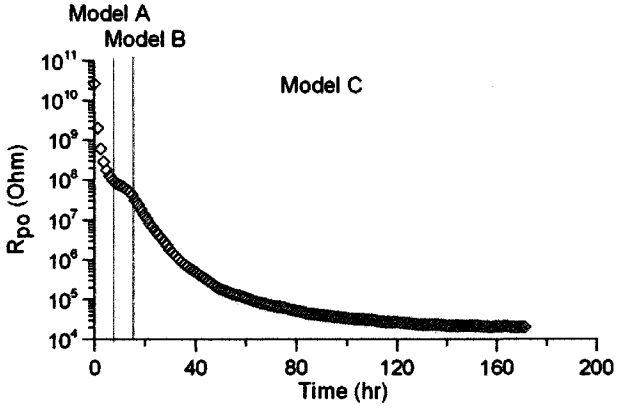

(b) Free-film Coating

Figure 6-29 The change in R_{po} for the REBC, bonded and free-film samples, exposed to 0.1M NaCl.

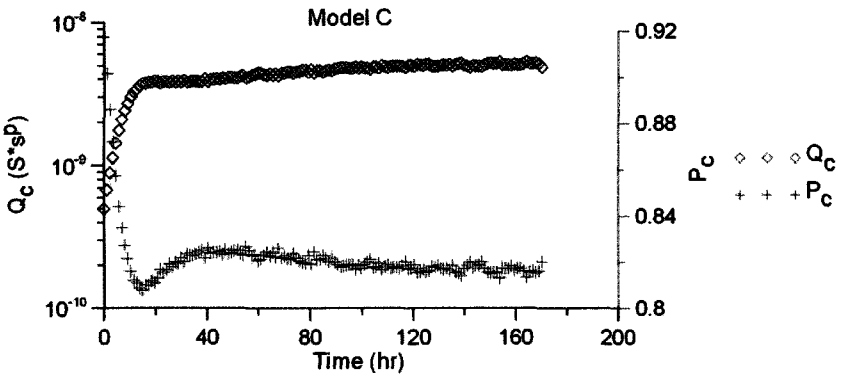

(a) Bonded Coating

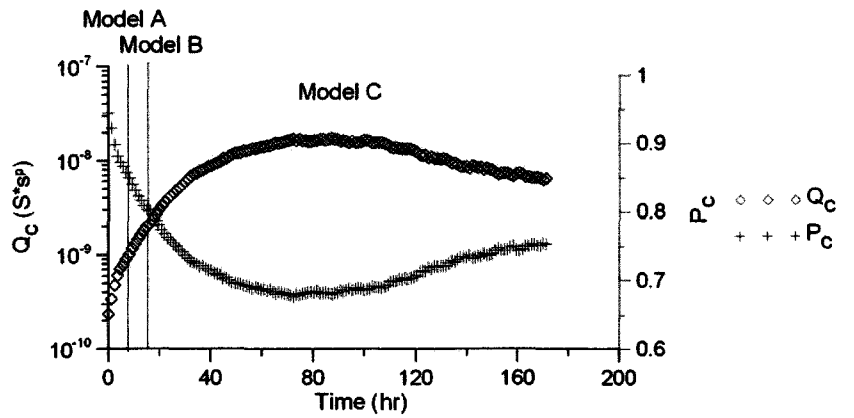

(b) Free-film Coating

Figure 6-30 The change in Q_c and P_c for the REBC, bonded and free-film samples, exposed to 0.1M NaCl.

6.3.2. Exposure to 0.1 M NaCl and pH 1 Sulphuric Acid Solution (test 3) at 60°C

The thickness of the bonded sample is provided in Table 6-8. Figure 6-31 and Figure 6-32 show respectively the variations with time of the modulus of the impedance and the phase angle for the free-film and the bonded-coating samples. The trends observed in the previous section concerning the behaviour of the modulus of the

impedance and phase angle were also observed in this test. The results indicated the ingress of solution into the coating. Although the changes in Zmod and phase angle were slightly faster for bonded samples than for free-film samples, this might be attributable to sample variations, such as variable thickness, and pore sizes of the coatings.

Table 6-8 Thickness of bonded sample.

	Mean	Standard deviation	Units
Metal thickness	1.25	0.026	mm
Metal and coating thickness	2.59	0.088	mm
Coating thickness	1.34		mm

With free-film samples, the typical tear failure in the coating was observed at 21 hours; the modulus of the impedance dropped significantly at all frequencies. The bonded samples did not fail in this manner, although there is a small discontinuity in the bonded-sample data at about 17.5 hours, which could be indicative of a breach in the coating. Although the evidence is that in all REBC samples the solution passed through the coating and reached the metal plate, the bonding of the coating to the metal electrode stopped the formation of a blister due to gas accumulation, thus preventing gross tearing of the coating. Even so, with no obviously visible tear in the coating, the barrier properties of the bonded samples were very low at the end of the test.

These observations were also confirmed with equivalent circuit modelling, as illustrated in Figure 6-33 and Figure 6-34. As shown in Figure 6-33, the R_{po} term of the bonded sample continued to decrease well beyond the resistance at which the free-film tore.

The CPE terms in both tests behaved similarly. For both coatings, there was an initial increase in the Q_c term, attributed to solution entering the coating (Figure 6-34). In

the case of the bonded samples, there was a rapid increase followed by a more gradual one, the latter indicating that the coating barrier was being increasingly penetrated. In the case of the free-film samples, the increase was more gradual and started to slow before the failure occurred.

One can conclude that bonding of the coating to the substrate decreases the degree of damage to the coating, but failure as a chemical barrier still occurs. For the bonded samples, penetrating electrolyte can only contact the metal at the bottom of pores. For the free films, once penetration occurs, there appears to be access to the complete electrode surface.

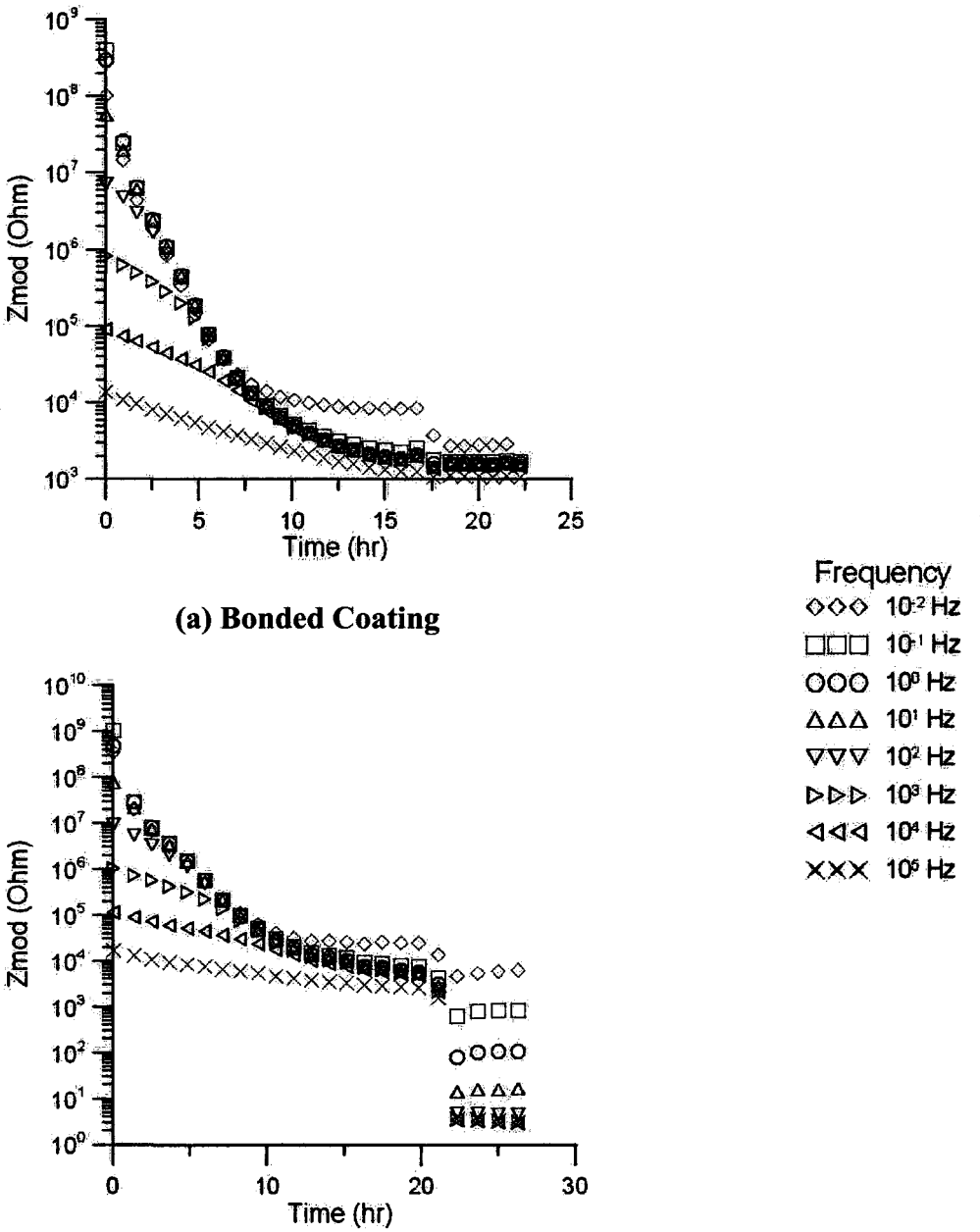

(a) Bonded Coating

(b) Free-film Coating

Figure 6-31 Change of the modulus of the impedance for the REBC samples, bonded and free-film, exposed to 0.1 M NaCl plus pH 1 sulphuric acid.

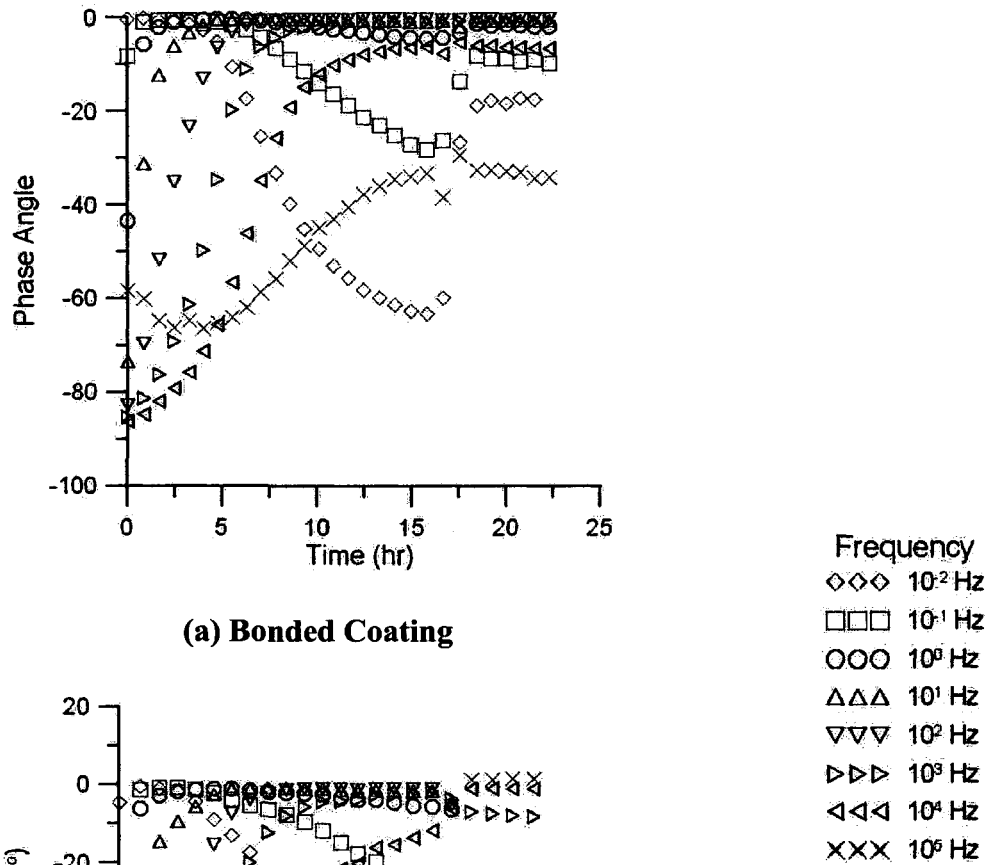

(a) Bonded Coating

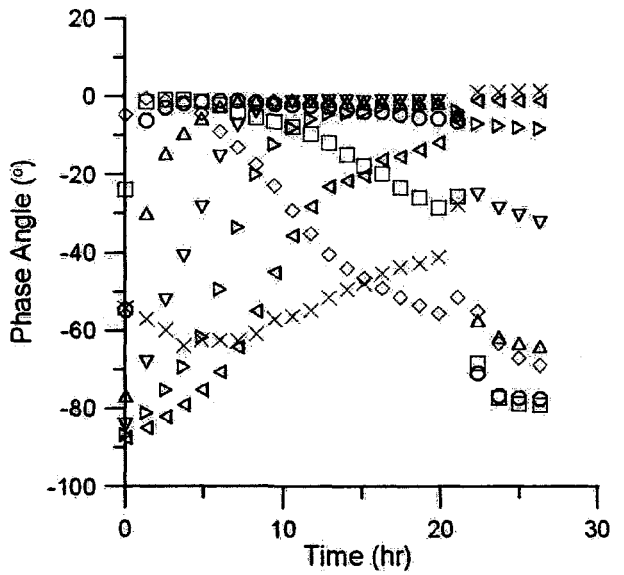

(b) Free-film Coating

Figure 6-32 Change of the phase angle for the REBC samples, bonded and free-film, exposed to 0.1 M NaCl plus pH 1 sulphuric acid.

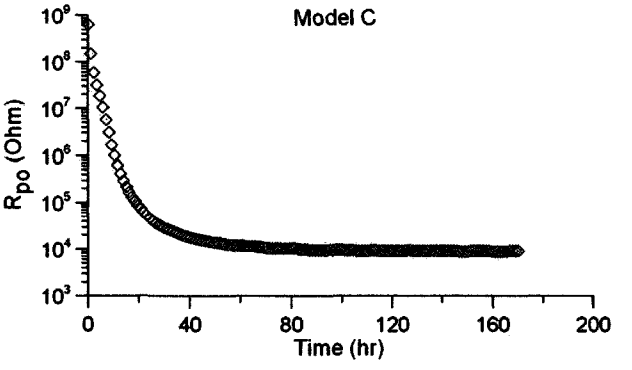

(a) Bonded Coating

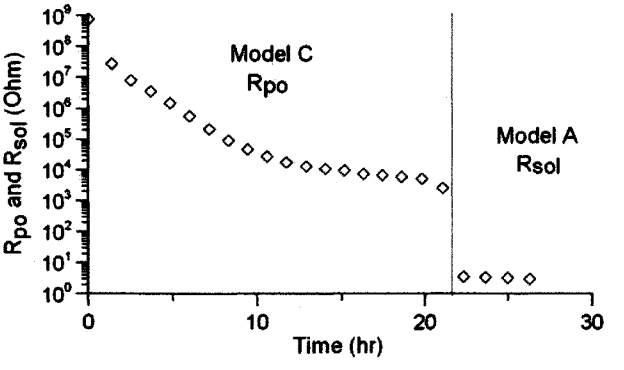

(b) Free-film Coating

Figure 6-33 The change in R_{po} for the REBC samples, bonded and free-film, exposed to 0.1 M NaCl plus pH 1 sulphuric acid.

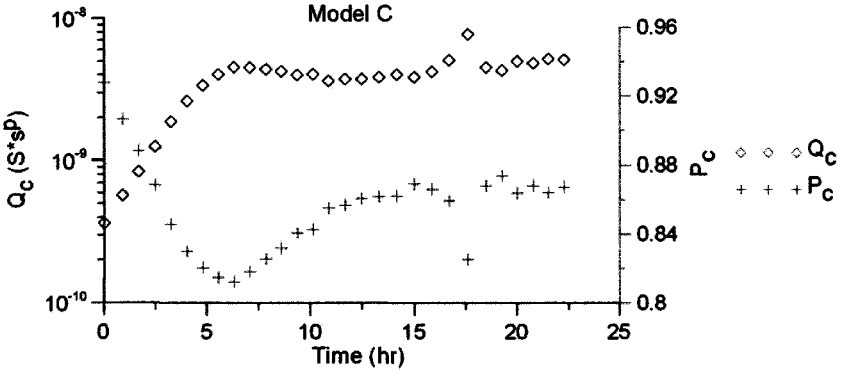

(a) Bonded Coating

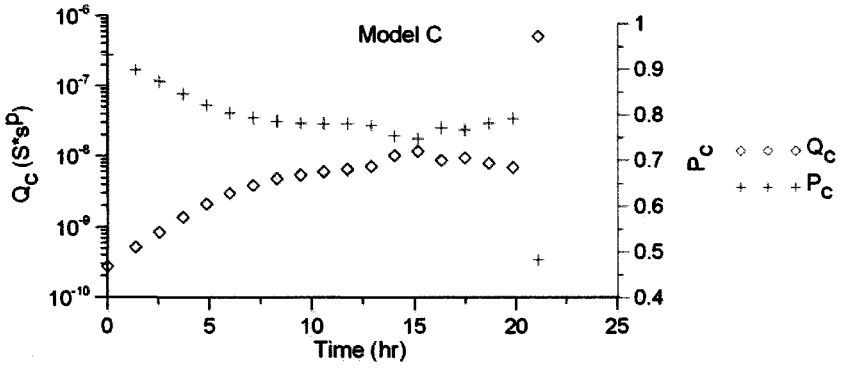

(b) Free-film Coating

Figure 6-34 The change in Q_c and P_c for the REBC samples, bonded and free-film, exposed to 0.1 M NaCl plus pH 1 sulphuric acid.

6.4. Conclusions

- In all tests and at all temperatures, the REBC started off as a high quality capacitor, with an exceedingly high resistivity, but as electrolyte entered the pores, the REBC transformed into a low value resistor. Eventually, the REBC became ineffective as a barrier coating. All of these effects were observable in the EIS spectra.

- When the electrolyte contained only NaCl, the EIS scans of the REBC samples showed that the solution was entering the coating. Since the NaCl solution did not degrade the coating, it can be concluded that a pre-existing network of pores was present in the sample. Though these pores, the NaCl solution was ultimately able to reach the surface of the metal plate.
- The electrolyte containing sulphuric acid caused electrochemical reactions on the metal surface, resulting in gas accumulation under the coating. The REBC samples failed after pressure had built up under the coating, eventually tearing the sample near the o-ring of the Tait cell. After this failure the coating was completely electrically bypassed. This was all observable by EIS
- Temperature played a significant role in the lack of performance of the REBC samples: at elevated temperatures the EIS scans indicated that the rate of ingress of solution into the coating was considerably increased.
- EIS showed that when the REBC samples, which had been previously saturated with the NaCl solution, were exposed to sulphuric acid, it may not be necessary for the sulphuric acid itself to penetrate the coating in order for there to be an electrochemical reaction on the surface of the metal electrode. In fact the NaCl, that already filled the pores, could act as a salt bridge, transferring charge between the metal electrode under the coating, and the bulk solution containing sulphuric acid above the coating.
- EIS measurements did not provide any evidence of a chemical reaction between the sulphuric acid and the REBC. This is in agreement with the traditional use of the REBC on floors where sulphuric acid might be spilled.

- When the REBC was bonded to the metal substrate, despite the solution still accessing the electrode through the pores, there was no evidence of blister formation due to gas accumulation. From this observation, it can be concluded that, in the traditional use of the coating to protect floors against acid spillage, the REBC should be bonded to the floors for best performance.
- The EIS technique is able to track the infiltration of electrolytes into coatings and through coatings. It can observe the time at which complete coating failure occurs.
- The Tait cell proved to be an effective means of performing in-situ EIS scans. The use of coatings that are not bonded to the underlying metal electrode, compared to coatings that are bonded, has significant advantages: lack of bonding accelerates the time to failure and magnifies the degree of failure.

7. Tait Cell Test Results for the PUBC

7.1. Introduction

This chapter focuses on the results of the Tait cell experiments carried out on the PUBC samples. Equivalent circuit modeling was also performed to analyze further the results of these experiments. The same general model used to model the REBC (see Figure 6-1 and Table 6-1) was also used to evaluate the performance of the PUBC samples, however, for the PUBC samples, only one variation of this general circuit, model B (Figure 7-1), was used to model the EIS data.

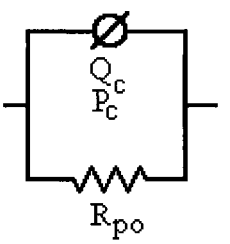

Figure 7-1 Equivalent circuit model B.

7.2. Effects of Temperature and Exposure Solution

In contrast to the REBC, the EIS spectra of the PUBC samples exposed in a Tait Cell to 0.1 M NaCl and 0.1 M NaCl / pH=1 H_2SO_4 solutions at temperatures up to 60°C did not show significant changes with time up to 58 days. In an attempt to see some reaction, additional Tait cell experiments were carried out at room temperature and 60°C using a significantly more aggressive solution containing 60% (vol.) H_2SO_4. The results of these experiments are presented in Section 7.2.3.

During analyses, it was found that high frequency data (range 50.12 to 100 kHz, 4 data points) was erroneous due to artefacts arising from the computer programming of the

Gamry potentiostat. These data points were removed from modeling and fitting of the data, therefore they do not impinge upon the overall experimental results or the conclusions.

7.2.1. Test 1: Exposure to 0.1 M NaCl solution

In this test, the PUBC samples were exposed to a solution of 0.1 M NaCl at room temperature (approximately 25°C), and at 40°C. Figure 7-2 and Figure 7-3, respectively, show the behaviour of the modulus of the impedance and the phase angle for this test. The tests were carried out for 34 days at room temperature (811 EIS scans) and for 58 days at 40°C (1589 EIS scans). Due to the large number of scans performed, only one in every 35 scans at room temperature and only one in every 75 scans at 40°C were plotted.

In the phase-angle plots (Figure 7-3), most data points were close to -90°, and after a short settling period, perhaps due to surface wetting, they remained constant throughout the remainder of the test.

Over the course of this PUBC experiment, in contrast to the REBC experiments, there was no significant change in the modulus of the impedance (Figure 7-2). There is no evidence that the electrolyte entered the coating. The Zmod values ranged from ~10^5 ohms for 10^4 Hz to ~10^{11} ohms for 10^{-2} Hz. As illustrated in Figure 7-2a and Figure 7-2b, changing the temperature did not have any effect on the measurements. If these values are compared with those of the REBC under the same conditions (Figure 6-6), it can be seen that the starting Zmod values of the PUBC are approximately one order of magnitude larger than those of the REBC samples, and also, unlike the REBC, the PUBC did not show any decrease of the modulus of impedance upon continuous exposure.

All the data demonstrate that the PUBC is in fact a very good barrier coating, even at elevated temperatures: there is no ingress of NaCl solution into the coating.

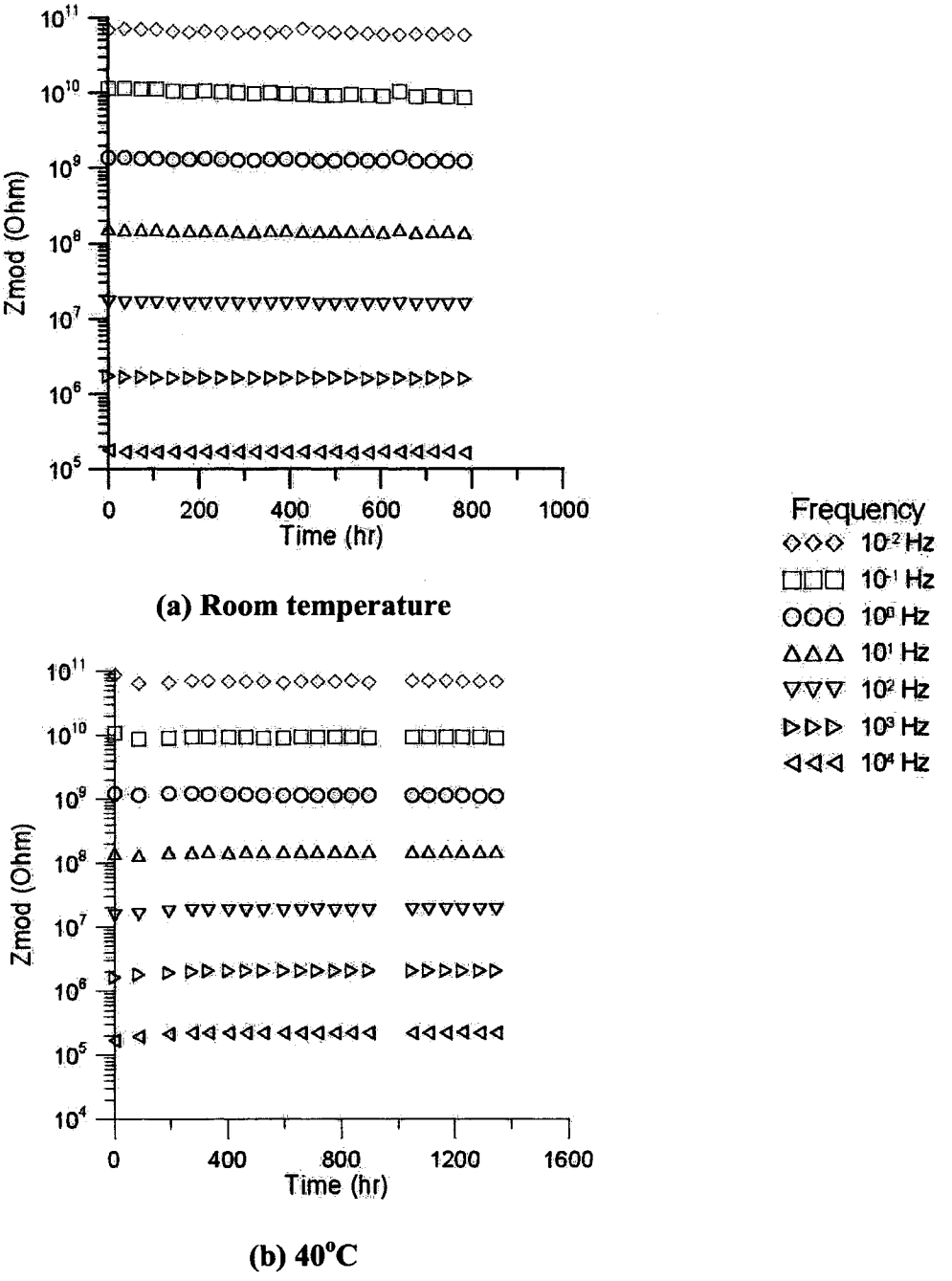

(a) Room temperature

(b) 40°C

Figure 7-2 Change with time of the modulus of the impedance of the PUBC samples exposed to 0.1 M NaCl solution at two different temperatures.

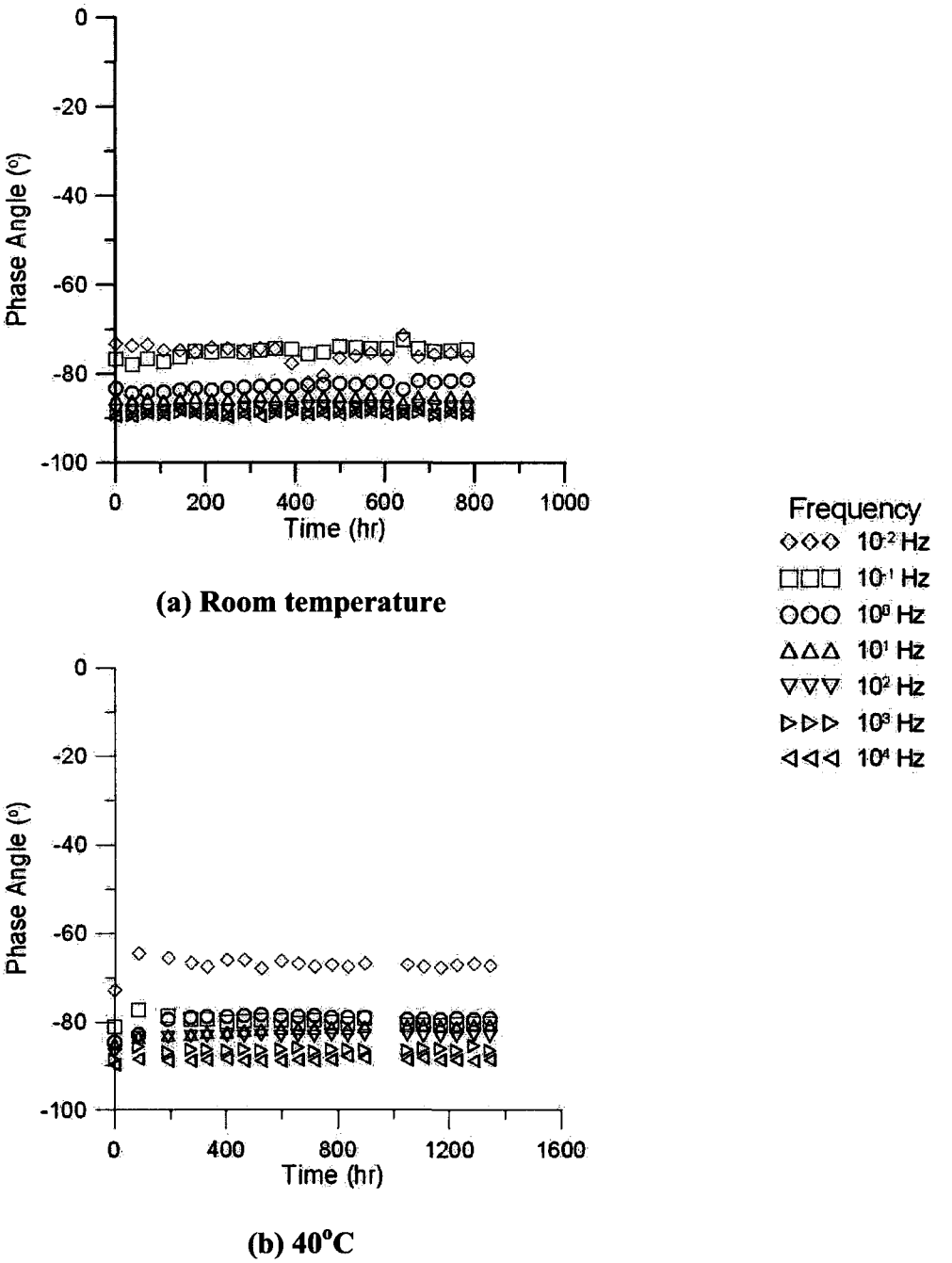

Figure 7-3 Change with time of the phase angle of the PUBC samples exposed to 0.1 M NaCl solution at two different temperatures.

Figure 7-4 shows a typical Bode plot and model-B fit of a PUBC sample exposed to 0.1 M NaCl. This simple model, which only really fits the bulk properties of the coating,

fits most but not all of the EIS data, which is perhaps to be expected because there are no elements for surface features, inhomogeneities, adsorption or chemical reactions. This scan was performed after approximately 370 hours of exposure; however similar behaviour was observed throughout the test. More information on the model fit is provided in Table 7-1. For all practical purposes, Q_c is almost a perfect capacitor. The plot in Figure 7-4 shows a horizontal line for the phase angle at approximately -90°, over the entire frequency range, with the exception of a small hump around 10^{-1} Hz. The log Zmod versus low ω plot is almost a perfectly straight line with a slope of -1. For the most part, this behaviour is very similar to that of a pure capacitor.

Table 7-1 Model B parameters of the PUBC sample exposed to 0.1 M NaCl for approximately 370 hours.

Parameter	Value	± Error	Units
R_{po}	$1.7x10^{11}$	$4x10^{9}$	ohms
Q_c	$1.5x10^{-10}$	$7x10^{-13}$	$S*s^{P}$
P_c	0.96	$6x10^{-4}$	
Goodness of Fit	1.8x10-2		
% Error of Fit	13		

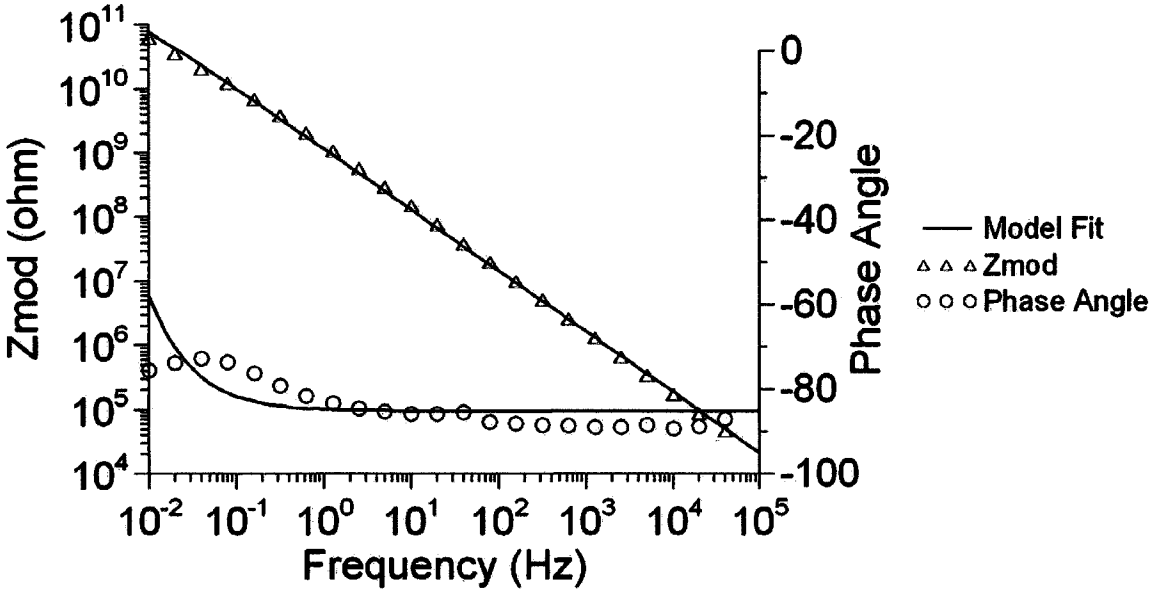

Figure 7-4 Typical Bode plot of the PUBC exposed to 0.1 M NaCl at room temperature, after 370 hours of exposure. Fitted to model B.

The coating properties, R_{po} and Q_c and P_c, are summarized in Table 7-2 Q_c is almost a pure capacitor for which P = 1. Over the course of the experiments, the model predicted small drifts in R_{po}, Q_c and P_c. Basically, Zmod remains constant, but the model has a small amount of redistribution between the in phase and out-of-phase components of the impedance. These drifts may arise from the simplicity of the model, which does not allow for surface effects, wetting and inhomogeneity.

In general, the minor experimental variations in Zmod and phase angle, and the minor model variations in R_{po} and Q_c suggest that the solution did not chemically or physically react with the PUBC. These samples behaved like good barrier coatings.

Table 7-2 Summary of the equivalent circuit modelling results of the PUBC in Test 1.

Parameter	40°C	Room Temperature
Duration of test (hours)	1391	811
Number of scans	1589	800
Maximum % Error of Fit	9	14
Average % Error of Fit	8	13
R_{po} at start of test (Ohms)	$2.8x10^{11}$	$1.6x10^{11}$
R_{po} at end of test (Ohms)	$2.0x10^{11}$	$1.8x10^{11}$
Q_c at start of test	$1.4x10^{-10}$	$1.4x10^{-10}$
P_c at start of test	0.96	0.95
Q_c at end of test	$1.6x10^{-10}$	$1.7x10^{-10}$
P_c at end of test	0.92	0.94
Model(s) used	B	B

7.2.2. Test 3: Coating exposed to 0.1 M NaCl and pH = 1 H_2SO_4

In this test, samples of the PUBC were exposed to a solution of 0.1 M NaCl and sulphuric acid (pH 1) in a Tait cell. Experiments were performed at room temperature, 40°C, and 60°C. The plots of the modulus of the impedance and the phase angle are shown in Figure 7-5 and Figure 7-6, respectively. At 40°C, a software problem prevented the recording of the EIS data for a short period around 800 hours of exposure. At 60°C, after the initial EIS scans stopped, the coating was left in the Tait cell, and additional EIS scans were taken after 1300 hours of exposure.

The plots of the modulus of the impedance and the phase angle of the tests performed at room temperature (Figure 7-5a) and at 40°C (Figure 7-5b) are very similar to those of test 1. They show little or no change throughout the duration of the test.

The test performed at 60°C (Figure 7-5c) behaved differently, but this was subsequently shown to arise from using a sample that was too small for the experimental

configuration. The low frequency plots of the modulus of the impedance showed a rapid drop, by approximately an order of magnitude, over the first several hours of the test. The plots then levelled out for the remainder of the test. In conjunction with this decrease in the low frequency modulus of the impedance, there was an increase in the phase angle at the low frequencies, with the 10^{-2} Hz frequency reaching a phase angle close to zero. This was indicative of a pure resistance at low frequencies. Additional short-term tests, less than 100 hours, were carried out using different PUBC samples to explain this phenomenon. These tests showed that, when the edge of the coating sample was too close to the edge of the o-ring of the Tait cell, the modulus of the impedance and the phase angle were inaccurately measured at low frequencies. There was an electrical conduction path around the edge of the sample. When a larger PUBC sample was used, so that the edges of the coating remained well outside the boundaries of the Tait cell, the measurements were not affected by the edge effect, and emulated the results at room temperature and 40°C.

It was concluded that there was no ingress of solution into the PUBC at temperatures up to 60°C over the time scale of these experiments, viz., up to 54 days.

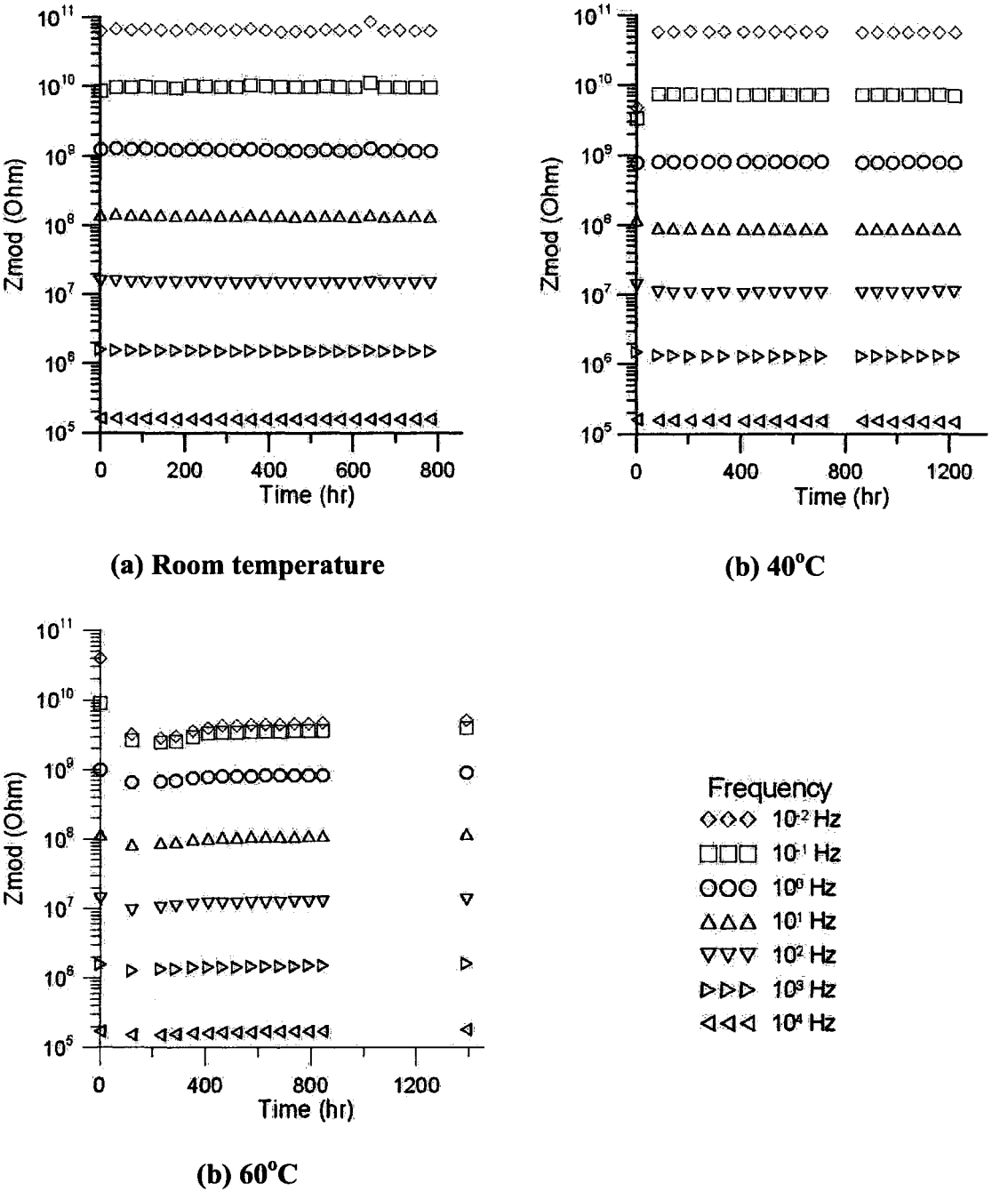

(a) Room temperature

(b) 40°C

(b) 60°C

Figure 7-5 Change with time of the modulus of the impedance of the PUBC samples exposed to 0.1 M NaCl and sulphuric acid (pH 1) at various temperatures.

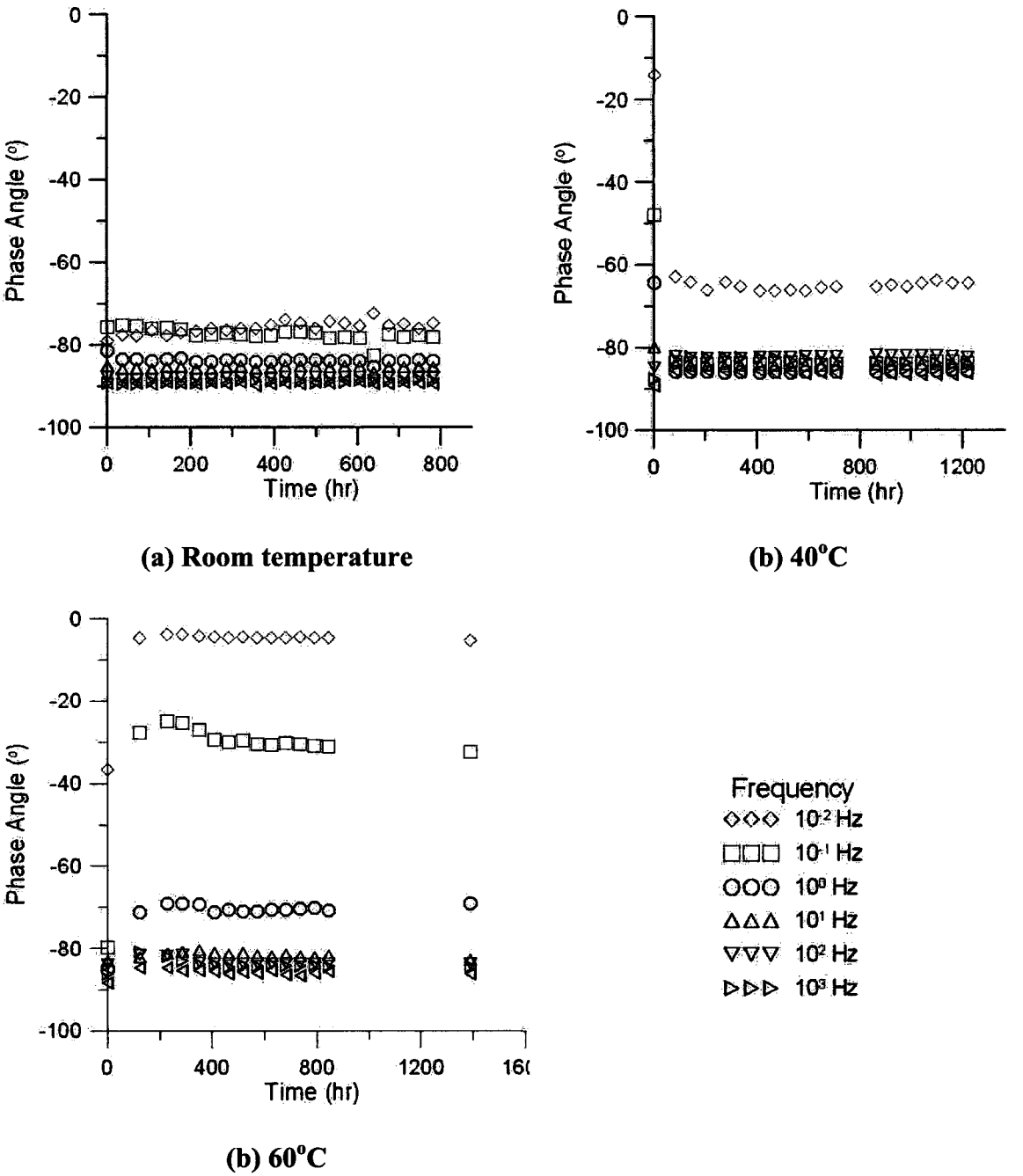

(a) Room temperature

(b) 40°C

(b) 60°C

Figure 7-6 Change with time of the phase angle of the PUBC samples exposed to 0.1 M NaCl and sulphuric acid (pH 1) solution at various temperatures.

The coating properties, R_{po}, Q_c and P_c, are summarized in Table 7-3. Similar comments can be made to those for the data in Section 7.2.1. Q_c is almost a pure

capacitor for which P = 1. Over the course of the experiments, the model predicted small drifts in R_{po}, Q_c and P_c. Basically, Zmod remains constant, but the model has small fluctuations between the in phase and out-of-phase components of the impedance. These drifts may arise from the simplicity of the model, which does not allow for surface effects, wetting and inhomogeneity.

The relatively low value of R_{po} at 60°C arises from the parallel resistive pathway around the edge of the sample, however, R_{po} and Q_c both showed stability over the long exposure time of this experiment, implying that no electrolyte penetrated the sample.

In general, the minor experimental variations in Zmod and phase angle, and the minor model variations in R_{po} and Q_c suggest that the solution did not chemically or physically react with the PUBC. These samples behaved like good barrier coatings.

Table 7-3 Summary of the equivalent circuit modelling results of the PUBC in Test 3.

Parameter	60°C	40°C	Room Temperature
Duration of test (hours)	1389	1218	811
Number of scans	1976	1352	801
Maximum % Error of Fit	7	6	14
Average % Error of Fit	4	5	11
R_{po} at start of test (ohm)	$1.2x10^{10}$	$1.3x10^{11}$	$2.7x10^{11}$
R_{po} at end of test (ohm)	$5.0X10^{9}$	$1.8x10^{11}$	$1.9x10^{11}$
Q_c at start of test	$2.2x10^{-10}$	$1.9x10^{-10}$	$1.7x10^{-10}$
P_c at start of test	0.93	0.94	0.94
Q_c at end of test	$1.9x10^{-10}$	$2.2x10^{-10}$	$1.6x10^{-10}$
P_c at end of test	0.93	0.94	0.95
Model(s) used	B	B	B

7.2.3. Coating exposed to 60% (vol) H_2SO_4

Due to the lack of apparent damage to the PUBC after exposure to pH 1 sulphuric acid, it was decided to test the PUBC samples in a more aggressive environment, viz., a solution of 60% by volume sulphuric acid. No NaCl was added to the solution.

Experiments were conducted in a Tait cell at room temperature and at 60°C for 120 hours, a much shorter time than previous experiments. The test at 60°C was performed in a hot water bath, which was placed inside a fume hood. In order to prevent direct contact of this water with the external components of the Tait cell, viz., the working electrode, alligator clips and cables, the Tait cell was placed inside two plastic bags prior to being placed inside the water bath. The opening of the plastic bags had to be kept above the water level. This configuration led to condensation inside the interior bag, causing a pool of water to form in the bag, which wetted the working plate electrode under the coating. When this happened, the EIS spectrum showed interfering noise at low frequencies. This problem was corrected by periodically removing the condensation.

At room temperature, there were no visible signs of deterioration of the coating samples. The EIS scans also showed that the PUBC remained unaffected by the strong acid solution. Figure 7-7 shows the modulus of the impedance and the phase angle at room temperature. It is obvious that there were no physical or chemical reactions between the sulphuric acid and the coating. Zmod is very high at low frequencies, and constant at all frequencies. All the phase angles are between -80° and -90° indicating capacitive behaviour with a very low conductivity. This is a very good barrier coating.

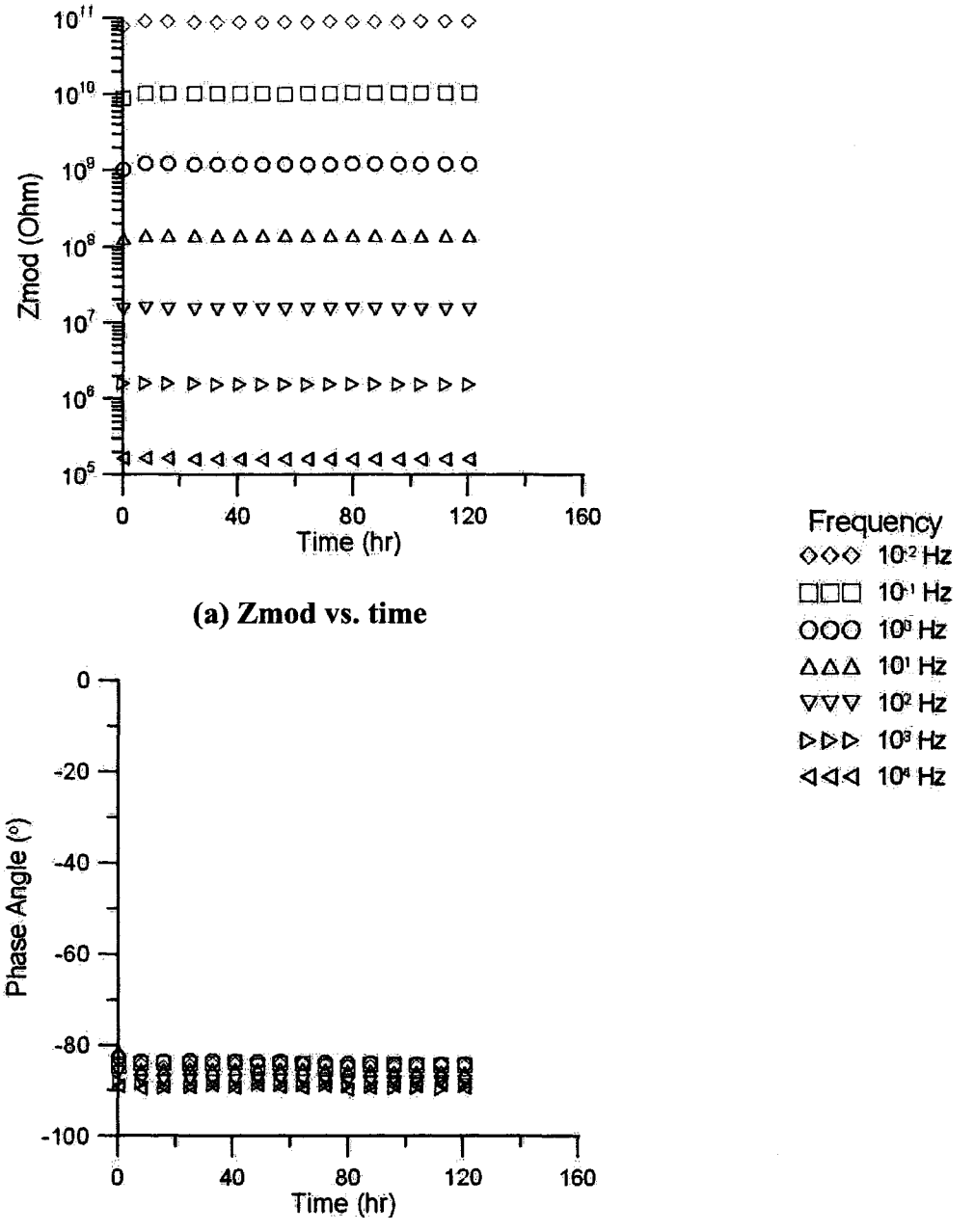

(a) Zmod vs. time

(b) Phase angle vs. time

Figure 7-7 Lack of change of the modulus of the impedance and phase angle of the PUBC samples exposed to 60% sulphuric solution at room temperature.

Results were different at 60°C where the coating showed significant visible deterioration. The solution started to turn brown during the early hours of exposure.

When the cell was disassembled at the end of the test, the coating had only half of its original thickness, and the solution was dark brown. There was a thin layer, ~ 0.1 mm, of brown residue on the coating which could be wiped off to observe the original yellow colour of the coating. When the coating was cut to see its cross section, it was observed that the remaining thickness of the sample had the original colour of the PUBC and had no visible signs of degradation or solution ingress. This suggested that strong acid chemically reacted with the surface of the PUBC, but did not enter the coating; and that the remaining coating was resistant to solution penetration. As will be seen, this was borne out by the EIS data. There were no signs of electrochemical activity on the surface of the metal plate under the sample.

The counter electrode was covered with a thick film, ~ 2 mm, of brown residue released from the coating (Figure 7-8), during the reaction of the sulphuric acid with it. When the film was wiped off, there were no visible signs of corrosion of the counter electrode (Hastelloy).

Figure 7-8 Counter electrode after 60°C test with 60% sulphuric acid.

Figure 7-9 shows the variation with time of the modulus of the impedance and the phase angle at 60°C. The modulus of the impedance is very stable at all frequencies except for 10^{-2} Hz, at which an initial fall is followed by a slow drift upwards. For all except the two lowest frequencies, 10^{-2} Hz and 10^{-1} Hz, the phase angles are constant between -80° and -90°. The phase angle at 10^{-1} Hz started off at -65° and decreased towards -90° as the test progressed. The phase angle at 10^{-2} Hz rapidly increased to -30° within the first hours of exposure, but later gradually decreased to -50°. Such changes are considerably larger than observed in any other PUBC experiment (see Figure 7-2, Figure 7-3, Figure 7-5, and Figure 7-6). These low-frequency changes are likely related to the chemical attack on the PUBC, and also perhaps to the accumulation of residue on the counter electrode.

According to the EIS data, especially the high Zmod values at low frequency, this coating still behaved as a good barrier to the concentrated sulphuric acid, even though chemical reaction was occurring on the surface of the coating. The effects of a diminution in coating thickness were not readily observable on a log(Zmod) plot (Figure 7-9), however, when Zmod was plotted against time on a linear axis, changes showed up clearly. Decreases in Zmod probably correspond to thinning of the polymer. Figure 7-9 shows the behaviour of the Zmod on a linear axis plot for four frequencies (0.01Hz, 10Hz, 100 Hz and 1000 Hz). As can be seen in these plots, there is a marked decrease in Zmod for the 60°C experiment. There were 16%, 17%, 21%, and 23% decreases in the values of the Zmod for the 0.01Hz, 10Hz, 100Hz, and 1000Hz frequencies, respectively. The 0.01Hz frequency shows an initial large decrease in Zmod, but over the remainder of the test it increases. Further work is required before an explanation for this behaviour can

be given. By comparison, there is a much smaller decrease in Zmod at room temperature. At the beginning of the exposures, Zmod values at both temperatures are similar, but they diverge (Figure 7-10). Some kind of perturbation occurred after 90 hours at 60°C. This can be seen clearly in Figure 7-9 and Figure 7-10. This may be related to the fouling of electrodes.

From these preliminary experiments, it is clear that the EIS technique was sensitive to the chemical degradation of a PUBC sample exposed to an aggressive environment. Further work is now needed to quantify how EIS spectra of coatings are affected by chemical changes of the kind observed during this current investigation.

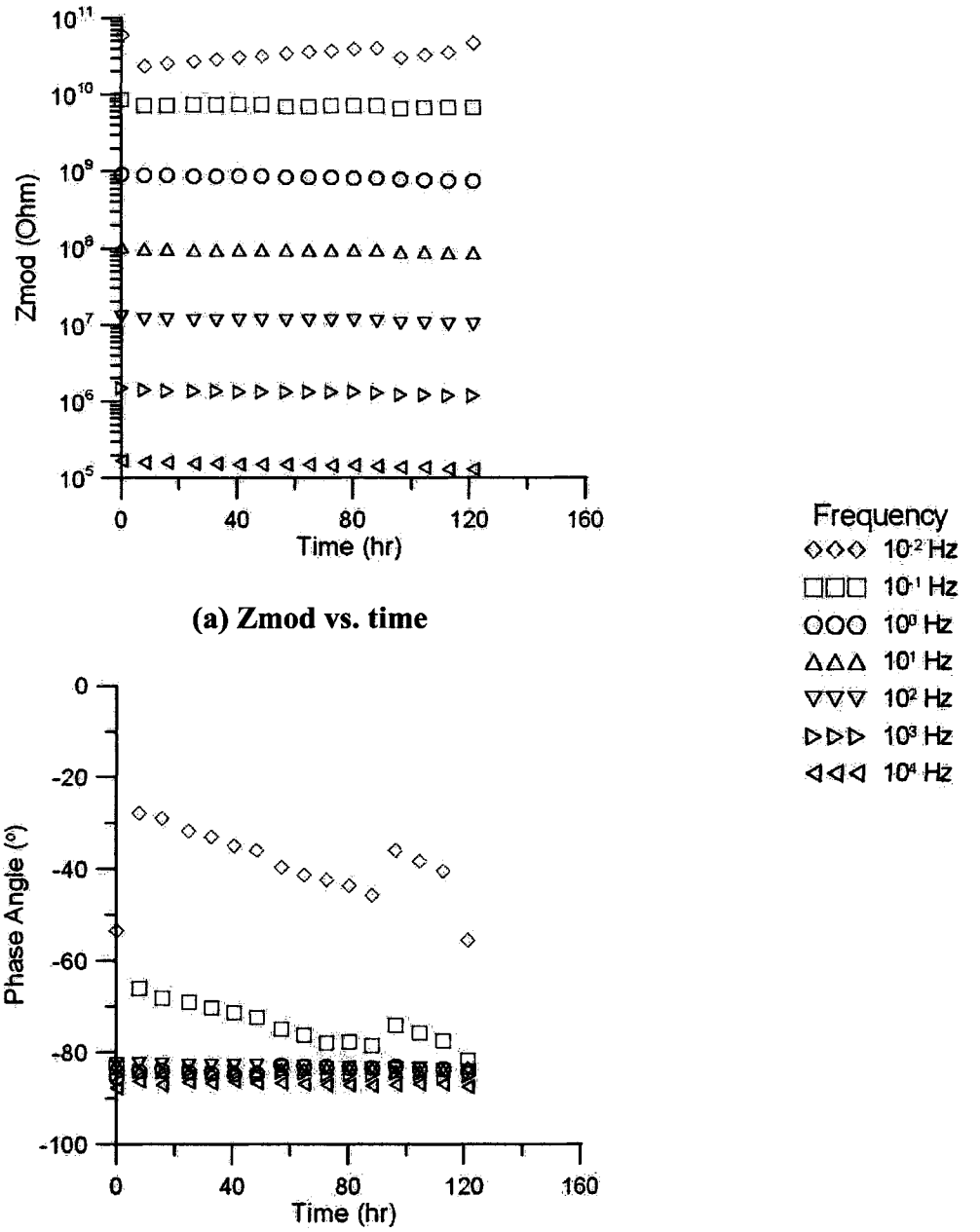

(a) Zmod vs. time

(b) Phase angle vs. time

Figure 7-9 Change of the modulus of the impedance and phase angle of the PUBC samples exposed to 60% sulphuric solution at 60°C.

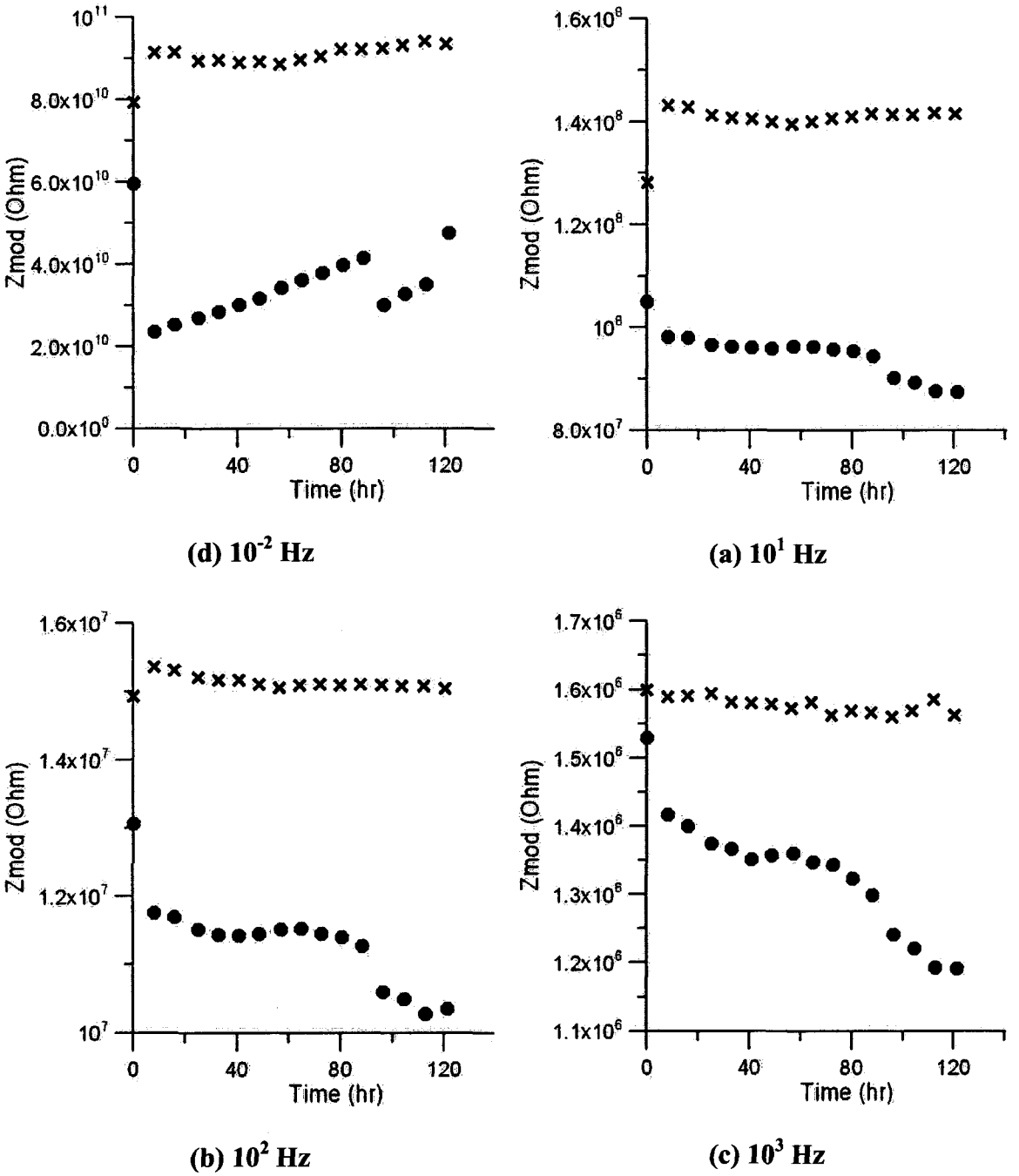

Figure 7-10 Variation of Zmod with time plotted on a linear axis for 4 different frequencies. In all four plots, the upper data are for room temperature, while the lower data are for 60°C.

7.3. Summary

In this investigation, the PUBC samples were exposed to different chemical environments, while continuous EIS spectra were recorded. The PUBC samples were exposed to: a 0.1 M NaCl test solution at 25°C and 40°C; a mixture of 0.1 M NaCl and pH 1 sulphuric acid at 25°C, 40°C and 60°C; and finally 60% by volume sulphuric acid at 25°C and 60°C. The conclusions derived from these experiments are presented in the following section.

7.3.1. Conclusions

Based on the results of the tests performed on the free film PUBC samples and the analyses of data, the following conclusions have been drawn:

- The Tait cell apparatus performed well over long testing periods, while exposed to high temperatures and strong acidic conditions, without any degradation of the cell or its electrodes: there were no observable signs of corrosion inside the cell, or on the counter and reference electrodes.
- It was observed that the coating's sample size had an important effect on the measurements. Samples must be prepared such that the edge of the coating is not near the edge of the o-ring of the Tait cell, otherwise the EIS spectra will be distorted by an electrical bypass around the edge of the coating.
- Throughout the testing (up to 58 days), the PUBC behaved as an excellent barrier coating. In contrast to the REBC, there was no penetration of electrolyte into the PUBC. EIS scans showed that the samples retained very high impedances and behaved like almost perfect capacitors over the entire duration of the 0.1 M NaCl experiments and the 0.1 M NaCl plus pH 1

sulphuric acid experiments. This was also the case at elevated temperatures (40°C and 60°C). EIS measurements reacted to variations in the coating samples, that could be attributed to differing surface properties, however, these were minor in comparison to the gross effects seen in the REBC samples in Chapter 6.

- At room temperature EIS scans showed that the PUBC was unaffected by 60% vol. sulphuric acid solution; it exhibited the properties of a very good barrier coating, with no obvious sign of chemical reaction.
- At 60°C, clear signs of degradation, viz., chemical product and a diminution in coating thickness, were observed in 60% vol. sulphuric acid. It was evident that the acid chemically reacted with the PUBC, but the EIS data showed that the acid did not penetrate the coating. The chemical reaction was on the surface. The remaining coating still acted as an excellent barrier layer. In contrast to experiences with the REBC (Chapter 6), there was no observable sign of electrochemical activity on the surface of the metal plate under the sample.
- The chemical attack of the coating in the strong acid test at 60°C was not readily observable on a log(Zmod) plot, however, it was clearly seen that Zmod was affected when plotted on a linear axis. Further work is needed to correlate chemical changes and formation of deposits with features of EIS spectra.
- It is generally observed that at low frequencies <0.1Hz, EIS spectra are more sensitive to noise. This arises because the highest impedances and

lowest currents are at low frequencies, and these take the longest times to measure.

- It was also observed in this present work (with the REBC and the PUBC), that it is at the low-frequency end of EIS spectra, that symptoms of barrier penetration or degradation are first observed.
- In agreement with the previous conclusion is the fact that low-frequency data were sensitive to a parallel conduction path around the edge of a sample, in an imperfect experimental setup.
- A very simple model that emulated only the bulk properties of the coating, gave a good fit to much of the EIS data. Fine structures in the EIS data need to be investigated in future work.

8. Conclusions and Future Work

8.1. General

In developed countries a large portion of the population is serviced by wastewater treatment plants. Solids (i.e. sludge that includes biomass and pathogens) produced during the wastewater treatment process are generally sent to anaerobic digesters where they are further cleaned using bacteria and are reduced to bio-solids and gaseous products. These digesters are mostly reinforced or prestressed concrete structures; however the treatment process of sludge in a digester creates an acidic environment known to be deleterious to concrete. The main method used to protect concrete is to apply high-performance barrier coatings on the interior faces of the digesters.

The performance of coatings in wastewater treatment plants is currently monitored using in-situ testing, which typically take two years or longer. There are both practical and economic motivations to reduce the time to evaluate the performance of coatings in wastewater digesters. Electrochemical impedance spectroscopy is known to be a sensitive technique to changes in electrical properties of coatings, films and oxides; therefore this research focused on the investigation of the potential use of EIS to quantify the performance of barrier coatings proposed for use in wastewater digesters under varying environmental conditions, and also to optimize the chemical conditions and the experimental method so as to obtain an accelerated test procedure.

To achieve these objectives a detailed experimental program has been carried out. This included the evaluation of two commercially available barrier coatings using EIS: a

Rubberized Epoxy Barrier Coating (REBC) and a PolyUrethane Barrier Coating (PUBC). The investigation was carried out in stages.

In the preliminary investigation, the feasibility and efficacy of EIS were investigated on the REBC and the PUBC samples that were sandwiched between two metal plates at room temperature and in dry conditions (*in air*). Using this method, coatings containing artificial defects and exposed to different environments were studied to determine if EIS could detect and measure faults in coatings.

Since the preliminary metal plate tests had limitations in that they did not permit the continuous monitoring of EIS spectra, in the next stage, an apparatus, called a Tait cell, was used to carry out repetitive real time in-situ EIS tests on the barrier coatings, without the need to remove the samples from solution for subsequent EIS measurements. The Tait cell setup also allowed us to carry out EIS tests on the coatings at different temperatures and using highly acidic solutions.

EIS data were analyzed by monitoring changes in the impedance of the coatings over time. These observations were supported by equivalent circuit modelling.

In general, the EIS technique was able to detect small changes in both coatings, and the Tait cell proved to be an effective means of performing accelerated in-situ EIS scans. The experiments have shown that REBC is not a good barrier coating, even at room temperature and when exposed to non-aggressive solutions like NaCl. On the other hand, PUBC showed excellent protective properties, even when exposed to highly acidic solutions at thermophyllic temperature ranges (50-57°C). Although further research is still necessary, the findings of this study suggest that the PUBC, which is currently

widely used in mesophyllic digesters that operate at 30-38°C, has the potential to be used in digesters that are operated at thermophyllic conditions.

The following specific conclusions have been drawn from the results of different stages of this experimental investigation. These conclusions have been previously stated in the conclusions of Chapters 4, 6, and 7.

8.2. Preliminary EIS Testing Using Metal Plates and Dry Cells

- Metal plate setup has been shown to be a very practical method to obtain a general idea about the properties of barrier coatings. The preliminary experiments showed that the EIS technique used in the metal plate setup can be very useful in assessing the barrier properties of coatings. It can detect flaws such as pinholes (holidays), and responds to different porosities in coatings. The tests did not show any great differences in EIS spectra for coatings that were thinned in places to make artificial depressions, but no quantitative analysis was done.
- It was possible to see from the metal plate tests that the two coating types tested in this research behaved in two completely unique manners. The PUBC sample appeared to be quite impermeable to electrolyte. Its impedance dropped when exposed to liquid, but it still retained good barrier properties. The REBC samples, however, absorbed an appreciable amount of electrolyte, which caused a dramatic reduction in impedance (5 orders of magnitude) compared to the dry coating.
- The metal plate tests had limitations in that they did not permit the continuous monitoring of EIS spectra, with a coating's surface completely exposed to a solution.

8.3. Tait Cell Tests on the REBC Samples

- In all tests and at all temperatures, the REBC started off as a high quality capacitor, with an exceedingly high resistivity, but as electrolyte entered the pores, the REBC transformed into a low value resistor. Eventually, the REBC became ineffective as a barrier coating. All of these effects were observable in the EIS spectra.
- When the electrolyte contained only NaCl, the EIS scans of the REBC samples showed that the solution was entering the coating. Since the NaCl solution did not degrade the coating, it can be concluded that a pre-existing network of pores was present in the sample. Through these pores, the NaCl solution was ultimately able to reach the surface of the metal plate.
- The electrolyte containing sulphuric acid caused electrochemical reactions on the metal surface, resulting in gas accumulation under the coating. The REBC samples failed after pressure had built up under the coating, eventually tearing the sample near the o-ring of the Tait cell. After this failure the coating was completely electrically bypassed. This was all observable by EIS.
- Temperature played a significant role in the lack of performance of the REBC samples: at elevated temperatures the EIS scans indicated that the rate of ingress of solution into the coating was considerably increased.
- EIS showed that when the REBC samples, which had been previously saturated with the NaCl solution, were exposed to sulphuric acid, it may not be necessary for the sulphuric acid itself to penetrate the coating in order for there to be an

electrochemical reaction on the surface of the metal electrode. In fact the NaCl, that already filled the pores, could act as a salt bridge, transferring charge between the metal electrode under the coating, and the bulk solution containing sulphuric acid above the coating.

- EIS measurements did not provide any evidence of a chemical reaction between the sulphuric acid and the REBC. This is in agreement with the traditional use of the REBC on floors where sulphuric acid might be spilled.
- When the REBC was bonded to the metal substrate, despite the solution still accessing the electrode through the pores, there was no evidence of blister formation due to gas accumulation. From this observation, it can be concluded that, in the traditional use of the coating to protect floors against acid spillage, the REBC should be bonded to the floors for best performance.
- The EIS technique is able to track the infiltration of electrolytes into coatings and through coatings. It can be used to observe the time at which complete coating failure occurs.
- The Tait cell proved to be an effective means of performing in-situ EIS scans. The use of coatings that are not bonded to the underlying metal electrode, compared to coatings that are bonded, has significant advantages: lack of bonding accelerates the time to failure and magnifies the degree of failure.

8.4. Tait Cell Tests on the PUBC Samples

- The Tait cell apparatus performed well over long testing periods, while exposed to high temperatures and strong acidic conditions, without any degradation of the

cell or its electrodes: there were no observable signs of corrosion inside the cell, or on the counter and reference electrodes.

- It was observed that the coating's sample size had an important effect on the measurements. Samples must be prepared such that the edge of the coating is not near the edge of the o-ring of the Tait cell, otherwise the EIS spectra will be distorted by an electrical bypass around the edge of the coating.
- Throughout the testing (up to 58 days), the PUBC behaved as an excellent barrier coating. In contrast to the REBC, there was no penetration of electrolyte into the PUBC. EIS scans showed that the samples retained very high impedances and behaved like almost perfect capacitors over the entire duration of the 0.1 M NaCl experiments and the 0.1 M NaCl plus pH 1 sulphuric acid experiments. This was also the case at elevated temperatures (40°C and 60°C). EIS measurements reacted to variations in the coating samples, that could be attributed to differing surface properties, however, these were minor in comparison to the gross effects seen in the REBC samples.
- At room temperature EIS scans showed that the PUBC was unaffected by 60% vol. sulphuric acid solution; it exhibited the properties of a very good barrier coating, with no obvious sign of chemical reaction.
- At 60°C, clear signs of degradation, viz., chemical product and a diminution in coating thickness, were observed in 60% vol. sulphuric acid. It was evident that the acid chemically reacted with the PUBC, but the EIS data showed that the acid did not penetrate the coating. The chemical reaction was on the surface. The remaining coating still acted as an excellent barrier layer. In contrast to

experiences with the REBC (Chapter 6), there was no observable sign of electrochemical activity on the surface of the metal plate under the sample.

- The chemical attack of the coating in the strong acid test at 60°C was not readily observable on a log(Zmod) plot, however, it was clearly seen that Zmod was affected when plotted on a linear axis. Further work is needed to correlate chemical changes and formation of deposits with features of EIS spectra.
- It is generally observed that at low frequencies <0.1Hz, EIS spectra are more sensitive to noise. This arises because the highest impedances and lowest currents are at low frequencies, and these take the longest times to measure.
- It was also observed in this present work (with the REBC and the PUBC), that it is at the low-frequency end of EIS spectra, that symptoms of barrier penetration or degradation are first observed.
- In agreement with the previous conclusion is the fact that low-frequency data were sensitive to a parallel conduction path around the edge of a sample, in an imperfect experimental setup.
- A very simple model that emulated only the bulk properties of the coating, gave a good fit to much of the EIS data. Fine structures in the EIS data need to be investigated in future work.

8.5. Recommendations for Future Work

- More extensive testing of the PUBC is required to determine if it is in fact suitable for use in wastewater digesters that are operated at the thermophyllic temperature range. This can be done by carrying out EIS scans though Tait cell

experiments on the coating over an extended time period, and at thermophyllic temperatures.

- Equivalent circuit modelling of the PUBC may be extended to cover elements for surface features, inhomogeneities, adsorption or chemical reactions.
- The testing of replicate REBC and PUBC samples would help gather more information on sample variation and strengthen the conclusions of this research.
- Sensitive and long-term mass gain tests using different electrolytes at different temperatures will allow us to gain additional engineering properties (e.g. transport properties) of the barrier coatings.
- Additional testing of the REBC and PUBC at varying coating thicknesses, and different application techniques, would determine if these factors have an effect on the performance of the coatings.
- Testing other barrier coatings would help develop further confidence in the methods used and developed in this research.
- The design of an EIS testing protocol that would allow the coating sample to be exposed to both gas (e.g. H_2S) and liquid (e.g. H_2SO_4) phases would more accurately represent the in-service conditions of a coating in a digester.
- The validity and accuracy of the results and conclusions of this work must be verified when coatings are applied on a concrete substrate.

References

A.S.M. International. Handbook Committee. *Metals Handbook.* 10th ed. Materials Park, Ohio: A.S.M. International., 1990.

Appleman, B. R., R. W. Drisko, and J. M. Neugebauer. *Inspection of Coatings and Linings: A Handbook of Basic Practice for Inspectors, Owners, and Specifiers.* SSPC, 1998.

ASTM D 6132. *Standard Test Method for Nondestructive Measurement of Dry Film Thickness of Applied Organic Coatings Over Concrete using an Ultrasonic Gage.* Philadelphia, PA: American Society of Testing and Materials, 1998.

ASTM D2240. *Standard Test Method for Rubber Property-Durometer Hardness.* Philadelphia, PA: American Society of Testing and Materials, 2001.

ASTM D2583. *Standard Test Method for Indentation Hardness of Rigid Plastics by Means of a Barcol Impressor.* Philadelphia, PA: American Society of Testing and Materials, 1998.

ASTM D3359. *Standard Test Methods for Measuring Adhesion by Tape Test.* Philadelphia, PA: American Society of Testing and Materials, 2008.

ASTM D4138. *Standard Practices for Measurement of Dry Film Thickness of Protective Coating Systems by Destructive, Cross-Sectioning Means.* Philadelphia, PA: American Society of Testing and Materials, 2007.

ASTM D4541. *Standard Test Method for Pull-Off Strength of Coatings using Portable Adhesion Testers.* Philadelphia, PA: American Society of Testing and Materials, 2002.

ASTM D5162. *Standard Practice for Discontinuity (Holiday) Testing of Nonconductive Protective Coating on Metallic Substrates.* Philadelphia, PA: American Society of Testing and Materials, 2008.

ASTM D6677. *Standard Test Method for Evaluating Adhesion by Knife.* Philadelphia, PA: American Society of Testing and Materials, 2007.

ASTM E1907. *Standard Guide to Methods of Evaluating Moisture Conditions of Concrete Floors to Receive Resilient Floor Coverings (Withdrawn 2008).* Philadelphia, PA: American Society of Testing and Materials, 2006.

Bacon, R. C., J. J. Smith, and F. M. Rugg. "Electrolytic Resistance in Evaluating Protective Merit of Coatings on Metals." *Industrial and Engineering Chemistry* 40, no. 1 (1948): 161-167.

Barsoukov, Evgenij, and J. Ross Macdonald. *Impedance Spectroscopy : Theory, Experiment, and Applications.* 2nd ed. Hoboken, N.J.: Wiley-Interscience, 2005.

Bierwagen, Gordon, Dennis Tallman, Junping Li, Lingyun He, and Carol Jeffcoate. "EIS Studies of Coated Metals in Accelerated Exposure." *Progress in Organic Coatings* 46, no. 2 (2003): 149-158.

Briand, Remi, and Nixon Randy. *A Novel Analytical Approach for Evaluating Protective Coatings Performance in Wastewater Environment.* WEFTEC 2003 Conference Proceedings, 2003.

CC Technologies Canada, Ltd. "NEWS, VIEWS, and UPDATES, CC Technologies." February 11 [cited 2008]. Available from http://www.cctechnologies.com/newsviews/newsviews/2005/FBEpipelinecoatings.htm.

City of Sante Fe, New Mexico. "Wastewater Treatment Plant." [cited 2008]. Available from http://www.santafenm.gov/index.asp?NID=852.

Cogdell, J. R. *Foundations of Electric Circuits.* Upper Saddle River, N.J.: Prentice Hall, 1999.

Crites, Ron, and George Tchobanoglous. *Small and Decentralized Wastewater Management Systems.* Boston: WCB/McGraw-Hill, 1998.

Deflorian, F., S. Rossi, l. Fedrizzi, and P. L. Bonora. "Statistical Analysis of Salt Spray and EIS Testing Data Concerning Organic Coated Metals." *Journal of Corrosion Science and Engineering* (1999).

Dehri, Ilyas. "Impedance Measurements of Polyester-Coated Galvanised Mild Steel in 10x Acid Rainwater After an Accelerated Wet-Dry Test." *Turk J Chem* 24, (2000): 239-245.

Department of the Navy, Naval Civil Engineering Laboratory. *Techdata Sheet Jun 1982 82-08, Paint Failures - Causes and Remedies.*1982.

Drever, James I. *The Geochemistry of Natural Waters.* 2nd ed. Englewood Cliffs, N.J.: Prentice Hall, 1988.

Duval, S., Y. Camberlin, M. Glotin, M. Keddam, F. Ropital, and H. Takenouti. "Characterisation of Organic Coatings in Sour Media in Influence of Polymer Structure on Corrosion Performance." *Progress in Organic Coatings* 39, (200): 15-22.

EPA. *Aging Water Infrastructure Research Program, Addressing the Challenge through Innovation.*2007.

EPA. *Primer for Municipal Wastewater Treatment Systems.*2004.

EPA. *Process Design Manual for Nitrogen Control.*1975.

Estoup, J. M., and R. Cabrillac. "Corrosion of Biological Origin Observed on Concrete Digestors." *Construction and Building Materials* 11, no. 4 (1997): 225-232.

Fairfield-Suisun Sewer District. "Fairfield-Suisun Sewer District." [cited 2008]. Available from http://www.fssd.com/indexSub.cfm?page=693825.

Fedrizzi, L., A. Bergo, and M. Fanicchia. "Evaluation of Accelerated Aging Procedures of Painted Galvanised Steels by EIS." *Electrochimica Acta* 51, (2006): 1864-1872.

Forsgren, Amy. *Corrosion Control through Organic Coatings.* Boca Raton, FL: CRC/Taylor & Francis, 2006.

Gamry Instruments. *Application Note, Basics of Electrochemical Impedance Spectroscopy.* 5th ed. Gamry Instruments, 2007.

Gamry Instruments. "EIS on Coatings - Potentiostat Limitations ." in Gamry Instruments [database online]. December 13, 2006 [cited 2008]. Available from http://gamry.com/App_Notes/EIS_Of_Coatings/EIS_Of_Coatings.htm.

Gamry Instruments. *PC4 Potentiostat/Galvanostat/ZRA Operator's Manual.* 4th ed. Gamry Instruments, 2001.

Girault, H. H. *Analytical and Physical Electrochemistry.* Lausanne, Switzerland; New York: Epfl; Marcel Dekker, 2004.

Grady, C. P. Leslie, Glen T. Daigger, and Henry C. Lim. *Biological Wastewater Treatment.* 2nd rev. and expand ed. New York: Marcel Dekker, 1999.

Gray, N. F. *Biology of Wastewater Treatment.* 2nd ed. London: Imperial College Press, 2004.

Hinderliter, B. R., S. G. Croll, D. E. Tallman, Q. Su, and G. P. Bierwagen. "Interpretation of EIS Data from Accelerated Exposure of Coated Metals Based on Modeling of Coating Physical Properties." *Electrochimica Acta* 51, no. 21 (2006): 4505-4515.

Islander, Robert L., Joseph S. Devinny, Florian Mansfeld, Adam Postyn, and Hong Shih. "Microbial Ecology of Crown Corrosion in Sewers." *Journal of Environmental Engineering* 117, no. 6 (1991): 751-751-770.

Khanna, Anand S., and Institute of Materials, Minerals, and Mining. *High-Performance Organic Coatings.* Cambridge, England :$bWoodhead Publishing ; England; Boca Raton, FL: Maney Publishing; CRC Press, 2008.

KMK Consultants Limited, and Black and Veatch Canada. *City of Toronto Biosolids and Residuals MASTER PLAN Executive Summary.*2004.

Kouloumbi, Niki J., and Stavros T. Kyvelidis. "Evaluation of the Anticorrosive Behaviour of Organic Coatings by using a Variant of Electrochemical Impedance Spectroscopy." *Mikrochimica Acta* 136, (2001): 175-180.

Liu, J., and C. Vipulanandan. "Long-Term Performance of Epoxy Coated Clay Bricks in Sulfuric Acid." *Journal of Materials in civil engineering* (2004): 349-355.

Liu, J., and C. Vipulanandan. "Testing Epoxy Coatings for Dry and Wet Concrete Wastewater Facilities." *Journal of Protective Coatings and Liningsno.* December (1999): 26-37.

Liu, Jie, and C. Vipulanandan. "Evaluating a Polymer Concrete Coating for Protecting Non-Metallic Underground Facilities from Sulfuric Acid Attack." *Tunnelling and underground space technology* 16, (2001): 311-321.

Loveday, D., P. Peterson, and B. Rodgers. "Evaluation of Organic Coatings with Electrochemical Impedance Spectroscopy, Part 3: Protocols for Testing Coatings with EIS." *JCT COATINGSTECH* (2005): 22-27.

Loveday, D., P. Peterson, and B. Rodgers. "Evaluation of Organic Coatings with Electrochemical Impedance Spectroscopy, Part 1: Fundamentals of Electrochemical Impedance Spectroscopy." *JCT COATINGSTECH* 1, no. 8 (2004): 46-52.

Loveday, D., P. Peterson, and B. Rodgers. "Evaluation of Organic Coatings with Electrochemical Impedance Spectroscopy, Part 2: Application of EIS to Coatings." *JCT COATINGSTECH* 1, no. 10 (2004): 88-93.

LSA Associates , INC. *Fieldcreast Villages ProjectT Environmental Impact Report.*2008.

Mansfeld, Florian. "Use of Electrochemical Impedance Spectroscopy for the Study of Corrosion Protection by Polymer Coatings." *Journal of Applied Electrochemistry* 25, (1995): 187-202.

Mansfeld, Florian. "Electrochemical Impedance Spectroscopy (EIS) as a New Tool for Investigating Methods of Corrosion Protection." *Electrochimica Acta* 35, no. 10 (1990): 1533-1544.

Masadeh, Sami. "Electrochemical Impedance Spectroscopy of Epoxy-Coated Steel Exposed to Dead Sea Water." *Journal of minerals and Materials Characterization and Engineering* 4, no. 2 (2005): 75-84.

Mills, Douglas, Steve Mabbutt, and Gordon Bierwagen. "Investigation into Mechanism of Protection of Pigmented Alkyd Coatings using Electrochemical and Other Methods." *Progress in Organic Coatings* 46, no. 3 (2003): 176-181.

Miskovic-Stankovic, V. B., D. M. Drazic, and Z. Kacarevic-Popovic. "The Sorption Characteristics of Epoxy Coatings Electrodeposited on Steel during Exposure to Different Corrosive Agents." *Corrosion Science* 38, no. 9 (1996): 1513-1523.

Neville, Adam M. *Properties of Concrete.* 3d ed. London: Pitman., 1981.

O'Dea, Vaughn. "Protecting Wastewater Structures Form Biogenic Sulfide Corrosion." *Journal of Protective Coatings and Liningsno.* October (2007): 52-56.

O'Dea, Vaughn. "Protecting Wastewater Structures from Biogenic Sulfide Corrosion." *Journal of Protective Coatings and Linings* (2007): 52-56.

O'Donoghue, Mike, Ron Garrett, Vijay Datta, Peter Roberts, and Terry Aben. "Electrochemical Impedance Spectroscopy: Testing Coatings for Rapid Immersion Service." *Coatings and Linnings* (2003): 36-36-41.

Oriol, Michael, and Kirk Howard. "Rehabilitating Primary Waste Treatment Structures: From Assessment to Waranty." *Journal of Protective Coatings and Liningsno.* october (2007): 24-32.

Ozcan, M., I. Dehri, and M. Erbil. "EIS Study of the Effect of High Levels of SO_2 on the Corrosion of Polyester-Coated Galzanised Steel at Different Relative Humidities." *Progress in Organic Coatings* 44, (2002): 279-285.

Peavy, Howard S., Donald R. Rowe, and George Tchobanoglous. *Environmental Engineering.* New York: McGraw-Hill, 1985.

Pletcher, Derek, and Frank Walsh. *Industrial Electrochemistry.* 2nd ed. London ; New York: Chapman and Hall, 1990.

Princeton Applied Research. *Condensed Catalogue 2002.*2002.

Research Solutions and Resources. "What is Chi-Squared?" November 27 [cited 2008]. Available from http://www.consultrsr.com/resources/eis/chi2.htm.

Scholz, F., and A. M. Bond. *Electroanalytical Methods : Guide to Experiments and Applications.* Berlin ; New York: Springer, 2002.

Shanghai Genesis Chemical Industry Co., Ltd. "Genesis Chemical, Ameron, Genesis, PPG, Industrial Coating, Marine Coating." [cited 2008]. Available from http://www.genesischemical.com/en/download/download.asp.

Shon, M., and H. Kwon. "Effects of Surface Modification with Amino Branched Polydimethylsiloxane (ABP) on the Corrosion Protection of Epoxy Coating." *Corrosion Science* 49, no. 11 (2007): 4259-4275.

Souto, R. M., M. L. Llorente, and L. Fernandez-Merida. "Accelerated Tests for the Evaluation of the Evaluation of the Corrosion Performance of Coil-Coated Steel Sheet: EIS Under Cathodic Polarization." *Progress in Organic Coatings* 53, (2005): 71-76.

SSPC: Society for Protective Coatings. *C-1 Fundamentals of Protective Coatings for Industrial Structures.* 13A.1 ed. SSPC, 2005.

Steele, Jon, and Jay Steele. "Performance Criteria for Coatings on Concrete in Chemical Exposures." *Journal of Protective Coatings and Liningsno.* July (1999): 29-35.

Tchobanoglous, George. *Wastewater Engineering : Treatment, Disposal, Reuse.* 2d ed. New York: McGraw-Hill, 1979.

Thomson, Graham. *Corrosion and Rehabilitation of Concrete Access/Inspection Chambers.*2000.

Turner, Rufus P., Stan Gibilisco, and Rufus P. Turner. *Principles and Practice of Impedance.* 2nd ed. Blue Ridge Summit, PA: Tab Books, 1987.

Turovskiy, I. S., and P. K. Mathai. *Wastewater Sludge Processing.* Hoboken, N.J.: Wiley-Interscience, 2006.

Vawter, Richard. "Parallel-Plate Capacitor." September 27 [cited 2008]. Available from http://www.ac.wwu.edu/~vawter/PhysicsNet/Topics/Capacitors/ParallCap.html.

Vipulanandan, C., and J. Liu. "Performance of Polyurethane-Coated Concrete in Sewer Environment." *Cement and Concrete Research* 35, (2005): 1754-1763.

Vipulanandan, C., and Jie Liu. "Glass-Fiber Mat-Reinforced Epoxy Coating for Concrete in Sulfuric Acid Environment." *Cement and Concrete Research* 32, (2002): 205-210.

Yang, X. F., J. Li, S. G. Croll, D. E. Tallman, and G. P. Bierwagen. "Degradation of Low Gloss Polyurethane Aircraft Coatings Under UV and Prohesion Alternating Exposures." *Polymer Degradation and Stability* 80, no. 1 (2003): 51-58.

Yang, X. F., D. E. Tallman, G. P. Bierwagen, S. G. Croll, and S. Rohlik. "Blistering and Degradation of Polyurethane Coatings Under Different Accelerated Weathering Tests." *Polymer Degradation and Stability* 77, no. 1 (2002): 103-109.

Yang, X. F., D. E. Tallman, S. G. Croll, and G. P. Bierwagen. "Morphological Changes in Polyurethane Coatings on Exposure to Water." *Polymer Degradation and Stability* 77, no. 3 (2002): 391-396.

Yang, X. F., C. Vang, D. E. Tallman, G. P. Bierwagen, S. G. Croll, and S. Rohlik. "Weathering Degradation of a Polyurethane Coating." *Polymer Degradation and Stability* 74, no. 2 (2001): 341-351.

Zhang, Shu-Yong, Yi-Fu Ding, Shan-Jun Li, Xiao-Wen Luo, and Wei-Fang Zhou. "Effect of Polymeric Structure on the Corrosion Protection of Epoxy Coatings." *Corrosion Science* 44, no. 4 (2002): 861-869.

Zhong, Shiyun, Meilun Shi, and Zhiyuan Chen. "The AC Response of Polymer-Coated Mortar Specimens." *Cement and Concrete Research* 32, (2002): 983-987.

Appendix A: Script Changes to Gamry Frameworks V3.5

This appendix provides details on all changes made to the Gamry scripts and why they were performed. The scripts are written in a proprietary programming language called "Explain". The first script shown was used to control the potentiostat to run multiple experiments in sequence, and to keep running the experiments for an extended period of time. The semi-colon (;) is used to denote comments in this language.

Table A - 1 Automatic EIS Script.

```
include "explain4.exp"
include "Auto Utilities.exp"
function Main()
        FileNameRoot1 = "2EIS REBC - 40 - 2 - 0.1M NaCl -"
        FileNameRoot2 = "2EIS PUBC - 40 - 0.1M NaCl -"

        i = 1
        j = 1

        while (i le 2000)

                ThisFileName1 = Sprint(FileNameRoot1, i, ".dta")
                ThisFileName2 = Sprint(FileNameRoot2, j, ".dta")
                i = i+1
                j = j+1

                if (LaunchWait("Auto Potentiostatic EIS.exp"
&               ,"TOMEIS.set"           ; set file
&               ,"EIS"                  ; set name
&               ,ThisFileName1          ; output file name
&               ,1                      ; potentiostat number
&               ,1) eq FALSE)           ; Multiplex channel
                return

                if (LaunchWait("Auto Potentiostatic EIS.exp"
&               ,"TOMEIS.set"           ; set file
&               ,"EIS"                  ; set name
&               ,ThisFileName2          ; output file name
&               ,1                      ; potentiostat number
&               ,2) eq FALSE)           ; Multiplex channel
                return
```

The following script changes were modified by Gamry after correspondence in an attempt to reduce the gain changes of the potentiostat that caused phantom peaks in the EIS spectra. The modified sections are highlighted in grey, and the original line is above the modified line, with a short explanation as to why the change was made. Script change 1 was a modification of a file called "classreadz.exp". The change in this script involved doubling the test frequency in order not to change the gain often during the experiment (Table A - 2). Figure A - 1 shows Bode plots of PUBC samples before and after this script change was made. It can be clearly seen that the many small changes visible in Figure A - 1a have been replaced with 1 change Figure A - 1b. In addition to reducing the number of gain changes, the script change shown in Table A - 2, had the side effect of causing significant error on the initial high frequency measurements for the PUBC samples, Figure A - 1b, these data points were omitted in the analysis.

Table A - 2 Gamry Script Change 1.

```
; *** RSR modification
; Increase the test frequency.  If it is OK at 2f, it will be better at f!

; _IERange = Pstat.TestIERangeAC (Abs (_Iac), Abs (AmplActual), Abs (_Idc), Abs
(DCAmplReq), Freq)

_IERange = Pstat.TestIERangeAC (Abs (_Iac), Abs (AmplActual), Abs (_Idc), Abs
(DCAmplReq), 2.0*Freq)
```

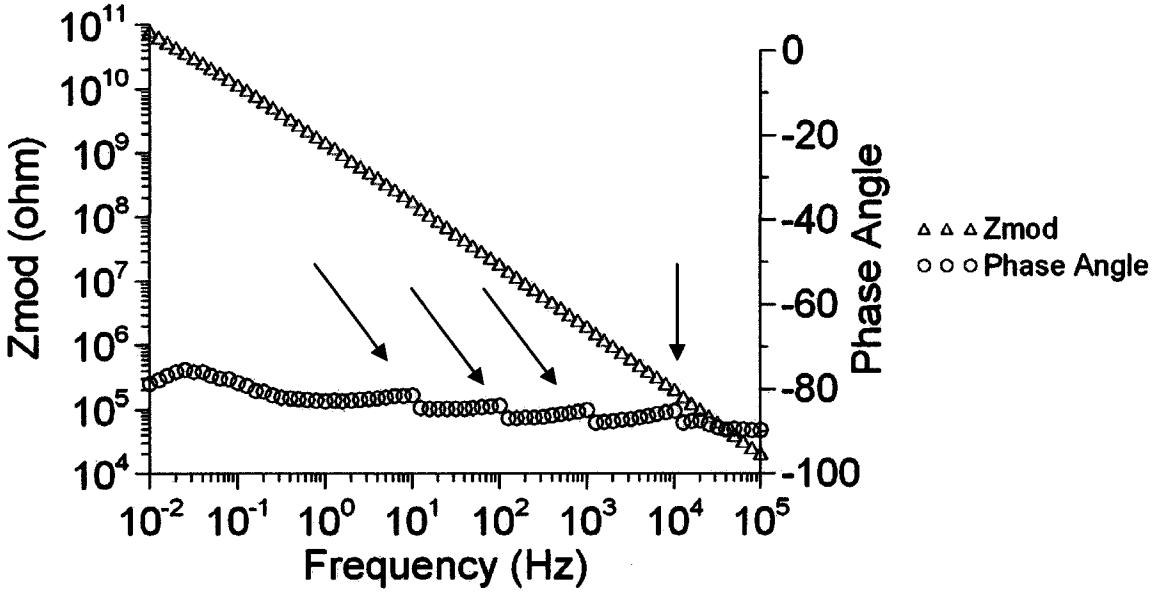

(a) Before script changes

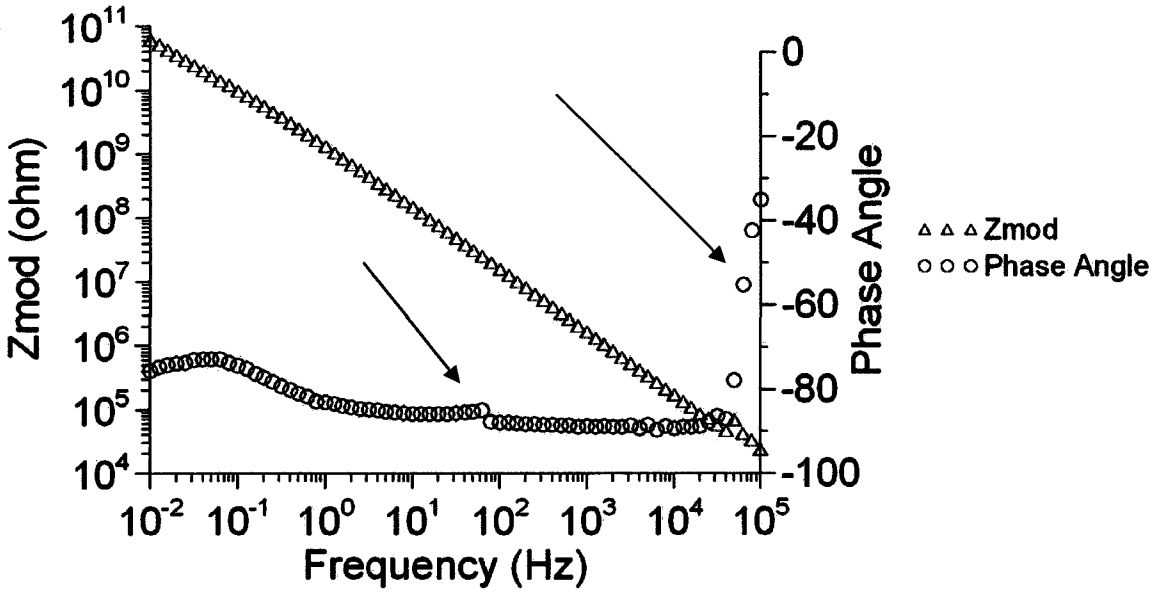

(b) After script changes

Figure A - 1 EIS scans of PUBC samples, performed in a Tait cell, before and after script changes.

Table A - 3 shows the second script modification performed; the name of the script is "multiplexed potentiostatic eis.exp". This modification was performed to compensate for the extra capacitance caused by attaching the multiplex unit to the Gamry system. Table A - 4 is a very similar script to that presented in Table A - 3, however the script in Table A - 4 is intended to be run without user input, and is called "Auto Potentiostatic EIS.exp", as such the same modification done to the script presented in Table A - 3 was done to the script in Table A - 4. The final script change performed was done on a file called "Common Functions.exp" and is presented in Table A - 5. This change was performed because the potentiostat was detecting an artificial error during the free potential measurements prior to the EIS. If the rate of change in the free potential was large, the potentiostat was aborting the test; the script change allowed us to continue the test.

Table A - 3 Gamry Script Change 2

```
; *** RSR modification: Increase IEStability to swamp out
; cable capacitance when using the ECM8
;       Pstat.SetStability (StabilityFast)
Pstat.SetStability (StabilityNorm)
```

Table A - 4 Gamry Script Change 3

```
; *** RSR modification: Increase IEStability to swamp out
; cable capacitance when using the ECM8
;       Pstat.SetStability (StabilityFast)
Pstat.SetStability (StabilityNorm)
```

Table A - 5 Gamry Script Change 4

```
;modfied by Thomas Miller, feb 20, 2008
;to stop cell from cutting out after a large change in voltage is measured
;       OcvCurve.StopAt (Slope, 1.0)
OcvCurve.Activate ()
```

Appendix B: System Specifications for the Gamry PC4/300 Potentiostat

Table B - 1 contains a list of specifications for the Gamry PC4/300 Potentiostat/ Galvanosatat/ZRA.

Table B - 1 Selected system specifications of the Gamry PC4/ 300. [Gamry Instruments 2001]

Control Amplifier	
Compliance Voltage	> ± 20 volts @ 150 mA
Output Current	> ± 300 mA
Differential Electrometer	
Input Impedance	> 1012 Ω in parallel with 5 pF
Input Current	< 10 pA
Voltage Measurement	
Full Scale Ranges	± 30V (±12 V usable), ± 3V, ± 300 mV, ± 30 mV
Resolution(16 Bits)	1 mV/bit, 100 μV/bit, 10 μV/bit,, 1 μV/bit
DC Accuracy	± 0.3% Range ± 1mV
Offset Range	± 12 V with 1.5 mV resolution
Current Measurement	
Analog Full Scale Ranges	± 3 nA to ± 300 mA in decades
Controller Board Gains	1, 10, 100
Resolution (16 bits)	0.1 pA/bit to 10 μA/bit
DC Accuracy (with 1X Controller Board Gain)	± 0.3% range ± 50 pA
Potentiostat Mode	
Applied E Range	± 11 volts
Accuracy	± 2 mV ± 0.3% of setting
Scan Ranges	± 6.4 V, ± 1.6V, and ± 0.4 V
Resolution	200 μV/bit, 50 μV/bit, 12.5 μV/bit